From the Department of Nutritional Science
Biochemistry and Molecular Biology

Trafficking and Sorting of Proteins to the Parasitophorous Vacuolar Membrane of *Plasmodium falciparum*: PfEXP1 as a Model

---

DISSERTATION

for the award of the doctoral degree (**Dr. rer. nat.**)
in the Faculty of Agricultural Sciences, Nutritional Sciences,
and Environmental Management at the
Justus Liebig University of Giessen

submitted by

Amin Abbasi

from Oroumieh, Iran

Giessen, 2026

With the permission of the Faculty of Agricultural Sciences, Nutritional Sciences and Environmental Management of the Justus Liebig University Giessen

1st reviewer: **Prof. Dr. Jude M. Przyborski**
Biochemistry and Molecular Biology
Faculty 09 – Agricultural, Nutritional and Environmental Sciences
Justus Liebig University Giessen

2nd reviewer: **Prof. Dr. Kai Thormann**
Institute of Microbiology and Molecular Biology
Faculty 08 – Biology and Chemistry
Justus Liebig University Giessen

Examiner: **Prof. Dr. Ross Douglas**
Institute of Veterinary Physiology and Biochemistry
Faculty 10 – Veterinary Medicine
Justus Liebig University Giessen

Examiner: **Apl. Prof. Dr. Elena Evguenieva-Hackenberg**
Institute of Microbiology and Molecular Biology
Faculty 08 – Biology and Chemistry
Justus Liebig University Giessen

Chairperson: **Prof. Dr. Jakob Santner**
Chair of Plant Nutrition
Faculty 09 – Agricultural, Nutritional and Environmental Sciences
Justus Liebig University Giessen

Declaration in accordance with the Doctoral Regulations of the Faculty 09 in the version of 29.05.2019 § 17 (2)

I declare that the doctoral thesis here submitted is entirely my own work, written without any unauthorised help by a third party and solely with the assistance referred to in the thesis. I have indicated in the text those texts that have been quoted from already published sources, either verbatim or by analogy and all statements based on verbally conveyed information. During the research carried out by me and referred to in the doctoral thesis, I have at all times followed the principles of good scholarly practice as defined in the Statute of Justus Liebig University Giessen for Ensuring of Good Academic Practice.

Giessen, 30/June/2026

_____

Amin Abbasi

Acknowledgment

I would like to start by expressing my deepest gratitude to my supervisor, **Prof. Dr. Jude M. Przyborski**. Our journey began with his efforts in coordinating with the German Embassy in Paris to make this opportunity possible from scratch. From the lab difficult moments to the opportunity to attend the MAM conference in Australia in 2024, his belief in me was constant.

A big thank you goes to all my colleagues for creating such a nice working atmosphere. I truly valued the knowledge you shared and the many discussions we had, both scientific and non-scientific. I especially want to thank Tina Roselt for the time we spent working together during her Master's project, and Eric Springer for being such a great office mate. I am also very grateful to Julian Barth and Nina Küster, not only for the memorable time we spent together at the MAM conference, but for their support throughout.

Last but certainly not least, I want to thank my wife, Sahar, and my family and friends. Your patience and support during this long journey were my foundation, and I could not have reached this milestone without you.

Abstract

During the asexual blood stage of malaria infection, *Plasmodium falciparum* develops inside a membrane-bound compartment within the host red blood cell. The membrane surrounding this compartment, the parasitophorous vacuolar membrane (PVM), forms an important interface between parasite and host cell. In addition to exporting soluble effector proteins, the parasite must also direct a specific set of membrane proteins to the PVM. PfEXP1 is a well-established membrane protein of the PVM, but the sequence features that govern its trafficking to this membrane remain unclear. The aim of this thesis was therefore to identify PfEXP1 sequence features that contribute to its targeting to the PVM.

To address this question, a panel of plasmid-expressed PfEXP1 variants was generated and analyzed by immunofluorescence microscopy in two parasite developmental stages. In parallel, a biochemical fractionation assay was used to compare whether the different variants behaved mainly as soluble or membrane-associated proteins.

Across the construct panel, distal C-terminal truncations generally retained PVM-like localization under the assay conditions used. These variants showed staining patterns consistent with PVM localization and were enriched in the membrane-associated fraction, suggesting that they remained capable of stable membrane association. This indicates that the distal C-terminus is not a dominant determinant of this behavior. In contrast, disruption of the N-terminal region more often resulted in less distinct localization and weaker biochemical evidence for stable membrane association. The transmembrane domain replacement experiments further showed that not all membrane anchors behaved in the same way. Constructs combining the PfEXP1 N-terminal region with a parasite-derived transmembrane segment were more often consistent with PVM-like localization, whereas constructs containing artificial hydrophobic helices did not reproduce clear PVM localization even when flanked by PfEXP1-derived N- and C-terminal regions. These findings argue against a model in which hydrophobicity alone is sufficient for correct targeting.

An important limitation of this study was the unexpected predominantly soluble behavior of the exogenous full-length PfEXP1 reference construct, indicating that construct architecture, including tag and linker context, can substantially affect the experimental readout. Taken together, the data support a model in which correct PfEXP1 targeting depends on N-terminal context acting together with an appropriate membrane anchor, whereas the distal C-terminal region appears broadly dispensable in this assay context. More broadly, this work highlights the need for follow-up experiments that directly resolve protein topology, particularly protease-protection assays.

Table of Contents

List of Figures

List of Tables

List of Abbreviations

AmpR	Ampicillin resistance
APS	Ammonium persulfate
bp	Base pair
BSA	Bovine serum albumin
CO_2	Carbon dioxide
DAPI	4',6-diamidino-2-phenylindole
ddH_2O	Double distilled water
DMSO	Dimethyl sulfoxide
DNA	Deoxyribonucleic acid
DTT	Dithiothreitol
E. coli	*Escherichia coli*
ECL	Enhanced chemoluminescence
EDTA	Ethylenediaminetetraacetic acid
EGTA	Ethylene glycol tetraacetic acid
EM	Erythrocyte membrane
ER	Endoplasmic reticulum
g	Gravitational force
GA	Glutaraldehyde
gDNA	Genomic DNA
GlcN	Glucosamine
h	Hour
HCl	Hydrochloric acid
hDHFR	human dihydrofolate reductase
HEPES	4-(2-hydroxyethyl)-1-piperazineethanesulfonic acid
HRP	horseradish peroxidase
IFA	Immunofluorescence assay
iRBC	Infected red blood cell
KCl	Potassium chloride
KOH	Potassium hydroxide
kDa	kilodalton
LB	Lysogeny broth
mg	milligram
min	Minute
mM	Millimolar

N_2	Nitrogen
NeoR	Neomycin resistance
nm	Nanometer
O_2	Oxygen
PBS	Phosphate buffered saline
PCR	Polymerase chain reaction
PEXEL	Plasmodium Export Element
Pf	*Plasmodium falciparum*
PFA	Paraformaldehyde
PfEXP1	*Plasmodium falciparum* Exported protein 1
PfEXP2	*Plasmodium falciparum* Exported protein 2
PfALD	*Plasmodium falciparum* Aldolase
PIC	Protease inhibitor cocktail
PMSF	Phenylmethylsulfonyl fluoride
PNEP	PEXEL-negative exported protein
PPM	parasite plasma membrane
PTEX	Plasmodium translocon of exported proteins
PV	parasitophorous vacuole
PVM	parasitophorous vacuolar membrane
RBC	Red blood cell
RNA	Ribonucleic acid
SDS	Sodium dodecyl sulfate
SP	Signal peptide
TAE	Tris acetate EDTA
TE	Tris EDTA
TEMED	N,N,N',N'-Tetramethyl ethylenediamine
TetR	Tetracycline repressor
TM	Transmembrane
TMD	Transmembrane domain
U	Unit
UTR	Untranslated region
V	Volt
WHO	World Health Organization
µg	Micrograms
µl	Microliter
µm	Micrometer
°C	Degree Celsius

1 Introduction

1.1 Malaria as a Global Disease

Malaria is a mosquito-borne parasitic disease caused by protozoa of the genus Plasmodium and transmitted to humans by infected female *Anopheles* mosquitoes. In 2023, malaria was estimated to cause 263 million cases and 597,000 deaths worldwide, an increase of approximately 11 million cases compared to 2022, which indicates stalled progress after previous gains (WHO-World health statistics 2024). The disease burden remains concentrated in the WHO African Region, with children under five years of age and pregnant women identified as the highest risk groups (WHO 2024; WHO 2025). In endemic regions, malaria imposes significant socioeconomic costs, including reduced productivity, increased strain on health systems, and long-term negative effects on child health and development (Gallup and Sachs 2001; Sachs and Malaney 2002). Malaria transmission primarily occurs in tropical and subtropical regions where ecological conditions support both vector survival and parasite development, resulting in a distinct global pattern of endemicity (Fig. 1) (Snow et al., 2017).

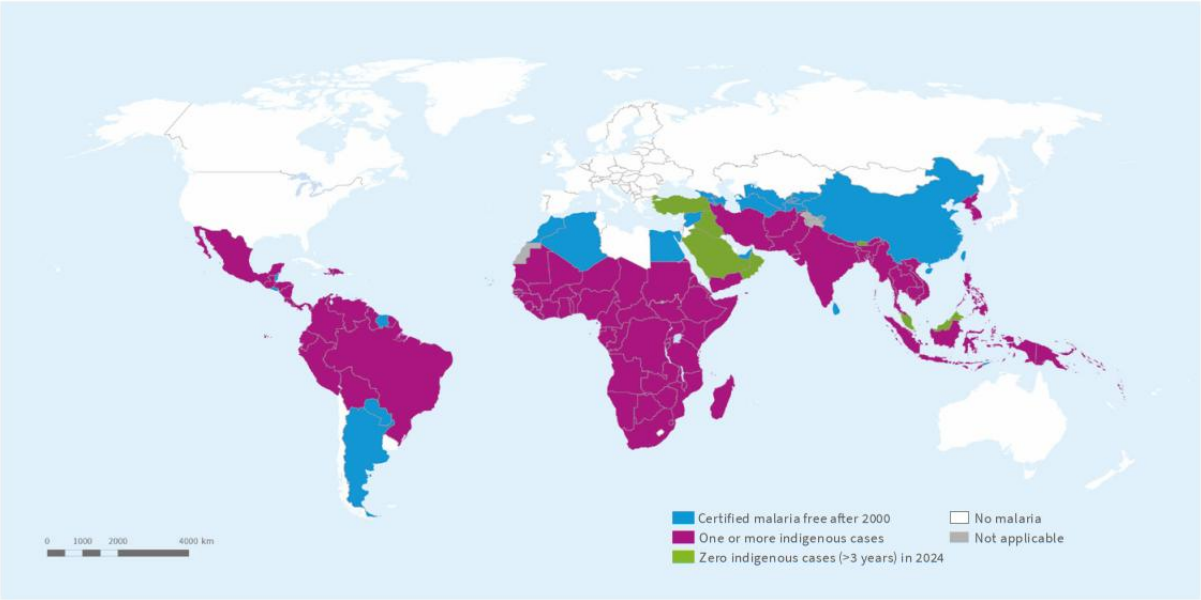

Fig. 1. Global distribution of malaria endemicity and elimination status.
Countries and areas with indigenous malaria cases in 2000 and their corresponding status by 2024. Areas with zero indigenous cases for at least three consecutive years are classified as having eliminated malaria.
Source: World Health Organization (WHO) database.

Despite large-scale implementation of insecticide-treated nets, indoor residual spraying, and improved access to effective antimalarial therapies, progress has been uneven and transmission continues in many areas (Bhatt et al. 2015; WHO 2024).

The emergence and spread of resistance represents a major threat to sustained malaria control. Rising insecticide resistance in *Anopheles* mosquitoes compromises vector control efforts, while declining parasite susceptibility to antimalarial drugs, including artemisinin-based combination therapies, threatens the effectiveness of current treatment regimens (Ashley et al. 2014; Dondorp et al. 2010).

1.2 Apicomplexa and the Exceptional Biology of *Plasmodium falciparum*

Malaria parasites belong to the phylum Apicomplexa, a diverse group of obligate intracellular eukaryotic pathogens that includes organisms of major medical and veterinary importance, such as *Toxoplasma gondii* and *Cryptosporidium* species (Adl et al., 2019). Members of this phylum share a conserved set of cellular and structural features that facilitate adaptation to an intracellular lifestyle (Cowman et al., 2017). Prominent among these are a highly specialized apical complex required for host-cell invasion and a relict non-photosynthetic plastid, the apicoplast, which supports essential metabolic pathways necessary for parasite survival (McFadden and Yeh, 2017). The principal morphological characteristics of apicomplexan parasites are illustrated in Fig. 2. The apical complex comprises several secretory organelles, including micronemes and rhoptries, which discharge their contents during host-cell invasion and promote establishment of the intracellular niche (Bradley and Sibley, 2007; Cova et al., 2022). The composition and spatial organization of these structures vary between species and life-cycle stages, and their presence represents a defining hallmark of the phylum and underpins the invasive capacity of apicomplexan parasites (Gubbels and Duraisingh, 2012; Katris et al., 2014).

Within the genus *Plasmodium*, several species are capable of infecting humans. Traditionally, five species were recognized as the principal causative agents of human malaria: *Plasmodium falciparum, Plasmodium vivax, Plasmodium malariae, Plasmodium ovale* and *Plasmodium knowlesi* (Antinori et al., 2012; Mace et al., 2022). Among them, *P. falciparum* is responsible for the most severe form of malaria and accounts for the majority of malaria-associated mortality worldwide (WHO report 2025; UK Health Security Agency (UKHSA) annual report 2024). The high virulence of *P. falciparum* is primarily due to its ability to reach high parasite densities in the bloodstream and alter infected erythrocytes. These changes promote sequestration of parasitized red blood cells in the microvasculature, enabling the parasite to evade splenic clearance and directly contribute to disease pathology (Miller et al., 2002; Buffet et al., 2011; Cowman et al., 2016).

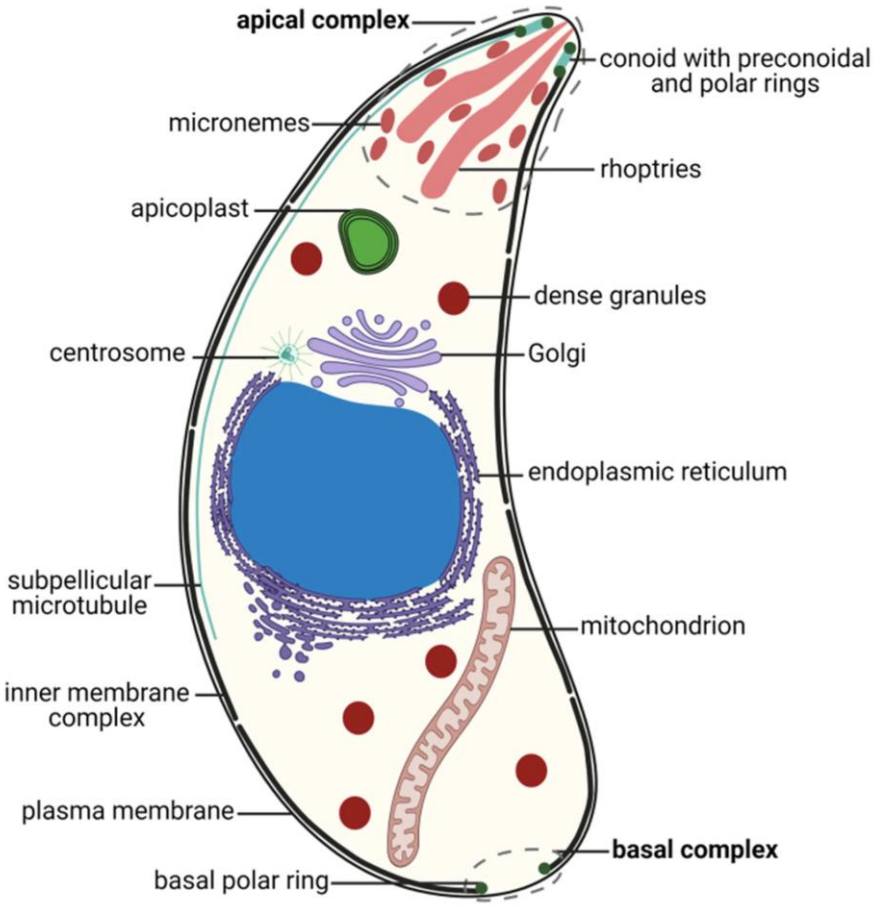

Fig. 2. Conserved cellular characteristics of apicomplexan parasites.

A schematic of a *Toxoplasma gondii* tachyzoite illustrates the major organelles and structural features characteristic of apicomplexan parasites. The apical complex, which includes secretory organelles such as micronemes and rhoptries, is indicated along with the basal complex. The apicoplast, a non-photosynthetic plastid surrounded by four membranes, is depicted as a distinct organelle essential for parasite metabolism. Although *T. gondii* is used for illustration, these features are broadly conserved across the phylum Apicomplexa, including *Plasmodium falciparum*. Source: Adapted from Delgado, Nolasco, et al. (2022)

Together, these characteristics distinguish *P. falciparum* from other human malaria parasites and underscore its central importance as a model organism for investigating the molecular and cellular mechanisms underlying malaria pathogenesis (Cowman et al., 2016; White, 2022).

1.2.1 The *Plasmodium falciparum* Life Cycle

The life cycle of *Plasmodium falciparum* alternates between the mosquito vector and the human host, encompassing several morphologically and metabolically distinct stages (Cowman et al., 2016) (Fig. 3). In humans, infection begins when sporozoites are transmitted during a blood meal by an infected female *Anopheles* mosquito.

After transmission, sporozoites quickly migrate to the liver, invade hepatocytes, and undergo extensive replication during the exoerythrocytic stage, producing thousands of merozoites from a single infected cell (Prudêncio et al., 2006). Once released into the bloodstream, merozoites invade erythrocytes and initiate the asexual intraerythrocytic developmental cycle. This cycle progresses through the ring, trophozoite, and schizont stages over approximately 48 hours (Bozdech et al., 2003; Cowman et al., 2016) (Fig. 3). At the end of each cycle, rupture of infected erythrocytes releases newly formed merozoites, leading to repeated rounds of invasion and parasite multiplication. This cyclical blood-stage replication causes the characteristic febrile episodes of malaria and is responsible for the major clinical manifestations of the disease (Miller et al., 2002).

In parallel with asexual replication, a subset of blood-stage parasites differentiates into sexual forms known as gametocytes. While these stages do not directly contribute to disease pathology, they are ingested by mosquitoes during subsequent blood meals and complete the parasite life cycle within the vector (Meibalan and Marti, 2017).

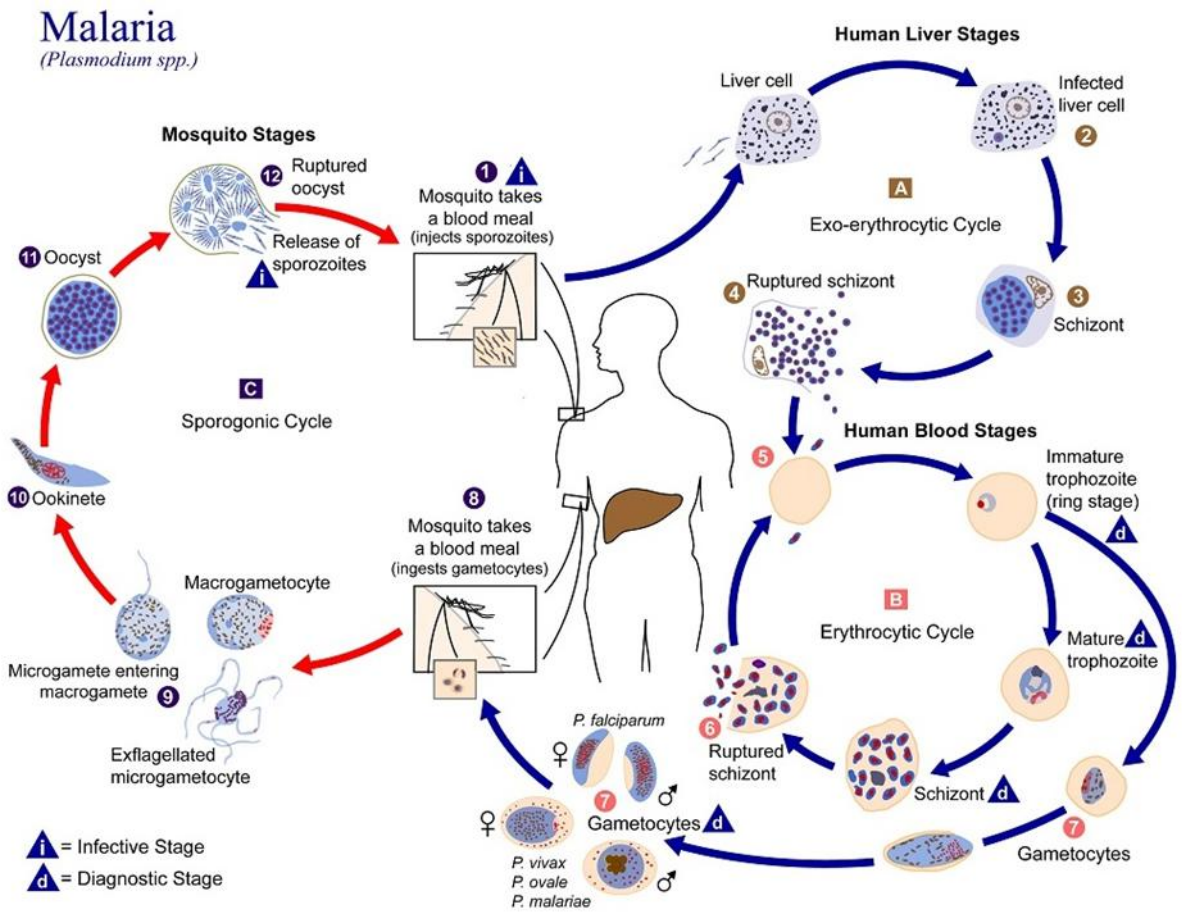

Fig. 3. Life cycle of *Plasmodium falciparum*

The parasite alternates between the human host and the *Anopheles* mosquito vector. After transmission during a blood meal, sporozoites infect hepatocytes and undergo exoerythrocytic replication, producing merozoites that invade erythrocytes. During the asexual blood stage, the parasite progresses through ring, trophozoite, and schizont stages, resulting in host-cell rupture and repeated replication cycles. A subset differentiates into sexual stages (gametocytes), which are ingested by mosquitoes during subsequent blood meals, thereby perpetuating the life cycle. Source: Centers for Disease Control and Prevention (CDC), DPDx; public domain image.

Throughout its life cycle, *P. falciparum* encounters a range of intracellular environments within both the human host and the mosquito vector. Transitions between these stages involve significant changes in parasite morphology, metabolism, and cellular organization. Investigating how the parasite adapts to these distinct intracellular niches is essential for elucidating the unique cell biology underlying malaria infection and transmission (Srivastava et al. 2016; Aly et al. 2009; Cowman et al. 2016).

1.2.2 The Asexual Blood Stage and the Infected Erythrocyte

Following erythrocyte invasion, *Plasmodium falciparum* initiates the asexual intraerythrocytic developmental cycle, which, as mentioned, is responsible for all clinical manifestations of malaria. (Fig. 4). During this stage, the parasite resides within a mature human red blood cell, a cell type that is specialized almost exclusively for oxygen transport (Haldar and Mohandas, 2009; Tilley et al., 2011; Pretini et al., 2019). Mature erythrocytes lack a nucleus, mitochondria, endoplasmic reticulum, Golgi apparatus, and endosomal system, and are therefore incapable of transcription, translation, or vesicular trafficking. As a consequence, they are unable to actively respond to intracellular infection or to support complex intracellular processes. For *P. falciparum*, survival within this highly restricted cellular environment requires extensive parasite-driven remodeling of the host cell (Maier et al. 2009; Moras et al. 2017). Immediately after invasion, the parasite is enclosed within a parasitophorous vacuole, a membrane-bound compartment that separates it from the host cell cytosol. Throughout intraerythrocytic development, the parasite significantly alters the structural and functional properties of the infected erythrocyte. These changes include modifications in membrane rigidity and permeability, reorganization of the host cytoskeleton, and the emergence of parasite-derived membranous structures within the host cell cytoplasm (Maier et al., 2009).

In addition to structural remodeling, infected erythrocytes acquire new biological properties that are central to malaria pathogenesis. Parasite-induced modifications promote adhesion of infected cells to endothelial receptors in the microvasculature, a process termed cytoadherence. This mechanism enables parasites to evade splenic clearance but directly contributes to disease severity (Miller et al., 2002; Lee et al., 2019).

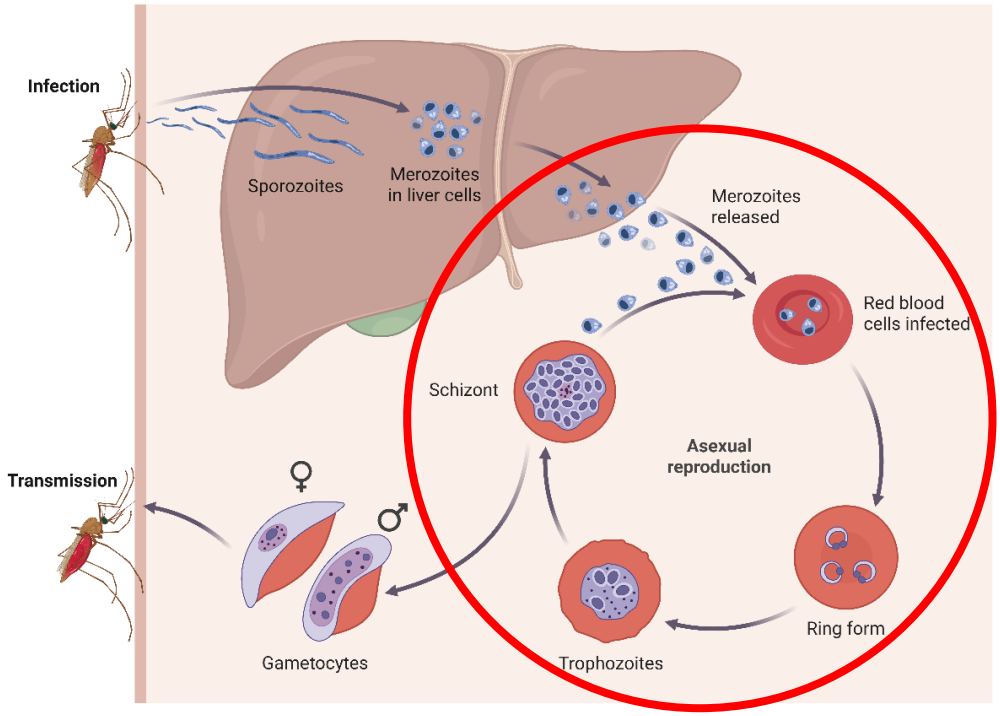

Fig. 4. Asexual blood-stage development of *Plasmodium falciparum*.
Schematic overview of the *P. falciparum* life cycle, highlighting the asexual intraerythrocytic developmental cycle (circled). After release from the liver, merozoites invade erythrocytes and progress through ring, trophozoite, and schizont stages, leading to host-cell rupture and repeated asexual replication. Sexual differentiation into gametocytes enables transmission to the mosquito vector. Adapted from BioRender.com

These changes also facilitate nutrient acquisition and support the parasite's rapid intracellular growth within an otherwise metabolically inert host cell. The extensive modification of the erythrocyte during the asexual blood stage highlights the exceptional degree of autonomy exhibited by *P. falciparum*. In the absence of host-derived biosynthetic and trafficking pathways, the parasite must establish and maintain its own systems to support intracellular survival. This unique host-parasite relationship makes the infected erythrocyte a highly specialized cellular environment and provides a powerful framework for investigating parasite-specific mechanisms of membrane organization, protein localization, and nutrient exchange (Przyborski and Lanzer 2005; Maier et al. 2009).

1.3 The Parasite Secretory Pathway

During the asexual blood stage, *Plasmodium falciparum* synthesizes a diverse array of proteins that require precise delivery to specific intracellular and host-associated compartments. Similar to other eukaryotes, protein biosynthesis begins on ribosomes within the parasite cytosol. Proteins targeted for secretion or membrane integration are co-translationally directed to the endoplasmic reticulum (ER) through N-terminal signal sequences and the signal recognition particle-Sec61 translocon system (Przyborski and Lanzer, 2005; Park and Rapoport, 2012).

After entering the ER, newly synthesized proteins undergo folding and initial quality control processes before advancing through the parasite's secretory pathway. Despite possessing a reduced and morphologically atypical endomembrane system, *P. falciparum* contains functional analogues of the Golgi apparatus and vesicle-mediated transport pathways. These structures facilitate the directional trafficking of proteins to downstream compartments (Struck et al. 2005; Florentin et al. 2020).

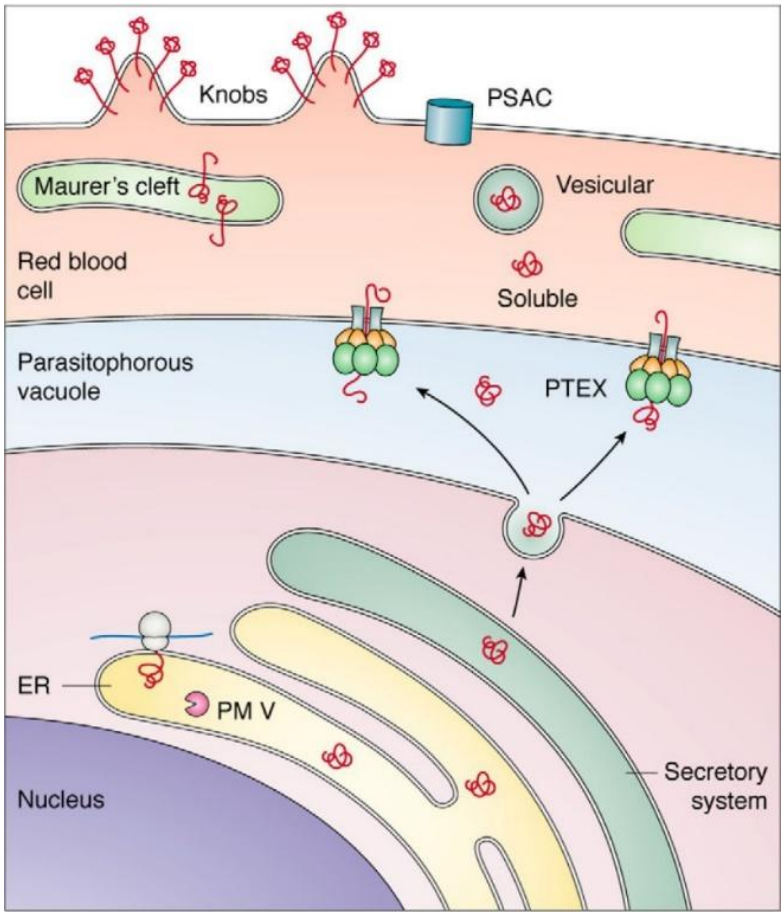

Fig. 5. Biosynthesis and trafficking of exported proteins in *Plasmodium falciparum*

Proteins destined for secretion or export are synthesized in the endoplasmic reticulum and traverse the parasite secretory system before reaching the parasitophorous vacuole. Exported proteins are translocated across the parasitophorous vacuole membrane via the PTEX complex and subsequently delivered to distinct compartments within the host erythrocyte, including the cytosol, Maurer's clefts, vesicular structures, and the erythrocyte membrane, where they contribute to host-cell modification.

Adapted from: (Nasamu *et al.*, 2020).

A major challenge for the parasite's secretory pathway is the accurate discrimination between proteins destined for different final destinations. These destinations include retention within the parasite, insertion into the parasite plasma membrane, delivery to the parasitophorous vacuole or its membrane, and export into the host erythrocyte. Accurate sorting is critical, as mislocalization of essential proteins can impair parasite viability and disrupt host-cell remodeling (Przyborski et al. 2016; Tonkin et al. 2006).

In contrast to nucleated host cells, mature erythrocytes lack intrinsic vesicular trafficking pathways. Therefore, all post-ER sorting decisions are determined and implemented exclusively by the parasite. This imposes significant functional demands on the parasite's secretory system, necessitating the integration of targeting signals, membrane translocation mechanisms, and regulated trafficking routes that function across multiple membrane barriers (Przyborski et al. 2016; Pretini et al. 2019). The presence of the parasitophorous vacuole and its membrane, which separate the parasite from the host cytosol, further increases the complexity of protein sorting. Proteins targeted for destinations beyond the parasite plasma membrane must cross this compartment in a tightly regulated manner. Understanding how the parasite secretory pathway interacts with the parasitophorous vacuole to achieve accurate protein localization remains a central question in *P. falciparum* cell biology and is essential for elucidating host-cell modification during blood-stage infection (De Koning-Ward et al., 2009; Mesén-Ramírez et al., 2019).

1.3.1 Parasitophorous Vacuolar Membrane as a Functional Compartment

During intraerythrocytic development, *Plasmodium falciparum* resides within the parasitophorous vacuole, a membrane-bound compartment that physically separates the parasite from the host erythrocyte cytosol. The membrane surrounding this compartment, the parasitophorous vacuolar membrane (PVM), is established during host-cell invasion (Fig. 6) and persists throughout the asexual blood stage (Geoghegan et al. 2021; Goldberg and Zimmerberg 2020). The PVM represents a unique biological membrane that differs fundamentally from classical eukaryotic organelle membranes. Although initially derived in part from the host erythrocyte plasma membrane, the PVM is rapidly modified following invasion and becomes enriched with parasite-encoded proteins. As a result, the PVM acquires properties that are not present in the host cell membrane and is functionally distinct from both the parasite plasma membrane and host-derived membranes (Lingelbach and Joiner 1998; Spielmann et al. 2006).

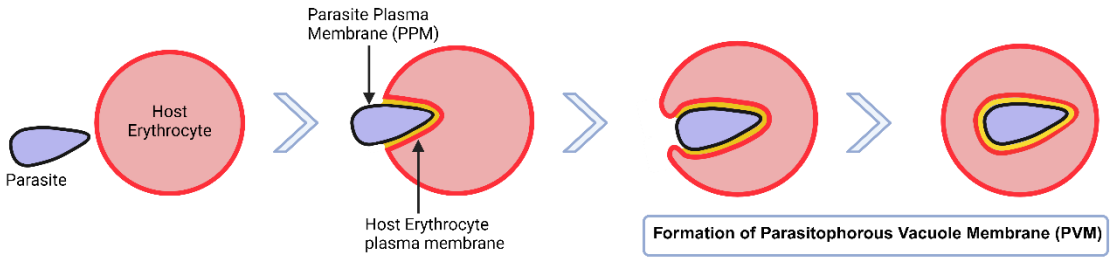

Fig. 6. Formation of the PVM during erythrocyte invasion

Schematic illustration depicting the establishment of the parasitophorous vacuole following invasion of an erythrocyte by *Plasmodium falciparum*. During invasion, the parasite becomes enveloped by host cell plasma membrane, giving rise to the parasitophorous vacuolar membrane (PVM). The PVM surrounds the intracellular parasite and separates it from the host erythrocyte cytosol, while the parasite plasma membrane (PPM) defines the parasite boundary within the vacuolar compartment. Created in BioRender.com

Functionally, the PVM acts as the principal interface between the parasite and its intracellular environment. It is required to maintain compartment integrity, shield the parasite from host-derived stresses, and facilitate the exchange of nutrients, metabolites, and proteins necessary for parasite growth. Achieving a balance between barrier function and permeability is critical for parasite survival within the highly restricted erythrocyte (Garten et al. 2018; Mesén-Ramírez et al. 2021). Unlike membranes of conventional intracellular organelles, the PVM functions without host-supported vesicular trafficking or membrane maintenance systems. Therefore, all aspects of PVM composition, organization, and function are actively established and maintained by the parasite. This requirement imposes exceptional demands on parasite-encoded proteins that localize to or operate at this membrane (Moras et al., 2017; Pretini et al., 2019). A growing body of evidence indicates that the PVM harbors a diverse set of resident parasite proteins with roles in membrane structure, transport, and host-parasite communication. Some of these proteins are involved in selective permeability to small solutes, while others appear to contribute to the organization or stability of the vacuolar compartment (Spielmann et al., 2006). However, the molecular mechanisms and signals governing the targeting, insertion, and function of PVM-resident proteins remain incompletely understood.

1.3.2 PVM-Resident Membrane Proteins

In addition to proteins that are exported into the host erythrocyte cytosol, the parasitophorous vacuolar membrane (PVM) contains a distinct set of parasite-encoded proteins that remain associated with or embedded within the membrane itself. These PVM-resident proteins are distinguished from exported proteins by their specific localization and functional roles, forming a separate class of molecules at the host-parasite interface (Przyborski et al. 2016; Spielmann et al. 2006). It is well established that the PVM is a specialized membrane enriched with parasite proteins, rather than merely a passive barrier between parasite and host cell. Later studies demonstrated that numerous parasite proteins are specifically targeted to the PVM and remain stably associated with this membrane throughout the asexual blood stage (Spielmann et al., 2003; Charpian and Przyborski, 2008). PVM-resident proteins localize to the parasite-host cell interface and support key processes required for intracellular survival (Spielmann et al. 2012). Genetic perturbation of several PVM proteins including PfEXP1, PfEXP2 and core components of a multi-molecular membrane machine called PTEX

(Plasmodium Translocon of Exported Proteins), causes severe growth defects or lethality, underscoring the functional importance of this membrane's proteins (Mesén-Ramírez et al., 2019). Despite their importance, the signals and mechanisms that govern targeting, membrane insertion, and retention of parasite proteins at the PVM remain poorly understood. In contrast to exported proteins, PVM-resident proteins do not consistently rely on canonical export signals, suggesting that distinct trafficking principles operate at this membrane.

Among known PVM-resident proteins, PfEXP1 is a conserved, well-studied example and therefore provides a suitable model for investigating protein trafficking to the parasitophorous vacuolar membrane.

1.3.3 PfEXP1 (*Plasmodium falciparum* Exported Protein 1)

PfEXP1 (*Plasmodium falciparum* Exported Protein 1) is a parasite-encoded membrane protein that localizes to the parasitophorous vacuolar membrane (PVM) during the asexual blood stage of *Plasmodium falciparum* (Hope et al., 1984, 1985). As one of the earliest identified PVM-associated parasite proteins, PfEXP1 has served as a widely used reference protein in studies of the PVM.

PfEXP1 is a small protein of approximately 23 kDa that is synthesized as an integral membrane protein. Early biochemical and cell-free translation studies demonstrated that PfEXP1 enters the parasite secretory pathway in a signal recognition particle-dependent manner and is co-translationally inserted into membranes via a hydrophobic stop-transfer sequence (Günther et al. 1991; Coppel et al. 1985). Biochemical extraction and protease accessibility experiments supported that PfEXP1 is an integral membrane protein rather than a peripheral membrane protein (Günther et al. 1991). PfEXP1 comprises an N-terminal signal peptide, a luminal region, a single transmembrane domain, and a C-terminal region (Fig. 7).

Fig. 7. Schematic domain organization of PfEXP1 used in this thesis

PfEXP1 is depicted with its N-terminal signal peptide, luminal region (residues 24–78), single transmembrane (TM) domain, and C-terminal region (residues 102–162). Residue numbering corresponds to the PfEXP1 sequence used for construct design in this study. Created in BioRender.com

Topology analyses indicate that PfEXP1 adopts a defined orientation at the PVM. The N-terminal domain faces the lumen of the parasitophorous vacuole, whereas the C-terminal domain is exposed to the host erythrocyte cytosol, consistent with asymmetric insertion into the PVM (Günther et al. 1991; Ansorge et al. 1997). Genetic studies indicate that PfEXP1 is essential for blood-stage parasite survival.

Conditional depletion of PfEXP1 leads to severe growth defects and parasite death *in vitro*, demonstrating that PfEXP1 is required during intraerythrocytic development (Mesén-Ramírez et al. 2019). In addition, PfEXP1 has been linked to functional properties of the PVM. Reduced PfEXP1 levels were reported to impair permeability across the PVM, consistent with a contribution to normal membrane function at the host–parasite interface (Mesén-Ramírez et al. 2021).

Despite PfEXP1 being a well-established PVM marker and an essential parasite protein, the molecular signals that direct PfEXP1 specifically to the PVM, rather than to PPM, remain unresolved. Its single-pass membrane topology, restricted localization, and tractable size therefore make PfEXP1 a suitable model to dissect the targeting information that governs selective localization to the PVM.

1.4 Trafficking to the Parasitophorous Vacuolar Membrane

Proteins that localize to the parasitophorous vacuolar membrane (PVM) require selective sorting within the parasite secretory pathway to maintain stable association with this compartment. Unlike soluble exported proteins, which are translocated across the PVM into the host erythrocyte cytosol, PVM-resident membrane proteins remain embedded in the vacuolar membrane and thus follow a distinct trafficking route (Tonkin et al. 2006; Spielmann et al. 2012). Early biochemical studies demonstrated that PfEXP1 is synthesized as an integral membrane protein and enters the parasite secretory pathway co-translationally, adopting a defined membrane topology that is preserved at the PVM (Günther et al. 1991). However, these studies did not clarify the mechanisms or signals by which PfEXP1 is selectively delivered to the PVM instead of remaining at the parasite plasma membrane or entering export pathways.

Several conceptual models have been proposed to explain how integral membrane proteins reach the PVM after departing the parasite plasma membrane. These models include vesicle-mediated transport, chaperone-assisted membrane extraction and reinsertion, and mechanisms involving the vacuolar translocon PTEX (Tribensky et al. 2017). Fig. 8 provides a schematic overview of these proposed trafficking routes.

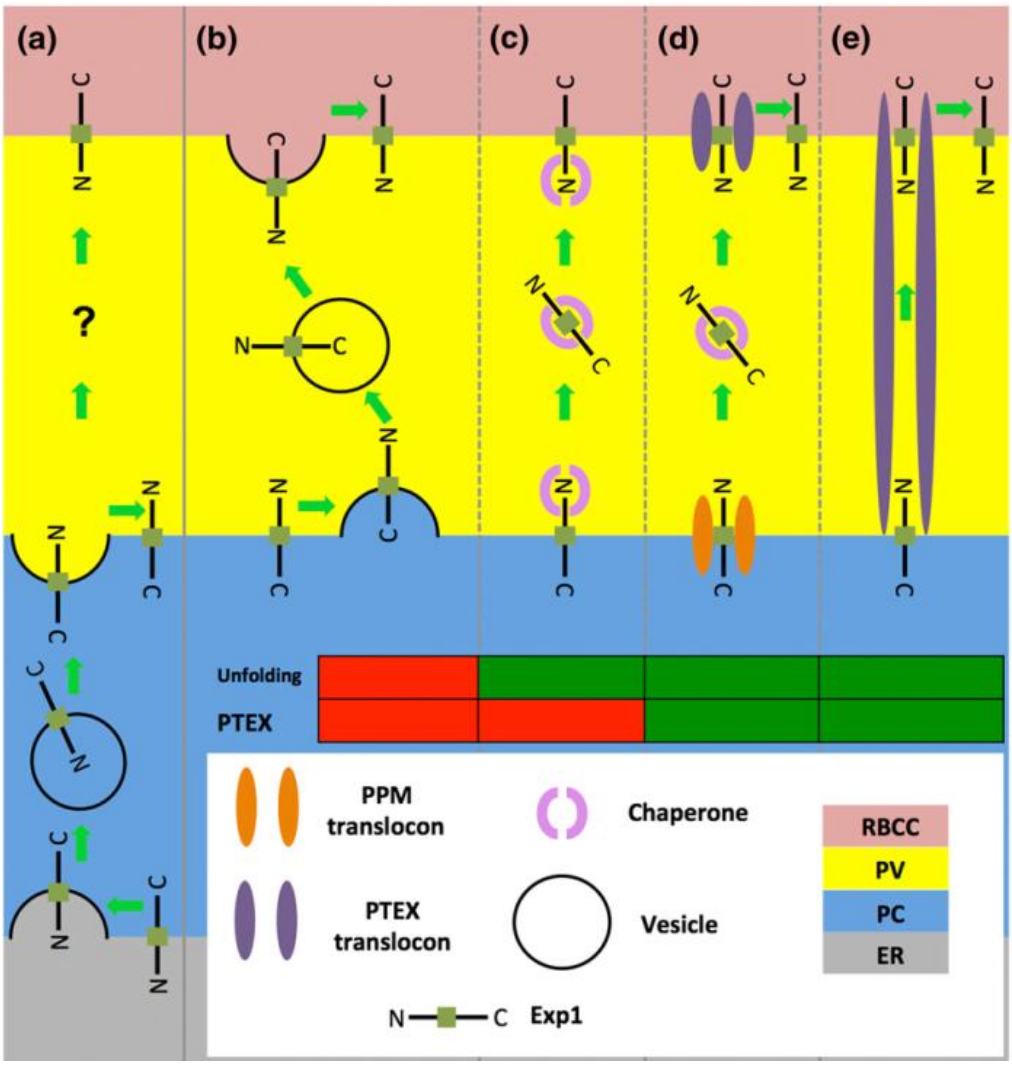

Fig. 8. Proposed models for trafficking of PfEXP1 to the PVM

Schematic overview of conceptual models proposed to explain how the integral membrane protein PfEXP1 might reach the parasitophorous vacuolar membrane (PVM) after synthesis and insertion into the parasite plasma membrane. The models include vesicle-mediated transport, chaperone-assisted membrane extraction and reinsertion, and mechanisms involving the vacuolar translocon PTEX. All models preserve the experimentally established topology of PfEXP1 at the PVM. The figure summarizes hypotheses addressed experimentally by Tribensky et al. (2017) and illustrates constraints on potential trafficking pathways rather than a confirmed mechanism.

Tribensky et al. (2017) made a significant advance by systematically analyzing PfEXP1 trafficking during the asexual blood stage. Through the use of reporter constructs, protein-folding interference, and genetic inactivation of essential PTEX components, the study demonstrated that PfEXP1 reaches and inserts into the PVM independently of both protein unfolding and the PTEX translocon. Inactivation of PTEX components effectively blocked export of soluble parasite proteins into the host cell but did not affect PfEXP1 localization, indicating that PfEXP1 does not utilize the canonical protein export pathway.

Together, these findings establish that PfEXP1 trafficking to the PVM is mechanistically distinct from protein export and exclude several previously proposed transport mechanisms. Furthermore, they demonstrate that delivery to the PVM cannot be explained solely by known export machinery. The mechanisms by which PfEXP1 is recognized as a PVM-destined protein and the molecular features that mediate its selective localization within the parasite secretory system, therefore, remain unresolved.

This unresolved question underscores the importance of identifying the targeting information that governs selective localization to the parasitophorous vacuolar membrane and forms the conceptual basis for the following section.

1.5 Determinants of PfEXP1 Localization at the PVM

The selective localization of membrane proteins to the parasitophorous vacuolar membrane (PVM) suggests that the parasite secretory system can distinguish between proteins destined for the parasite plasma membrane, the PVM, or export beyond the vacuole. In the case of PfEXP1, experimental evidence demonstrates that this discrimination is not accounted for by known export machinery or general trafficking mechanisms alone (Tribensky et al., 2017).

Therefore, selective PVM localization likely depends on targeting information intrinsic to the protein. However, the specific nature of this information remains undetermined. It is unclear whether PVM targeting relies on a discrete linear sequence motif, structural features, properties of the transmembrane domain, contributions from flanking regions, or a combination of these elements. Determining which regions of PfEXP1 are necessary for trafficking from the PPM to the PVM remains a central unresolved question. Identifying this targeting information offers a direct experimental strategy to elucidate how membrane proteins are selectively recognized within the parasite secretory system and serves as the conceptual foundation for the construct-based analyses presented in this thesis.

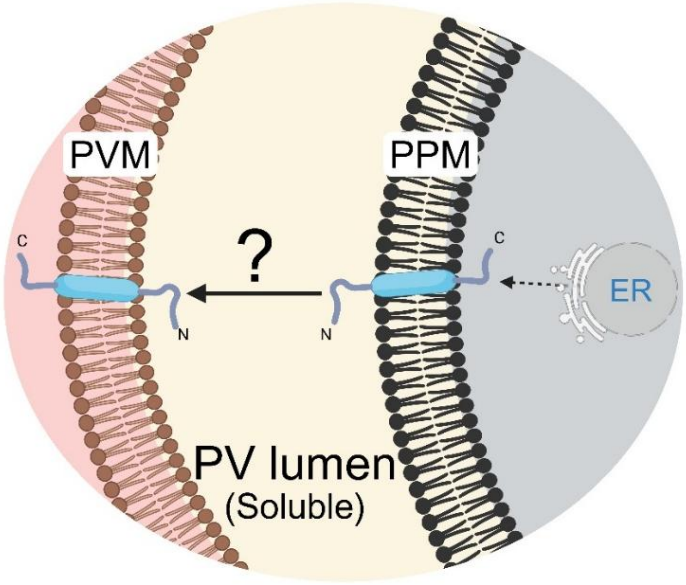

Fig. 9. Schematic representation of PfEXP1 localization at the PVM

The schematic depicts a *Plasmodium falciparum*-infected erythrocyte, highlighting the parasite, the parasitophorous vacuole (PV), and the parasitophorous vacuolar membrane (PVM). PfEXP1 is illustrated as an integral membrane protein at the PVM with defined topology. The question mark denotes that the molecular determinants responsible for the selective targeting and insertion of PfEXP1 at the PVM are currently unknown. Created in BioRender.com

1.6 Aims of this Thesis

Plasmodium falciparum develops within a parasitophorous vacuole membrane (PVM) inside the host erythrocyte. The PVM provides a platform for many parasite proteins that function at this boundary. How PVM proteins are selectively targeted to the PVM, rather than retained at the parasite plasma membrane (PPM), remains incompletely understood. In particular, it is unclear whether PVM targeting depends primarily on the luminal N-terminus, the cytosolic C-terminus, or the identity and properties of the transmembrane domain (TMD). Therefore, the overall aim of this study was to identify the PfEXP1 sequence determinants that govern selective targeting to the parasitophorous vacuolar membrane during the asexual blood stage of *P. falciparum*. To address this aim, PfEXP1 variant proteins were expressed from plasmids and localization was assessed by immunofluorescence microscopy in trophozoite and schizont stages, using compartment markers to interpret peripheral localization.

This study aimed to determine whether PfEXP1 localization depends on N-terminal and/or C-terminal sequence information by analyzing progressive truncations at each end. Additionally, we tested whether the transmembrane domain is the primary determinant of PfEXP1 PVM targeting by comparing the native domain with alternative PVM transmembrane helices, including a PVM-derived helix (PfETRAMP10.1) and synthetic helices.

2 Results

2.1 Design, generation and validation of the PfEXP1 construct panel

To investigate which regions of PfEXP1 may contribute to transport to the parasitophorous vacuolar membrane (PVM), a panel of PfEXP1-derived constructs was generated and expressed episomally in *Plasmodium falciparum* 3D7. Because PfEXP1 is essential during blood-stage development, the endogenous gene was not altered in this study. Instead, all constructs were expressed from the episomal vector pVP1 (Fig. 11), which is based on pARL2 (Fig. 10) and carries the PfEXP1 promoter. This allowed analysis of mutant PfEXP1 variants without interfering with endogenous PfEXP1 function.

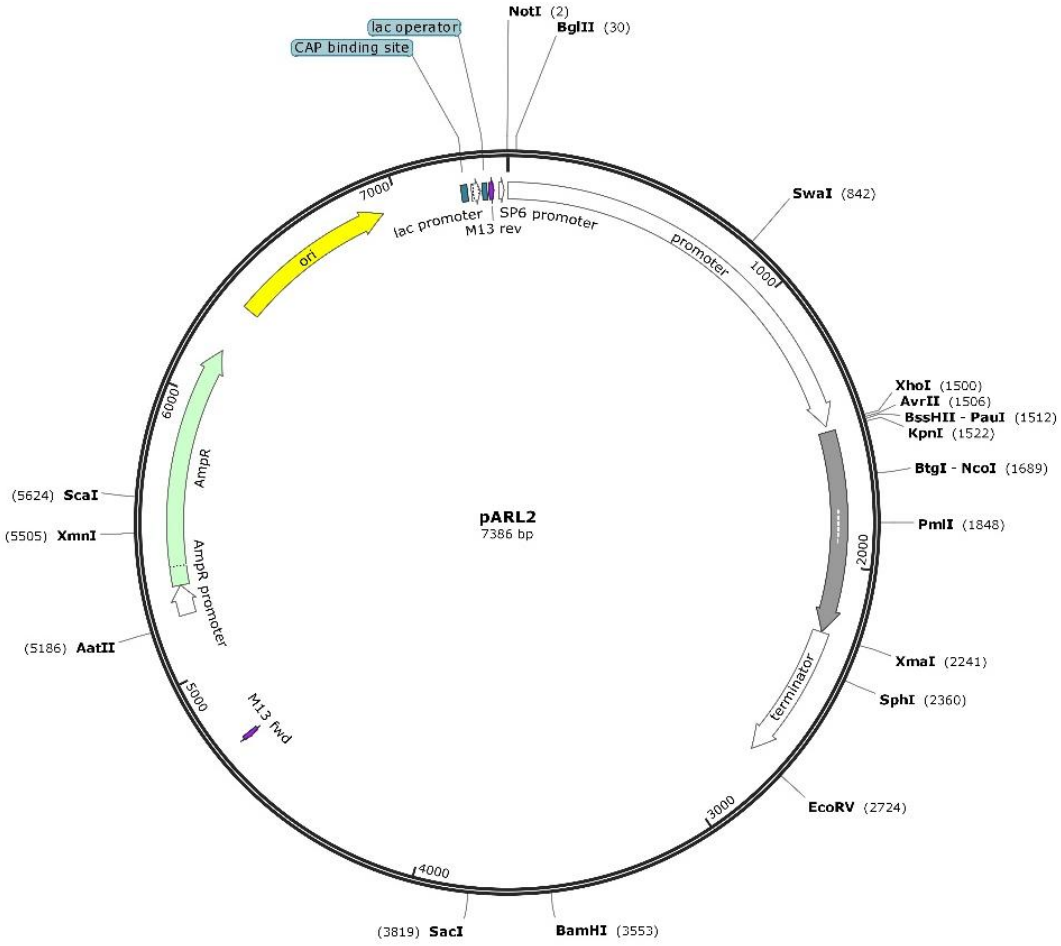

Fig. 10. Parental pARL2 plasmid backbone used for generation of pVP1

Circular plasmid map of the parental pARL2 vector used as the starting backbone for generation of pVP1. Major vector elements and restriction sites are indicated. (Created with SnapGene)

Fig. 11. pVP1 episomal expression vector carrying the PfEXP1 promoter

Circular plasmid map of pVP1, derived from pARL2 after insertion of the PfEXP1 5′ regulatory region. All PfEXP1-derived constructs analyzed in this study were cloned into pVP1 for episomal expression in *Plasmodium falciparum* 3D7. (Created with SnapGene)

2.1.1 First design phase: deletion constructs

In an earlier phase of the project, a deletion construct series was generated to test whether sequence information in the N-terminus or C-terminus contributes to PfEXP1 transport to the PVM. For this reason, progressive truncation constructs were designed in both directions, while leaving the signal peptide and the transmembrane domain intact. The idea was that if removal of one terminal region changed localization, this could indicate that this region contains information important for correct trafficking. PfEXP1 was amplified from 3D7-derived RNA/cDNA, and a 3×HA tag was introduced by overlap-extension PCR either N-terminal or C-terminal to the transmembrane domain, generating two tagged PfEXP1 templates. These tagged templates were then used to generate the truncation series (Fig. 12). In one series, 10, 20, 30, 40 or 50 amino acids were removed from the C-terminus (Fig. 13); in the other series, the same stepwise deletions were made from the N-terminus (Fig. 14). In each case, the HA tag was placed on the opposite side so that the truncated constructs could still be detected by immunofluorescence assay and Western blot. In this way, the first construct series (group 1) covered both terminal regions of PfEXP1 outside the signal peptide and transmembrane domain.

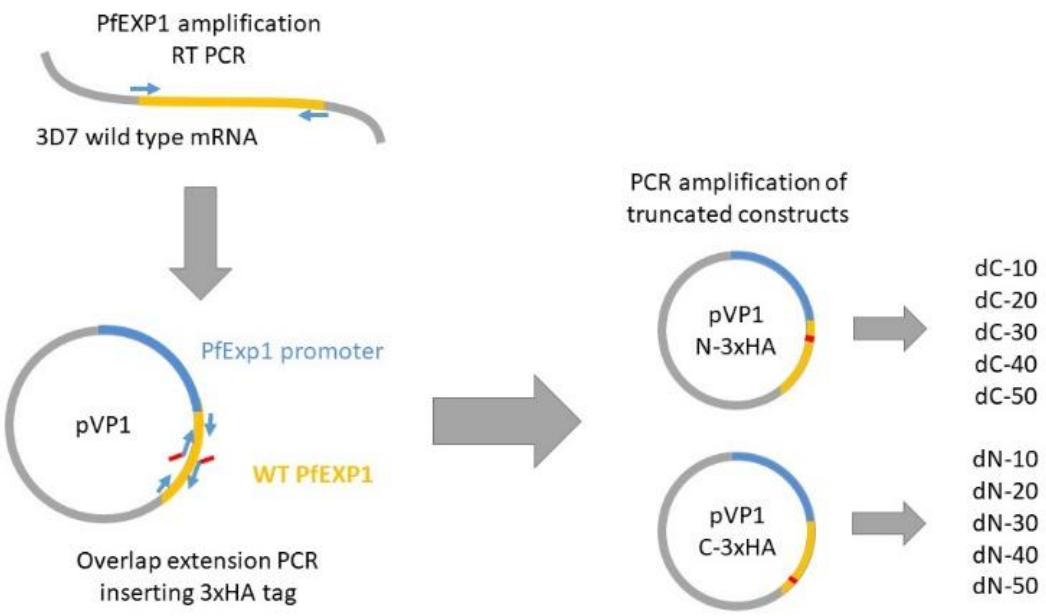

Fig. 12. Cloning workflow for generation of the PfEXP1 deletion construct series

Schematic overview of the cloning strategy used to generate the deletion constructs. PfEXP1 was amplified from 3D7 wild-type RNA/cDNA and cloned into pVP1. A 3×HA tag was introduced by overlap-extension PCR either N-terminal or C-terminal to the transmembrane domain to generate tagged PfEXP1 templates, which were then used for PCR amplification of the progressive truncation constructs.

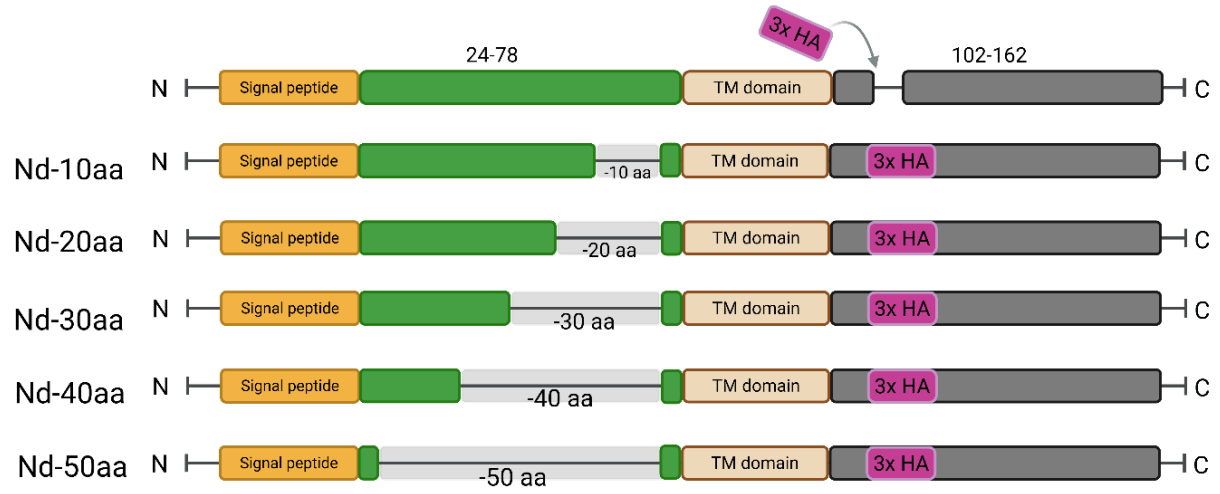

Fig. 13. Schematic overview of the N-terminal PfEXP1 deletion construct series

Construct design of the N-terminal deletion variants ΔN10 to ΔN50. Progressive deletions of 10-50 amino acids were introduced from the N-terminus while leaving the signal peptide and transmembrane domain intact. A C-terminal 3×HA tag was used to allow detection of the truncated proteins by immunofluorescence assay and Western blot. Created in BioRender.com

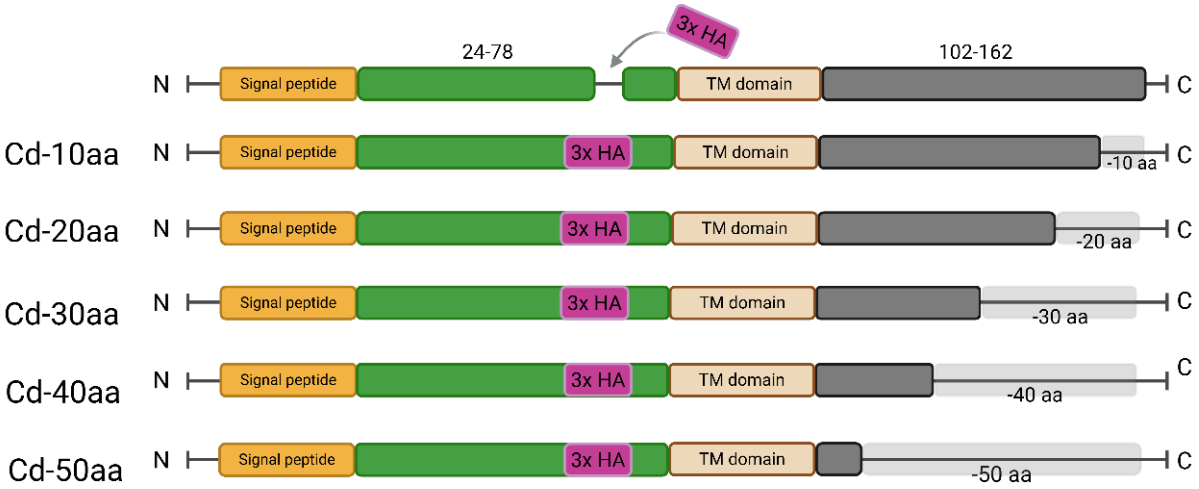

Fig. 14. Schematic overview of the C-terminal PfEXP1 deletion construct series

Construct design of the C-terminal deletion variants ΔC10 to ΔC50. Progressive deletions of 10–50 amino acids were introduced from the C-terminus while leaving the signal peptide and transmembrane domain intact. An N-terminal 3×HA tag was used to allow detection of the truncated proteins by immunofluorescence assay and Western blot. Created in BioRender.com

2.1.2 Second design phase: transmembrane-domain constructs

In the second phase, the focus shifted to the transmembrane domain, to test whether PfEXP1 localization to the PVM depends mainly on the identity of this region. For this purpose, a second construct series was designed in a more standardized format. The endogenous signal peptide (SP) of PfEXP1 was retained, because it is cleaved during co-translational insertion into the ER and was therefore not expected to affect the later transport step being tested here. Except for the signal peptide and the transmembrane domain, the remaining body of the protein was replaced by linker sequences and tags. This was done to exclude signals not related to the transmembrane domain, to avoid complicated structure, and to keep the constructs similar in overall length and organization to PfEXP1. The use of flexible linkers was based on linker designs with described flexibility in fusion-protein studies (Huang et al., 2016). Within this shared design, different transmembrane-domain settings were compared. One construct contained the native PfEXP1 transmembrane domain (group 2). A second contained the transmembrane domain of PfETRAMP10.1 (group 3). PfETRAMP10.1 was chosen because PfEXP1 belongs to the ETRAMP family, and PfETRAMP10.1 represented the most suitable related member with the best similarity of the transmembrane-domain sequence among the candidates considered. The third set used synthetic hydrophobic helices, named 23L and 23LG (group 4). The synthetic constructs were included to test whether hydrophobicity alone might be sufficient for PVM localization. 23L consisted of a poly-leucine helix, based on previously used synthetic transmembrane-domain designs (Grau et al., 2017). 23LG was based on the same idea but included glycine residues in reference to the glycine-containing motifs present in the native PfEXP1 transmembrane domain. In particular, the native PfEXP1 transmembrane domain contains GXXG motifs, which were of interest because such motifs have been discussed in relation to transmembrane-domain function and helix–helix interactions (Zhao et al., 2012; Teese and Langosch, 2015; Bugge et al., 2016) (Fig. 15).

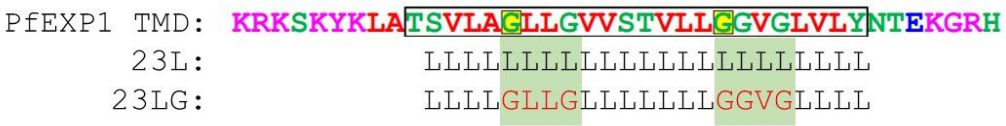

Fig. 15. Artificial TMD modules compared in the standardized construct series

Schematic comparison of the transmembrane-domain modules used in the standardized construct series. The native PfEXP1 transmembrane domain was compared with the synthetic hydrophobic helices 23L and 23LG. The 23LG construct includes glycine residues in reference to the glycine-containing motifs present in the native PfEXP1 transmembrane domain.

For this second construct series (group 2, 3 and 4), a 3×HA tag was placed at the N-terminus and a 3×Ty tag at the C-terminus. Different tags were used on the two sides to preserve flexibility for later N- or C-terminal modifications (Fig. 16).

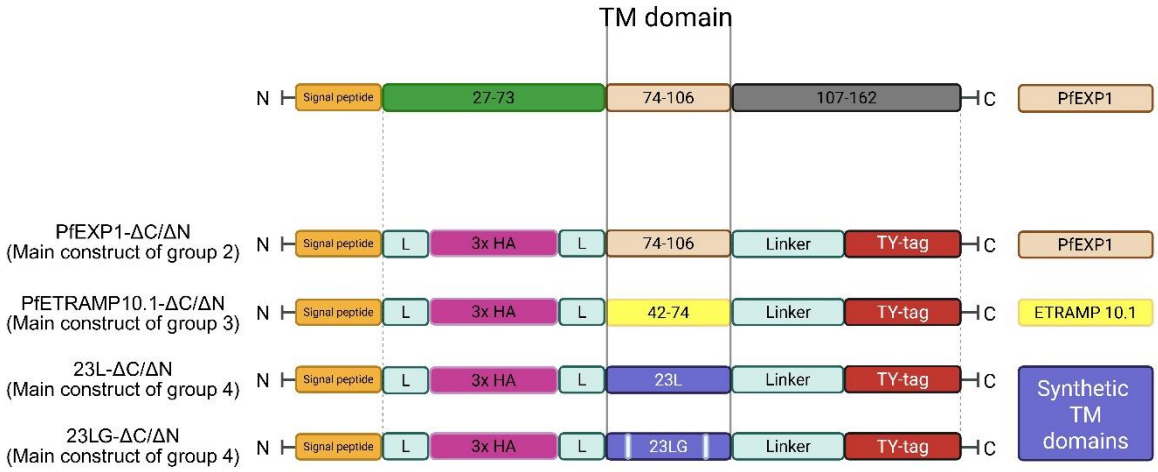

Fig. 16. Standardized architecture of the transmembrane-domain construct panel

Schematic overview of the common construct design used for Groups 2-4. The endogenous PfEXP1 signal peptide was retained, whereas the remaining body of the protein was replaced by linker and tag modules surrounding the transmembrane domain. Within this shared format, constructs containing the native PfEXP1 transmembrane domain, the PfETRAMP10.1 transmembrane domain, or the synthetic 23L and 23LG helices were generated. A 3×HA tag was placed at the N-terminus and a 3×Ty tag at the C-terminus. Created in BioRender.com

Control constructs containing the endogenous PfEXP1 N- and/or C-terminal regions were included within the same design framework to assess whether the added tags and linkers themselves affected localization (Fig. 17). If a construct still containing all endogenous PfEXP1 parts failed to localize correctly, then interpretation of the TMD-swap constructs would have to be made with caution.

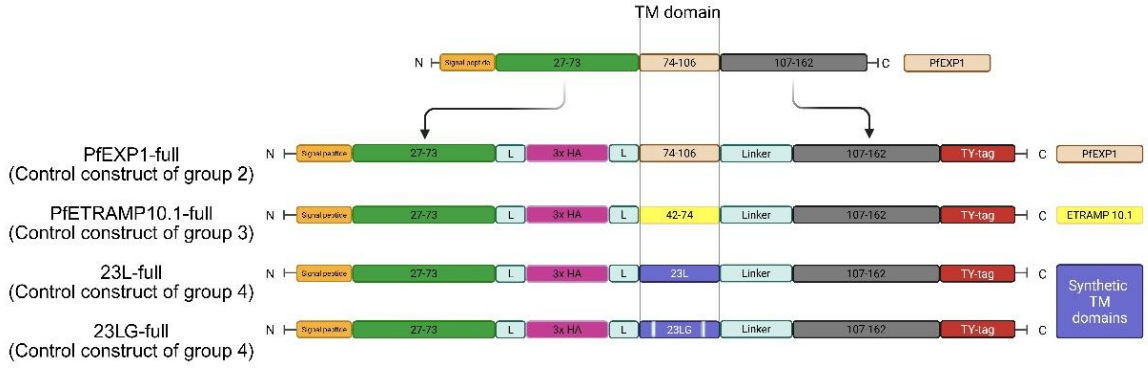

Fig. 17. Control constructs retaining endogenous PfEXP1 terminal regions

Control constructs used within the standardized design framework for Groups 2-4. These constructs retained endogenous PfEXP1 N- and/or C-terminal regions despite the presence of linkers and tags and were included to assess whether the modified construct architecture itself affected PfEXP1 localization. Created in BioRender.com

Taken together, the second phase was designed to ask whether the PfEXP1 transmembrane domain is itself a major determinant of PVM localization, and whether it can be replaced either by the transmembrane domain of another ETRAMP protein or by a synthetic hydrophobic helix.

2.1.3 Construct generation and cloning workflow

All final constructs used in this study were cloned into pVP1. PfEXP1 was amplified from 3D7-derived RNA/cDNA, and the tagged PfEXP1 templates were generated by overlap-extension PCR. These templates were then used for PCR amplification of the progressive N-terminal and C-terminal truncation constructs, which were subsequently cloned into the pVP1 episomal expression vector.

For the second construct series, a more modular cloning strategy was used. A synthetic construct containing PfEXP1-derived N- and C-terminal regions, linker sequences, detection tags, and multiple restriction sites was used as the basis for the transmembrane-domain panel. This synthetic construct was first cloned into pVP1, after which different transmembrane domains were inserted and the corresponding N- and C-terminal variants were generated. In this way, the full-length, ΔN, ΔC and ΔC/ΔN versions of the PfEXP1, PfETRAMP10.1, 23L and 23LG constructs were produced within the same overall cloning framework.

To facilitate this workflow, multiple restriction sites were incorporated into the construct design (Fig. 18). These were arranged around the transmembrane-domain region and the surrounding modules so that the transmembrane-domain segment could be exchanged and the N- and/or C-terminal parts could be removed where required. This modular setup made systematic generation of the construct panel possible.

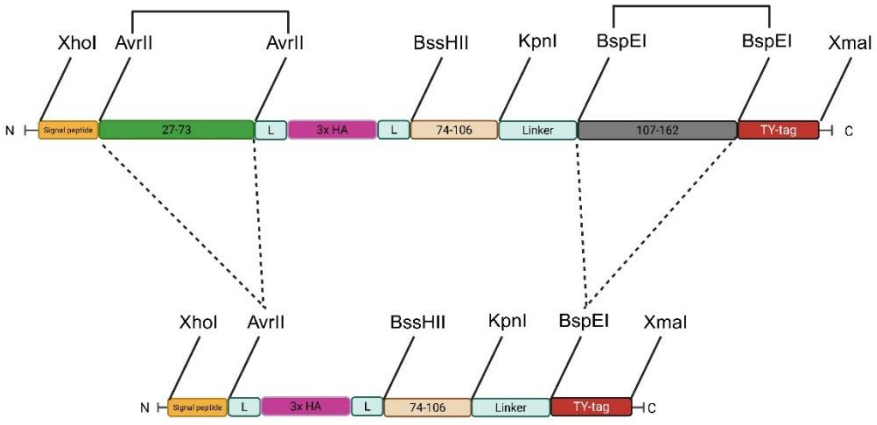

Fig. 18. Modular cloning strategy for TMD exchange and terminal deletions

Schematic representation of the modular cloning design used for the transmembrane-domain construct panel. Multiple restriction sites were positioned around the transmembrane-domain region and adjacent modules to allow exchange of transmembrane domains and generation of the corresponding ΔN, ΔC and ΔC/ΔN variants within the same overall construct framework

After cloning, all final plasmid constructs were confirmed by restriction analysis and were additionally checked by sequencing before transfection. Plasmid preparations were then made for parasite transfection.

2.1.4 Generation and validation of transfectant parasite lines

After plasmid preparation, all constructs were introduced into *P. falciparum* 3D7 by electroporation. For transfection, 150 µg plasmid DNA was precipitated and used for each transfection. The transfected parasites were then returned to culture and maintained under WR99210 selection to enrich parasite populations carrying the episomal plasmids.

Following transfection, genomic DNA (gDNA) was extracted from the parasite populations, and PCR was used to confirm the presence of episomal plasmid material in the transfectants. This provided confirmation that the intended construct had been introduced into the parasite line. As a second validation step, expression of the recombinant proteins was examined by Western blot. This was used to confirm that the construct was not only present in the transfected parasite population but also expressed at the protein level before further analysis. After confirmation of construct presence and expression, the parasite lines were analyzed by immunofluorescence assay. In trophozoites, localization of the recombinant proteins was assessed relative to PfEXP2 as a PVM marker. In schizonts, PfMSP1 was used instead in order to visualize the parasite plasma membrane (PPM) and merozoite outlines separately from the PVM. The generated parasite lines were then used for the localization and fractionation analyses described in the following sections.

2.2 Overview (cell lines)

Throughout this chapter, results are presented in a uniform format to facilitate comparison between variants. For each cell line, the corresponding figure first shows a schematic of the episomal construct design, followed by immunofluorescence assays (IFA) in trophozoites and schizonts, and finally a biochemical fractionation assay used to assess protein solubility versus membrane integration.

Localization was evaluated by IFA in two developmental stages. In trophozoites, the PVM is in very close apposition to the parasite plasma membrane (PPM), and fluorescence microscopy cannot reliably distinguish PVM and PPM signals based on the staining pattern alone. Therefore, each variant was analyzed in schizonts in addition to trophozoites. In trophozoites, samples were co-stained with anti-PfEXP2 as a PVM marker. In schizonts, samples were co-stained with anti-PfMSP1 as a PPM/merozoite membrane marker; in this stage, the PPM appears as multiple small circles surrounding individual merozoites, whereas the PVM appears as one large circle surrounding the entire schizont (O'Donnell et al., 2001).

In the fractionation assay, SN denotes the soluble supernatant fraction, C the carbonate-extractable fraction, and P the final pellet fraction. SN therefore indicates soluble proteins, C weak or high-pH-sensitive membrane association, and P stably membrane-integrated proteins. For PfEXP1-derived constructs, enrichment in P would be expected.

For clarity, the PfEXP1 construct panel was organized into four design classes, summarized in Table 1.

Table 1. Overview of the PfEXP1 construct panel analyzed in this study

Group	Construct name
Group 1: C- and N-terminal deletion constructs	ΔC-10aa
	ΔC-20aa
	ΔC-30aa
	ΔC-40aa
	ΔC-50aa
	ΔN-10aa
	ΔN-20aa
	ΔN-30aa
	ΔN-40aa
	ΔN-50aa
Group 2: PfEXP1 reference constructs (Control constructs)	PfEXP1-full
	PfEXP1-ΔC
	PfEXP1-ΔN
	PfEXP1-ΔC/ΔN
Group 3: PfETRAMP10.1 TMD swapping constructs	PfETRAMP10.1-full
	PfETRAMP10.1-ΔC
	PfETRAMP10.1-ΔN
	PfETRAMP10.1-ΔC/ΔN
Group 4: Synthetic TMD swapping constructs	23L-full
	23L-ΔC
	23L-ΔN
	23L-ΔC/ΔN
	23LG-full
	23LG-ΔC
	23LG-ΔN
	23LG-ΔC/ΔN

2.3 Strategy for cell line selection and dataset completeness

In the terminal deletion series, we started by testing the largest deletions first. This method helped us see if removing the whole terminal region would change localization. If the largest deletion still showed a PVM-like pattern, we did not test smaller stepwise deletions, since further truncations were unlikely to add useful information for this screen.

In addition, the order of Results presentation reflects the underlying biological questions rather than the chronological order in which experiments were performed. As a consequence, not all planned variant series are complete. Biochemical fractionation was used as a quality-control step to verify that the expressed proteins behave as expected for membrane-associated species. During this control analysis, the main positive-control parasite line ("PfEXP1-full") used throughout the study was found to be predominantly soluble under the fractionation conditions. Following this observation, further work on the remaining planned variants was stopped. The implications of this finding are addressed in the Discussion.

2.4 Deletion constructs (Group 1)

2.4.1 C-terminal deletion screening: ΔC50

To test whether the C-terminal region contributes to PfEXP1 localization, the largest C-terminal deletion variant (ΔC50) was analyzed by immunofluorescence microscopy in trophozoites and schizonts and by biochemical fractionation. In trophozoites, the ΔC50 signal showed staining at the parasite boundary and overlapped with the PVM marker PfEXP2 in all analyzed images (n = 30 trophozoites) (Fig. 19, A). In mature schizonts, the ΔC50 signal displayed a PVM-like pattern in all analyzed images (n = 17 schizonts) (Fig. 19, B). Biochemical fractionation showed ΔC50 predominantly in the parasite pellet (P) fraction, consistent with behavior expected for a membrane-associated species under these conditions (Fig. 19, C).

A.

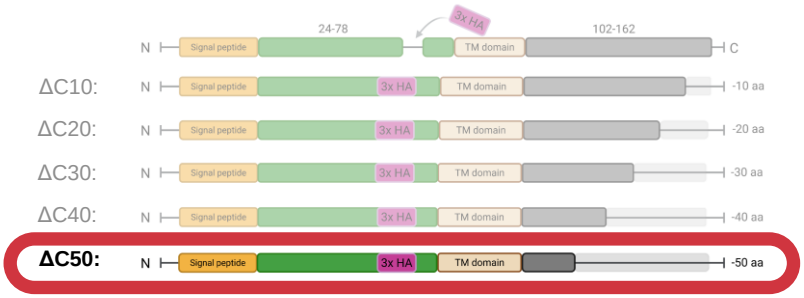
3x HA
24-78
102-162
N
Signal peptide
TM domain
C
ΔC10:
ΔC20:
ΔC30:
ΔC40:
ΔC50:
3x HA
-10 aa
-20 aa
-30 aa
-40 aa
-50 aa

B.

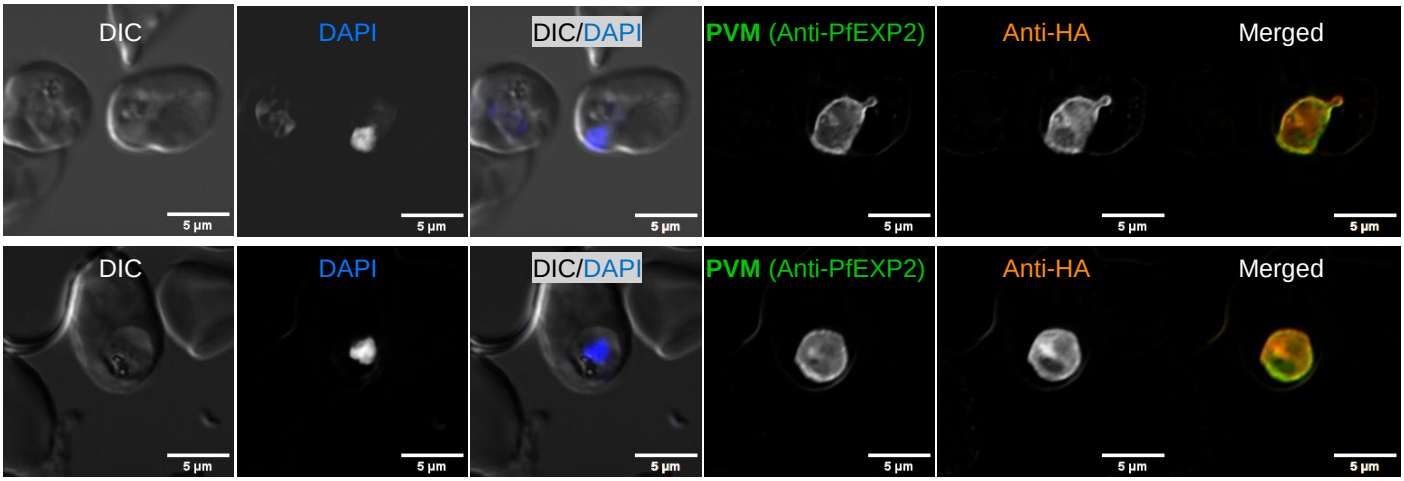
DIC
DAPI
DIC/DAPI
PVM (Anti-PfEXP2)
Anti-HA
Merged
5 µm

C.

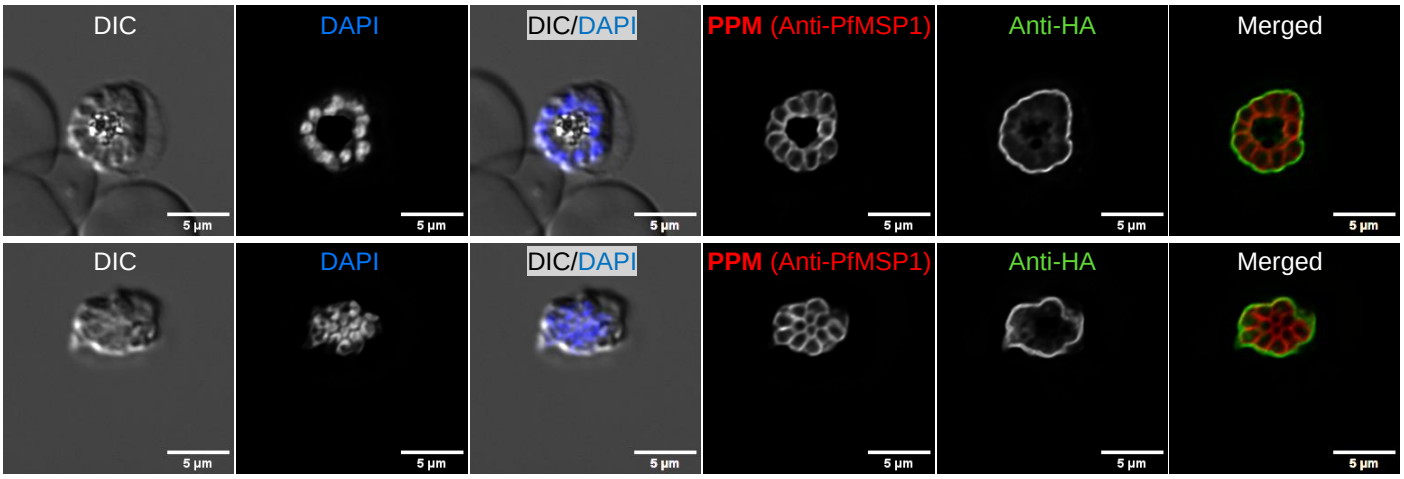
DIC
DAPI
DIC/DAPI
PPM (Anti-PfMSP1)
Anti-HA
Merged
5 µm

D.

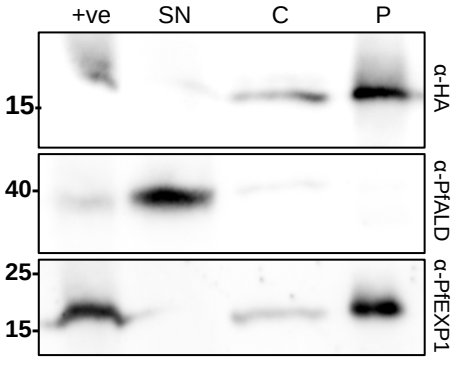
+ve
SN
C
P
15
40
25
15
α-HA
α-PfALD
α-PfEXP1

Fig. 19. IFA images and biochemical fractionation of the PfEXP1 ΔC50

(A) Schematic representation of the C-terminal deletion strategy; the red bar indicates the ΔC50 variant. Created in BioRender.com. **(B)** Trophozoite-stage immunofluorescence analysis of parasites expressing ΔC50, stained with anti-HA and anti-PfEXP2 (PVM marker). The HA tag signal shows staining at the parasite boundary and overlaps with PfEXP2 (n = 30 trophozoites). DAPI stains parasite nuclei; DIC shows parasite morphology. **(C)** Mature Schizont-stage immunofluorescence analysis of parasites expressing ΔC50, stained with anti-HA and anti-PfMSP1 (PPM marker). The HA signal shows a PVM-like pattern as a single large outline surrounding the schizont, distinct from PfMSP1 staining of individual merozoites (n = 17 schizonts). DAPI stains parasite nuclei; DIC shows parasite morphology. **(D)** Biochemical fractionation of ΔC50 analyzed by Western blot. Samples were loaded as input (+ve; full cell lysate), supernatant (SN; soluble proteins), carbonate (C; carbonate-extractable fraction), and pellet (P; insoluble/membrane fraction). Anti-HA detects ΔC50 predominantly in the pellet (P) fraction. PfALD serves as a soluble control; anti-PfEXP1 detects endogenous PfEXP1 as a membrane-integrated positive control.

Taken together, the microscopy and fractionation data indicate that ΔC50 is consistent with membrane-insertion behavior and PVM-like localization. These results are consistent with the C-terminal 50 amino acids not being essential for PfEXP1 localization in this assay; however, definitive conclusions about localization and topology are addressed in the Discussion section.

2.4.2 N-terminal deletion screening: ΔN50

To test whether the N-terminal region contributes to PfEXP1 targeting, the largest N-terminal deletion variant (ΔN50) was analyzed by immunofluorescence microscopy in trophozoites and schizonts. A total of 30 trophozoite images and 21 schizont images were evaluated. In trophozoites, the ΔN50-HA signal showed staining at the parasite boundary, and an overlap with the PVM marker PfEXP2 was observed in a subset of images (Fig. 20, B). In mature schizonts, the ΔN50 staining pattern was not interpretable. Across all analyzed images, the signal did not reproducibly form a clear ring around the schizont or did not show co-localization with the PPM marker PfMSP1 (Fig. 20, C).

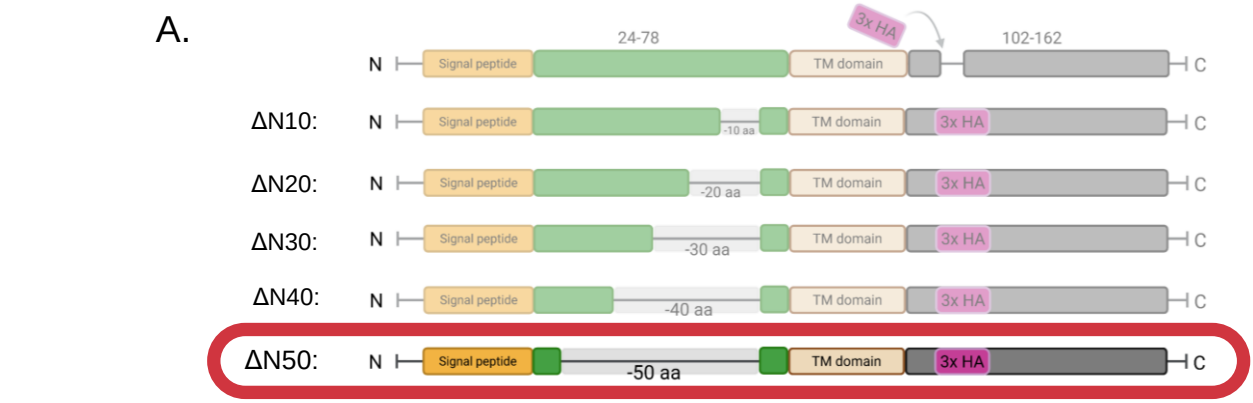

B.

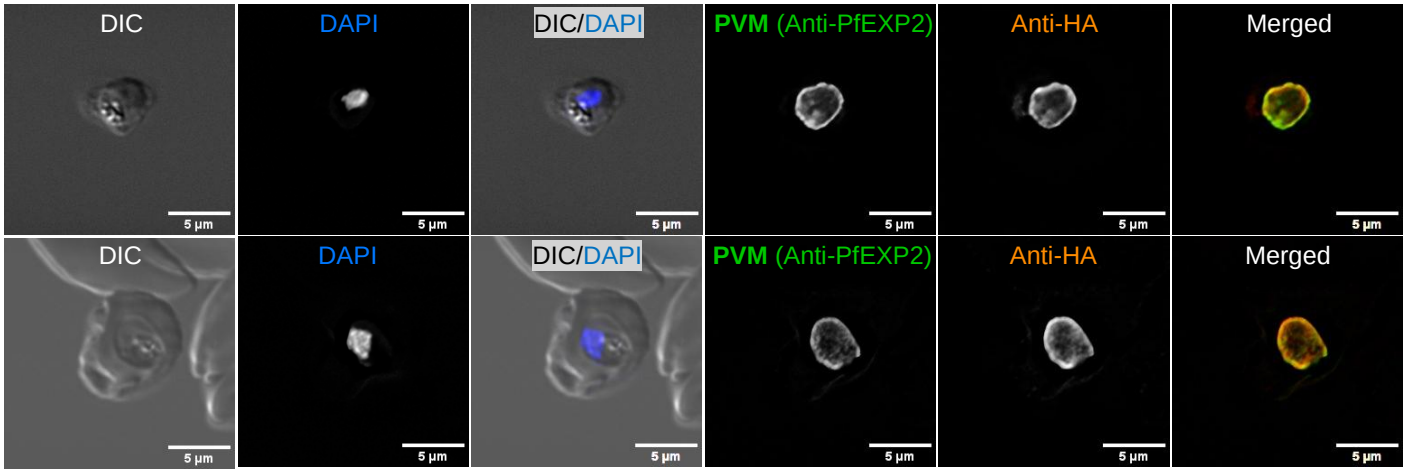

C.

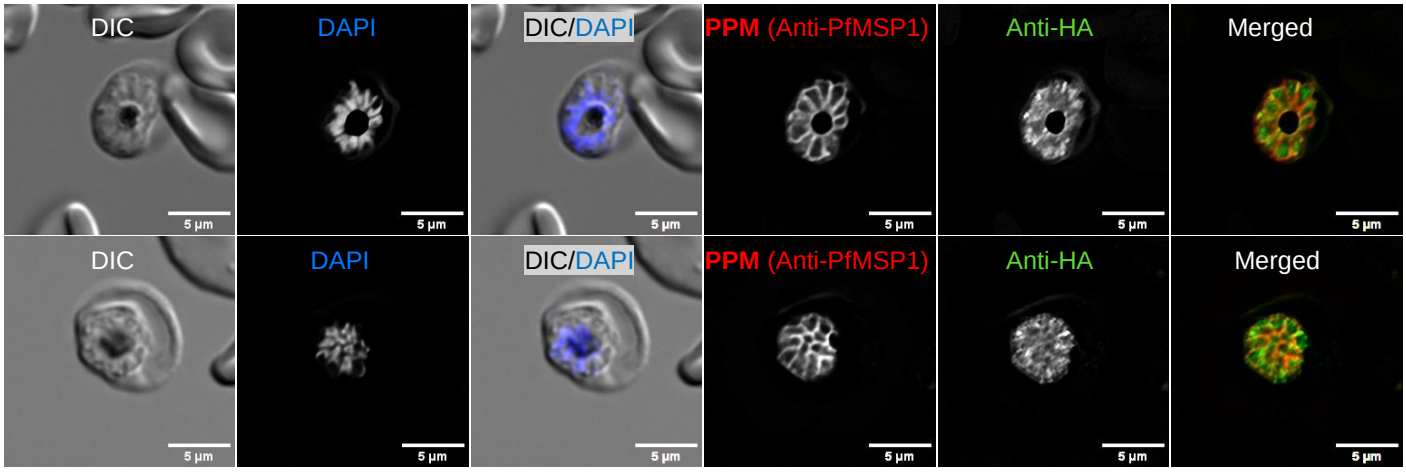

Fig. 20. IFA images of the ΔN50 PfEXP1 variant

(A) Schematic representation of the ΔN50 variant analyzed in this experiment. Created in BioRender.com. **(B)** Trophozoite-stage IFA of parasites expressing ΔN50, stained with anti-HA and anti-PfEXP2 (PVM marker; green). The HA signal is detected at the parasite boundary and lies close to the PfEXP2 signal. DAPI stains parasite nuclei; DIC shows parasite morphology. **(C)** Mature Schizont-stage IFA of parasites expressing ΔN50, stained with anti-HA and anti-PfMSP1 (PPM marker; red). The HA signal shows no consistent ring-like outline around the schizont and no clear overlap with the PfMSP1 signal in this dataset. DAPI stains parasite nuclei; DIC shows parasite morphology. n = 30 trophozoites; n = 21 schizonts.

2.4.3 N-terminal deletion screening: ΔN10

Based on the observations obtained for the largest N-terminal deletion (ΔN50), the N-10aa variant (ΔN10) was analyzed next, to test whether short N-terminal sequence elements contribute to PfEXP1 localization. Trophozoite-stage IFA showed a staining pattern similar to ΔN50, with overlap with the PVM marker PfEXP2 visible in most of the images (Fig. 21, B). A total of 22 mature schizont images were evaluated. In schizonts, the HA signal was not interpretable across the dataset and did not show a clear ring-like outline or overlap with PfMSP1 (Fig. 21, C). Biochemical fractionation was performed twice for the ΔN10 parasite line. In both experiments, HA was detected predominantly in the supernatant (SN) fraction (soluble) with additional signal in the carbonate (C) fraction and little to no signal in the pellet (Fig. 21, D). Since endogenous PfEXP1 is an integral membrane protein, this predominantly soluble/carbonate-extractable behavior, which does not support stable membrane integration of ΔN10, was unexpected and is discussed further in the Discussion.

A.

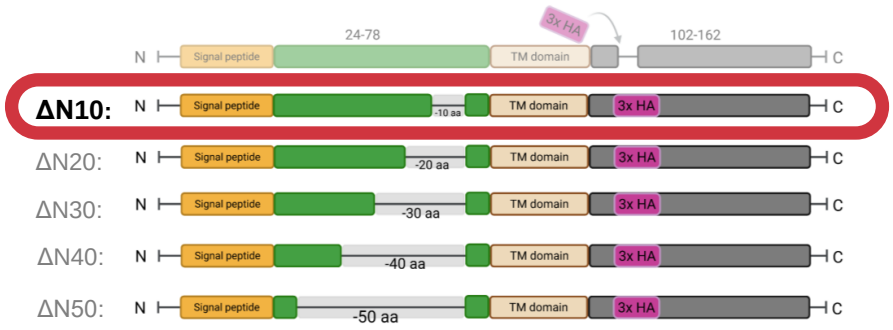
3x HA
24-78
102-162
N
Signal peptide
TM domain
C
ΔN10:
-10 aa
ΔN20:
-20 aa
ΔN30:
-30 aa
ΔN40:
-40 aa
ΔN50:
-50 aa
3x HA

B.

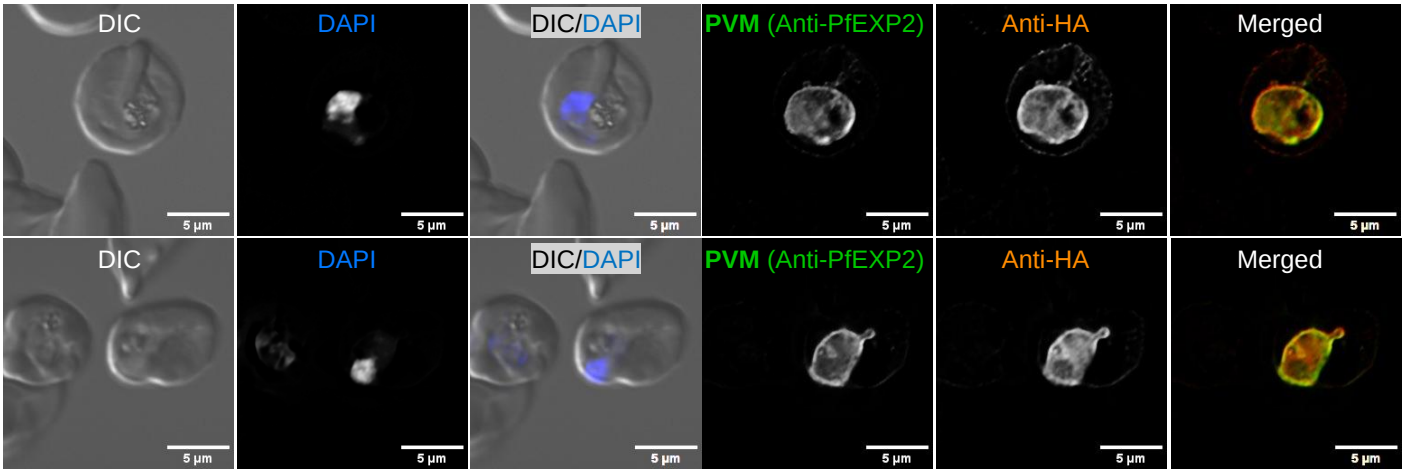
DIC
DAPI
DIC/DAPI
PVM (Anti-PfEXP2)
Anti-HA
Merged
5 µm

C.

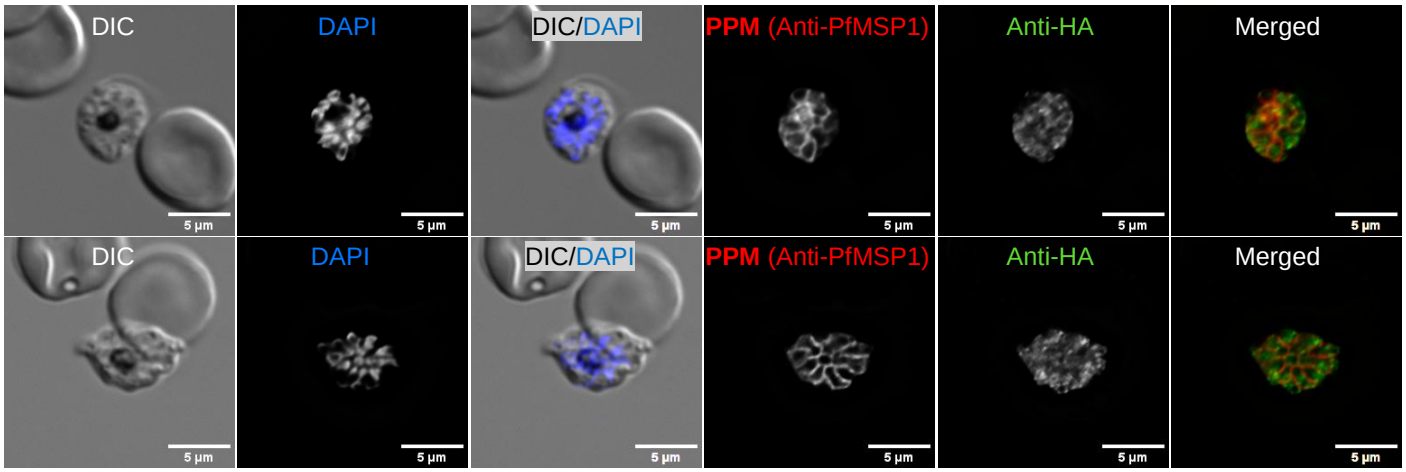
DIC
DAPI
DIC/DAPI
PPM (Anti-PfMSP1)
Anti-HA
Merged
5 µm

D.

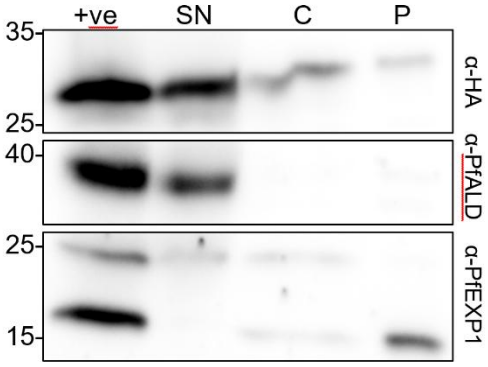
+ve
SN
C
P
35
25
40
25
15
α-HA
α-PfALD
α-PfEXP1

Fig. 21. IFA images and fractionation behavior of the ΔN10

(A) Schematic representation of the N-terminal deletion strategy; the red bar indicates the ΔN10 variant. Created in BioRender.com. **(B)** Trophozoite-stage immunofluorescence analysis of parasites expressing ΔN10, co-stained with anti-HA and anti-PfEXP2 (PVM marker). The HA signal is detected at the parasite boundary and lies close to the PfEXP2 signal. DAPI stains parasite nuclei; DIC shows parasite morphology. **(C)** Mature Schizont-stage immunofluorescence analysis of parasites expressing ΔN10, co-stained with anti-HA and anti-PfMSP1 (PPM marker). Across this dataset (n = 22 schizonts), the HA signal shows no consistent ring-like outline and no clear overlap with the PfMSP1 signal. DAPI stains parasite nuclei; DIC shows parasite morphology. **(D)** Biochemical fractionation of the ΔN10 parasite line analyzed by Western blot. Fractionation was performed twice; one representative experiment is shown. Samples were loaded as input (+ve; full cell lysate), supernatant (SN), carbonate (C), and pellet (P) fractions. The +ve (input) lane confirms expression and antibody reactivity in the unfractionated cell lysate. Anti-HA detects ΔN10 predominantly in SN with additional signal in C. PfALD serves as a soluble control; anti-PfEXP1 detects endogenous PfEXP1 as a membrane-integrated positive control.

2.5 Control constructs (Group 2)

2.5.1 PfEXP1-full

PfEXP1-full served as the primary architectural control for this study because it was intended to test whether the tagged and linker-containing expression format used across the TMD-swapping constructs still allowed full-length PfEXP1 to behave as an appropriate reference construct and integrate into the membrane. In trophozoites, the PfEXP1-full signal was detected at the parasite periphery and showed overlap with the PVM marker PfEXP2 (Fig. 22, B). Since fluorescence microscopy cannot reliably distinguish PVM and PPM signals in trophozoites, PfEXP1-full was additionally analyzed in schizonts. Across 21 mature schizont images, the staining pattern was generally not interpretable, and only a subset of images showed weak or partial overlap with the PPM marker PfMSP1 (Fig. 22, C). Biochemical fractionation was performed four times for PfEXP1-full. In each repeat, PfEXP1-full was detected predominantly in the supernatant (SN) and/or carbonate (C) fractions, with little to no signal in the pellet (P) fraction (Fig. 22, D). This indicates that PfEXP1-full does not behave as a stably membrane-integrated species under these conditions. These data are consistent with PfEXP1-full being largely soluble in the parasitophorous vacuole (PV) lumen.

A.

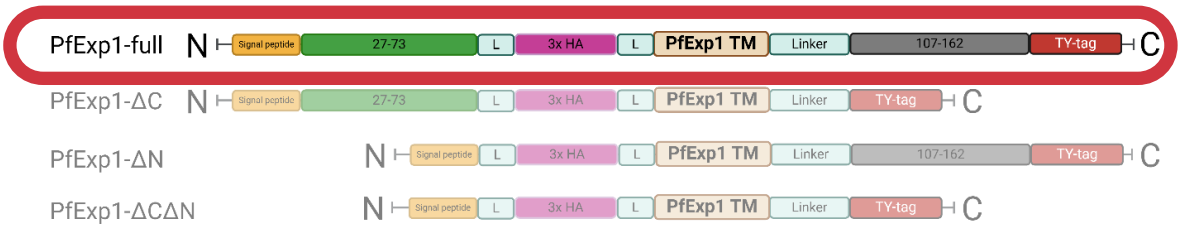
PfExp1-full
N
Signal peptide
27-73
L
3x HA
L
PfExp1 TM
Linker
107-162
TY-tag
C
PfExp1-ΔC
PfExp1-ΔN
PfExp1-ΔCΔN

B.

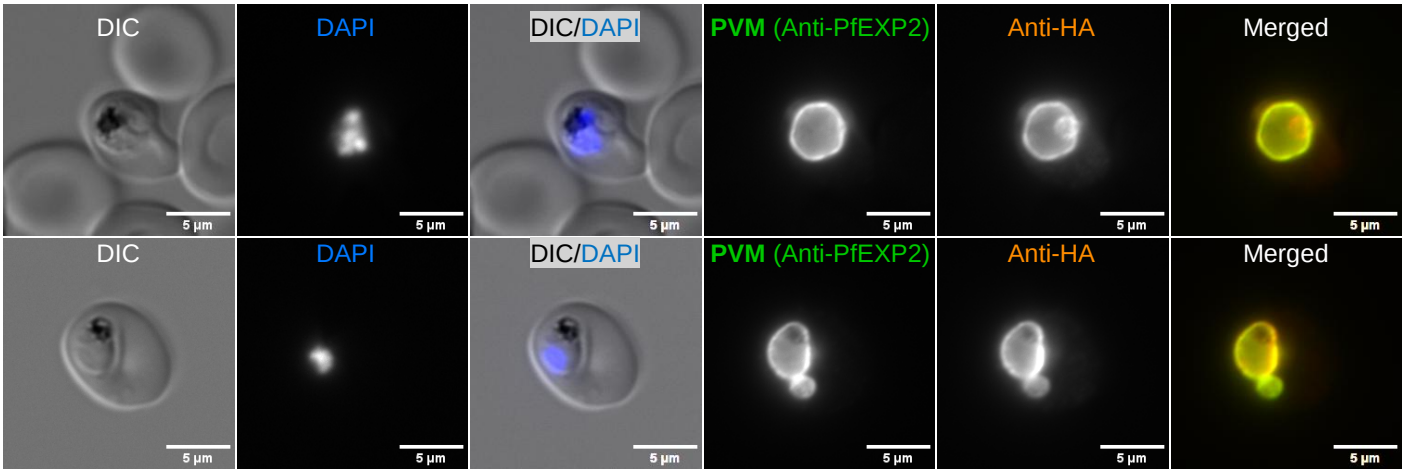
DIC
DAPI
DIC/DAPI
PVM (Anti-PfEXP2)
Anti-HA
Merged
5 µm

C.

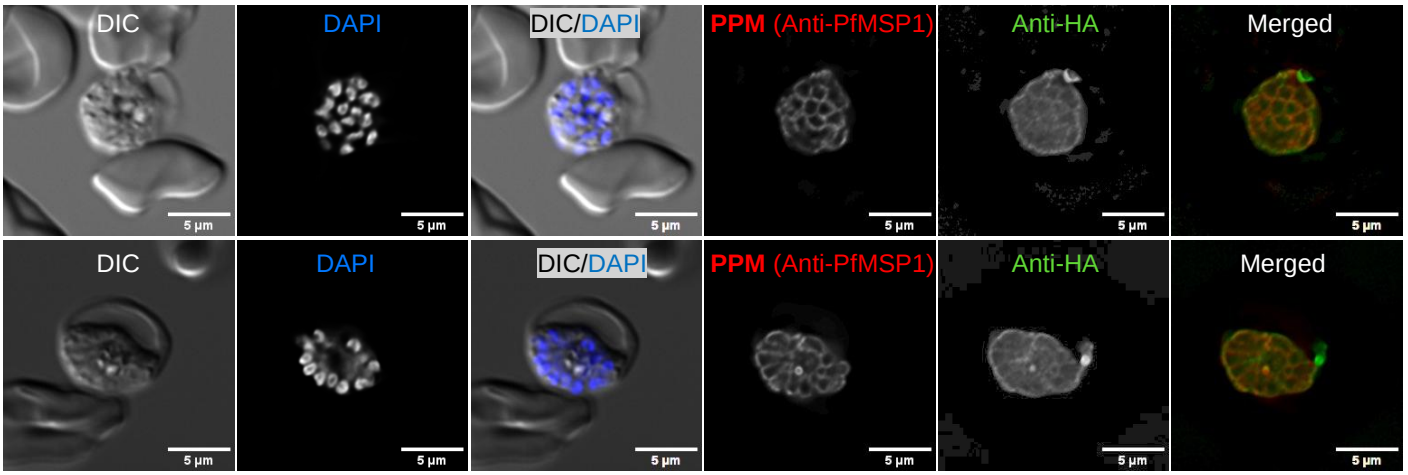
DIC
DAPI
DIC/DAPI
PPM (Anti-PfMSP1)
Anti-HA
Merged
5 µm

D.

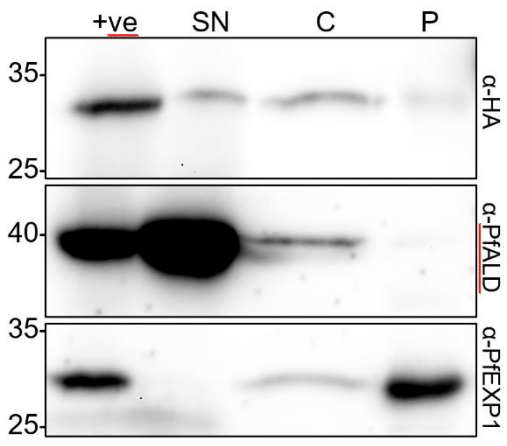
+ve
SN
C
P
35
25
40
35
25
α-HA
α-PfALD
α-PfEXP1

Fig. 22. IFA images and solubility of the PfEXP1-full reference plasmid (Group 2)

(A) Schematic representation of the PfEXP1-full plasmid design. Created in BioRender.com. **(B)** Trophozoite-stage immunofluorescence analysis of parasites expressing PfEXP1-full, co-stained with anti-HA and anti-PfEXP2 (PVM marker). The PfEXP1-full signal is detected at the parasite boundary and lies close to the PfEXP2 signal. DAPI stains parasite nuclei; DIC shows parasite morphology. **(C)** Mature Schizont-stage immunofluorescence analysis of parasites expressing PfEXP1-full, co-stained with anti-HA and PfMSP1 (PPM marker). Across this dataset (n = 21 schizonts), the PfEXP1-full signal shows no consistent ring-like outline and no clear overlap with the PfMSP1 signal. DAPI stains parasite nuclei; DIC shows parasite morphology. **(D)** Biochemical fractionation of PfEXP1-full analyzed by Western blot. Samples were loaded as input (+ve; full cell lysate), supernatant (SN), carbonate (C), and parasite pellet (P) fractions. Fractionation was performed 4 times; one representative experiment is shown. PfEXP1-full is detected predominantly in SN and/or C, with little to no signal in P. PfALD serves as a soluble control; anti-PfEXP1 detects endogenous PfEXP1 as a membrane-integrated positive control.

2.5.2 PfEXP1-ΔC

PfEXP1-ΔC, like PfEXP1-full, was included as a control to confirm that the tagged expression format used in this study does not, by itself, disrupt construct localization to PVM. Since the C-terminal region was not expected to be required for targeting, PfEXP1-ΔC was expected to show PVM-like localization even in the presence of the additional tag and linker elements. In trophozoites, PfEXP1-ΔC showed staining at the parasite boundary and overlapped with the PVM marker PfEXP2 in all analyzed images (n = 25 trophozoites) (Fig. 23, B). In schizonts, a PVM-like pattern (single large outline around the schizont) was observed in 22 of 28 images, whereas 6 of 28 images showed slight overlap with the PPM marker PfMSP1 (Fig. 23, C). Biochemical fractionation was performed twice; in both experiments, PfEXP1-ΔC was detected predominantly in the pellet (P) fraction with a minor signal in the carbonate (C) fraction (Fig. 23, D). Overall, these observations are consistent with PfEXP1-ΔC being largely membrane-associated and consistent with a PVM localization.

A.

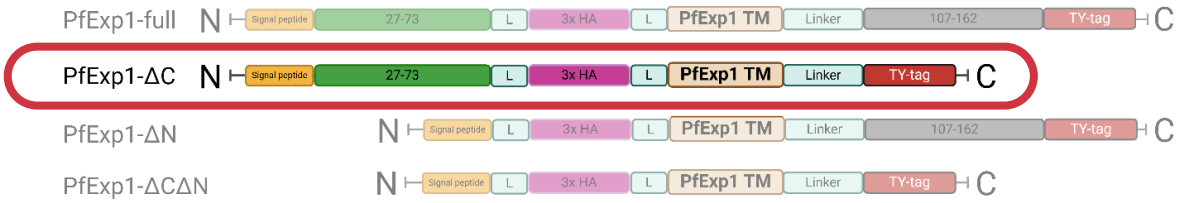
PfExp1-full
N
Signal peptide
27-73
L
3x HA
L
PfExp1 TM
Linker
107-162
TY-tag
C
PfExp1-ΔC
PfExp1-ΔN
PfExp1-ΔCΔN

B.

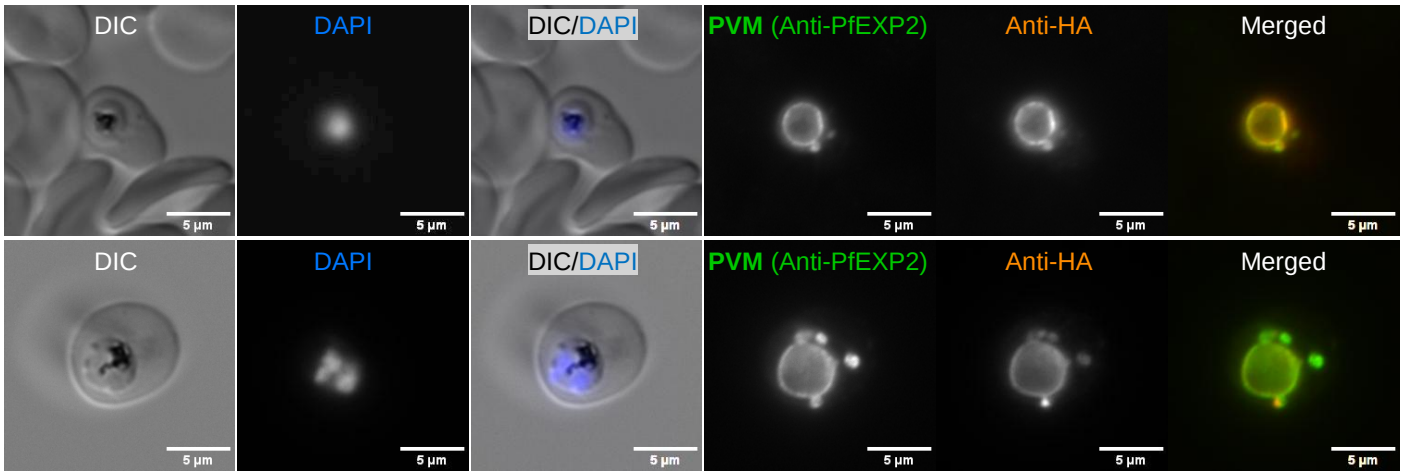
DIC
DAPI
DIC/DAPI
PVM (Anti-PfEXP2)
Anti-HA
Merged
5 µm

C.

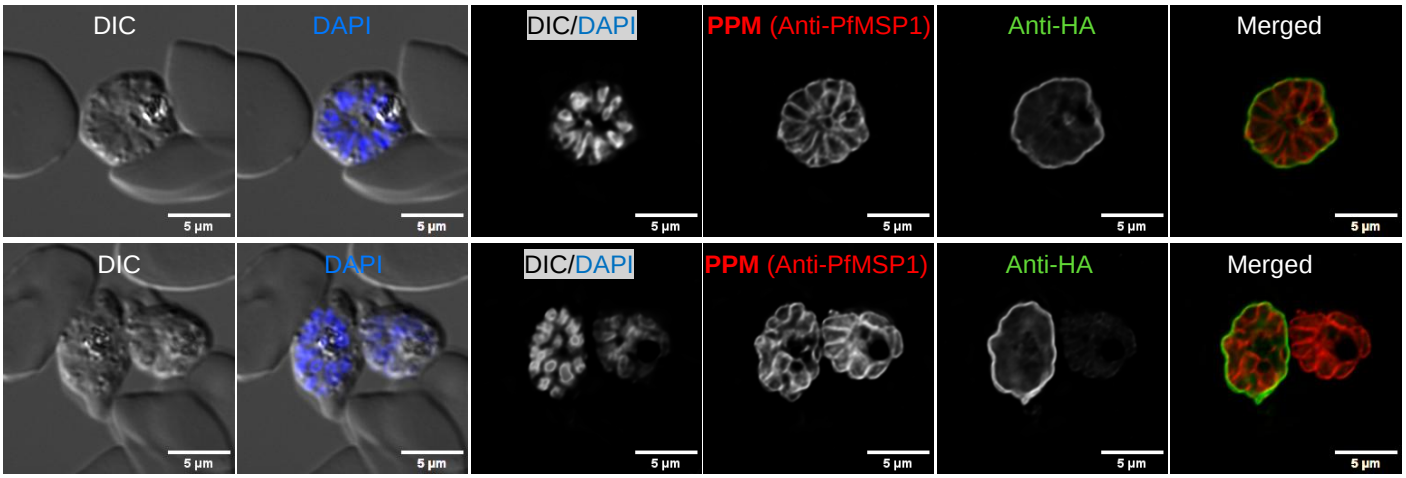
DIC
DAPI
DIC/DAPI
PPM (Anti-PfMSP1)
Anti-HA
Merged
5 µm

D.

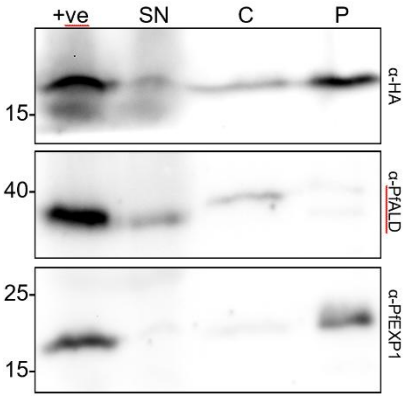
+ve
SN
C
P
15-
40-
25-
15-
α-HA
α-PfALD
α-PfEXP1

Fig. 23. IFA images and biochemical fractionation of PfEXP1-ΔC (Group 2)

(A) Schematic representation of the PfEXP1-ΔC plasmid design. Created in BioRender.com. **(B)** Trophozoite-stage immunofluorescence analysis of parasites expressing PfEXP1-ΔC, co-stained with anti-HA and anti-PfEXP2 (PVM marker). The PfEXP1-ΔC signal shows staining at the parasite boundary and overlaps with PfEXP2 (n = 25 trophozoites). DAPI stains parasite nuclei; DIC shows parasite morphology. **(C)** Schizont-stage immunofluorescence analysis of parasites expressing PfEXP1-ΔC, co-stained with anti-HA and PfMSP1 (PPM marker). A PVM-like pattern was observed in 22/28 schizonts; 6/28 schizonts showed only weak/partial overlap with PfMSP1. DAPI stains parasite nuclei; DIC shows parasite morphology. **(D)** Biochemical fractionation of PfEXP1-ΔC (two repeats; one representative experiment shown). Samples were analyzed by Western blot as input (+ve; full cell lysate), supernatant (SN; soluble fraction), carbonate (C; carbonate-extractable fraction), and pellet (P; insoluble/membrane fraction). PfEXP1-ΔC is detected predominantly in P with a minor signal in C. PfALD serves as a soluble control; anti-PfEXP1 detects endogenous PfEXP1 as a membrane-integrated positive control.

2.5.3 PfEXP1-ΔN

PfEXP1-ΔN, like other members of Group 2, was included as a control to confirm that the tagged expression format used in this study does not, by itself, disrupt PfEXP1 construct localization. Since the N-terminal region was not expected to be required for targeting, PfEXP1-ΔN was expected to show localization to the PVM even in the presence of the additional tag and linker elements. PfEXP1-ΔN was analyzed by immunofluorescence microscopy in trophozoites and schizonts and by biochemical fractionation. Trophozoite-stage IFA showed a staining pattern similar to the other Group 2 controls, with overlap with the PVM marker PfEXP2 (Fig. 24, B). In schizonts, PfEXP1-ΔN showed slight overlap with PfMSP1 in 15 of 19 analyzed images (Fig. 24, C). Biochemical fractionation was performed twice. In both experiments, PfEXP1-ΔN was detected predominantly in the carbonate (C) fraction with a minor signal in the supernatant (SN) fraction (Fig. 24, D). These data are consistent with a predominantly soluble and/or weakly membrane-associated fraction of PfEXP1-ΔN within the parasitophorous vacuole lumen.

A.

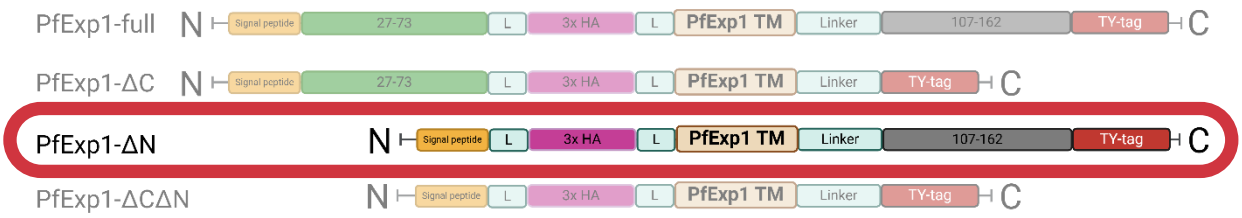
PfExp1-full
N
Signal peptide
27-73
L
3x HA
L
PfExp1 TM
Linker
107-162
TY-tag
C
PfExp1-ΔC
N
Signal peptide
27-73
L
3x HA
L
PfExp1 TM
Linker
TY-tag
C
PfExp1-ΔN
N
Signal peptide
L
3x HA
L
PfExp1 TM
Linker
107-162
TY-tag
C
PfExp1-ΔCΔN
N
Signal peptide
L
3x HA
L
PfExp1 TM
Linker
TY-tag
C

B.

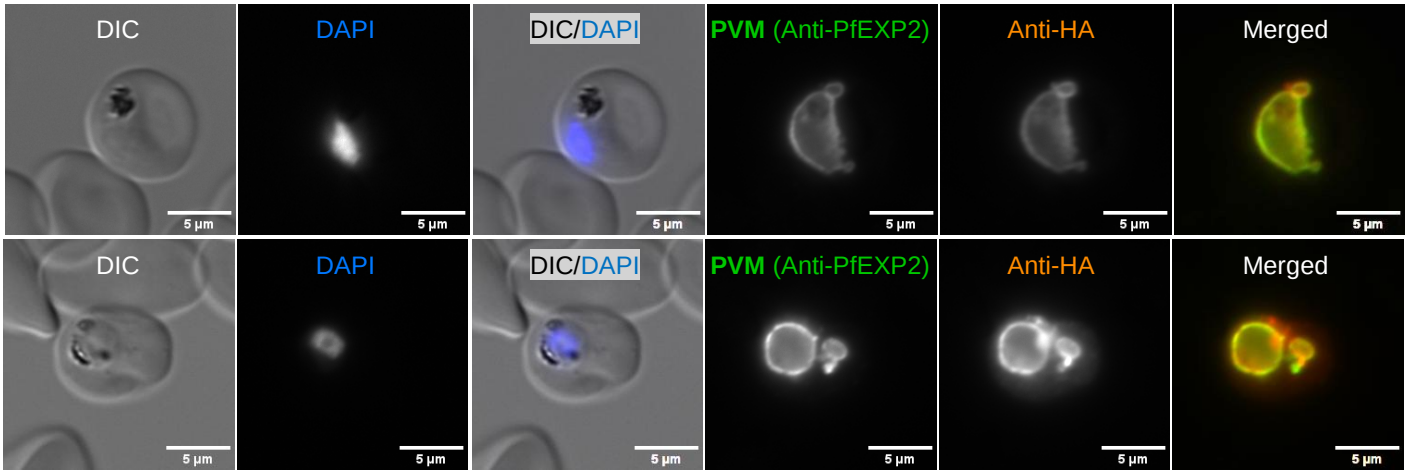
DIC
DAPI
DIC/DAPI
PVM (Anti-PfEXP2)
Anti-HA
Merged
5 µm

C.

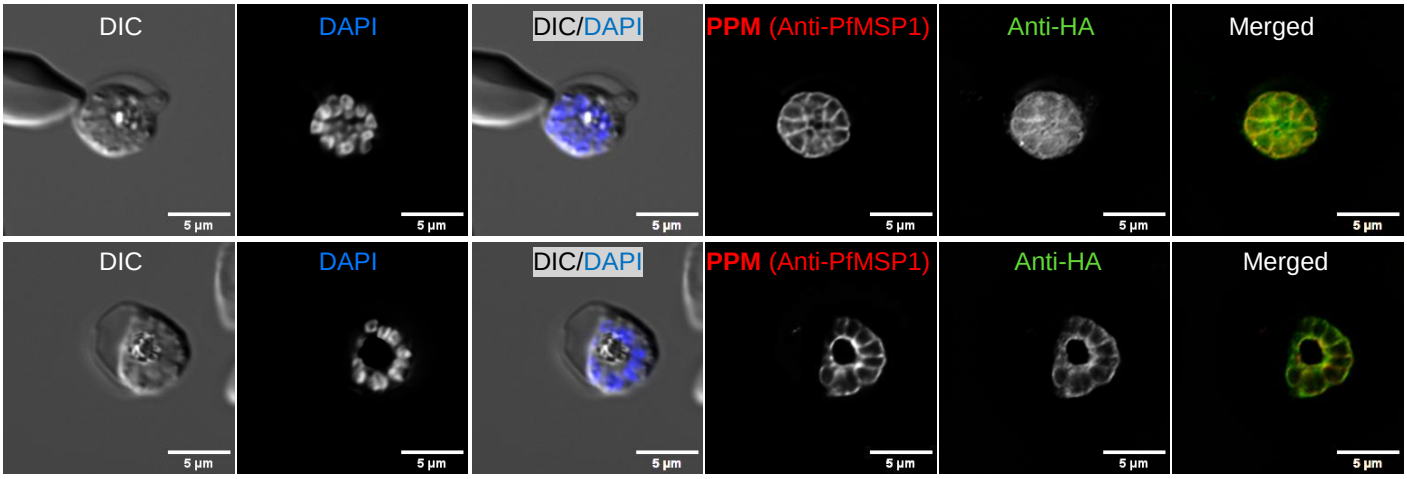
DIC
DAPI
DIC/DAPI
PPM (Anti-PfMSP1)
Anti-HA
Merged
5 µm

D.

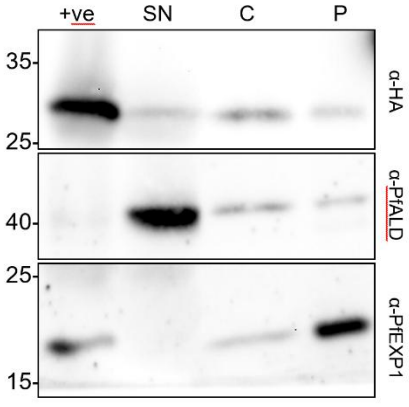
+ve
SN
C
P
35
25
40
25
15
α-HA
α-PfALD
α-PfEXP1

Fig. 24. IFA images and biochemical fractionation of PfEXP1-ΔN (Group 2)

(A) Schematic representation of the PfEXP1-ΔN plasmid design. Created in BioRender.com. **(B)** Trophozoite-stage immunofluorescence analysis of parasites expressing PfEXP1-ΔN, co-stained with anti-HA and anti-PfEXP2 (PVM marker). The HA tag signal shows staining at the parasite boundary and overlaps with PfEXP2. DAPI stains parasite nuclei; DIC shows parasite morphology. **(C)** Schizont-stage immunofluorescence analysis of parasites expressing PfEXP1-ΔN, co-stained with anti-HA and PfMSP1 (PPM marker). Slight overlap with PfMSP1 was observed in 15/19 schizonts (n = 19 schizonts). DAPI stains parasite nuclei; DIC shows parasite morphology. **(D)** Biochemical fractionation of PfEXP1-ΔN was performed twice; one representative experiment is shown. Samples were analyzed by Western blot as input (+ve; full cell lysate), supernatant (SN; soluble fraction), carbonate (C; carbonate-extractable fraction), and pellet (P; insoluble/membrane fraction). Anti-HA detects PfEXP1-ΔN predominantly in C with a minor signal in SN. PfALD serves as a soluble control; anti-PfEXP1 detects endogenous PfEXP1 as a membrane-integrated positive control.

2.5.4 PfEXP1-ΔC/ΔN

PfEXP1-ΔC/ΔN was analyzed by immunofluorescence microscopy in trophozoites and schizonts, together with biochemical fractionation. In trophozoites, the HA signal was detected at the parasite boundary and overlapped with the PVM marker PfEXP2 (Fig. 25, B); however, as described above, the close apposition of PVM and PPM at this stage limits membrane-level assignment by fluorescence microscopy. In schizonts, 26 of 30 analyzed images showed slight overlap with the PPM marker PfMSP1 (n = 30 schizonts) (Fig. 25, C). Biochemical fractionation was performed twice; in both experiments, PfEXP1-ΔC/ΔN was detected predominantly in the carbonate (C) fraction with a minor signal in the supernatant (SN) fraction (Fig. 25, D). Taken together, these results fit better with PfEXP1-ΔC/ΔN being present as a soluble (or loosely associated) pool in the PV lumen rather than as a clearly membrane-integrated PVM protein.

A.

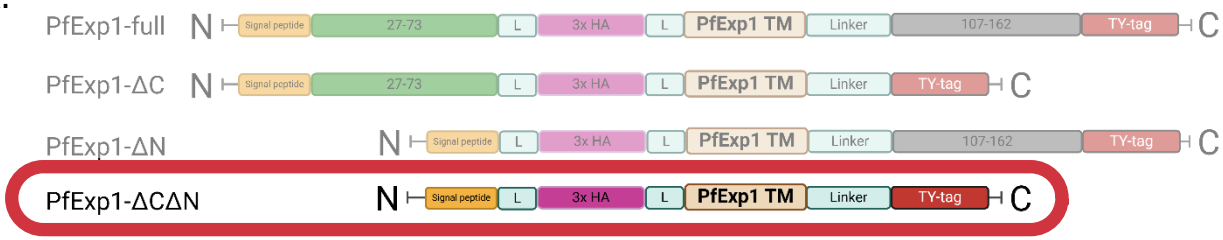
PfExp1-full
N
Signal peptide
27-73
L
3x HA
L
PfExp1 TM
Linker
107-162
TY-tag
C
PfExp1-ΔC
N
Signal peptide
27-73
L
3x HA
L
PfExp1 TM
Linker
TY-tag
C
PfExp1-ΔN
N
Signal peptide
L
3x HA
L
PfExp1 TM
Linker
107-162
TY-tag
C
PfExp1-ΔCΔN
N
Signal peptide
L
3x HA
L
PfExp1 TM
Linker
TY-tag
C

B.

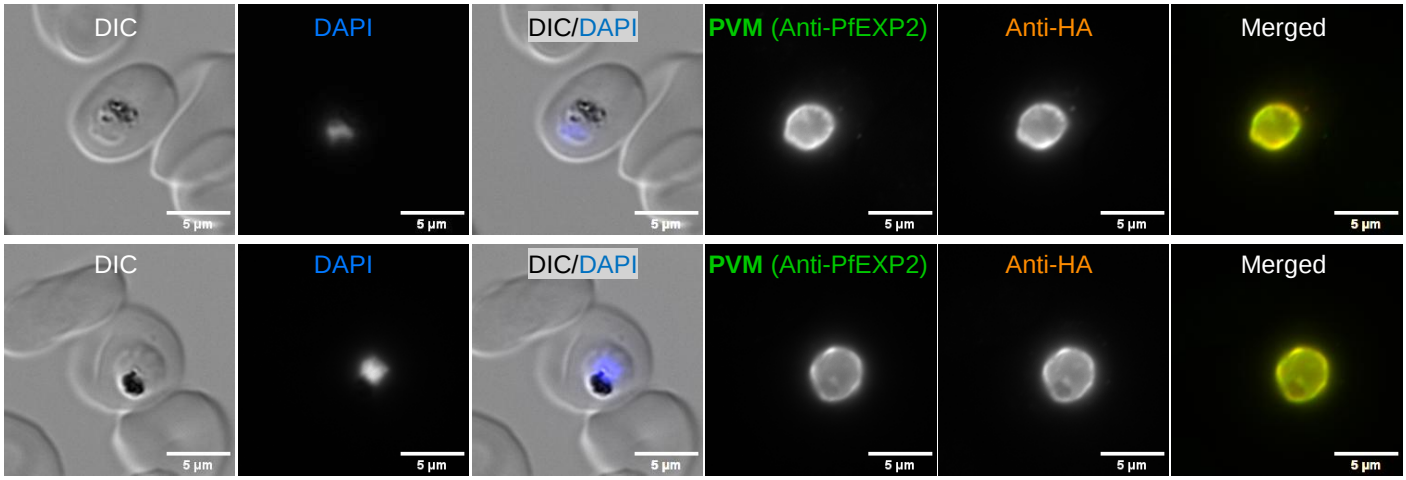
DIC
DAPI
DIC/DAPI
PVM (Anti-PfEXP2)
Anti-HA
Merged
5 µm

C.

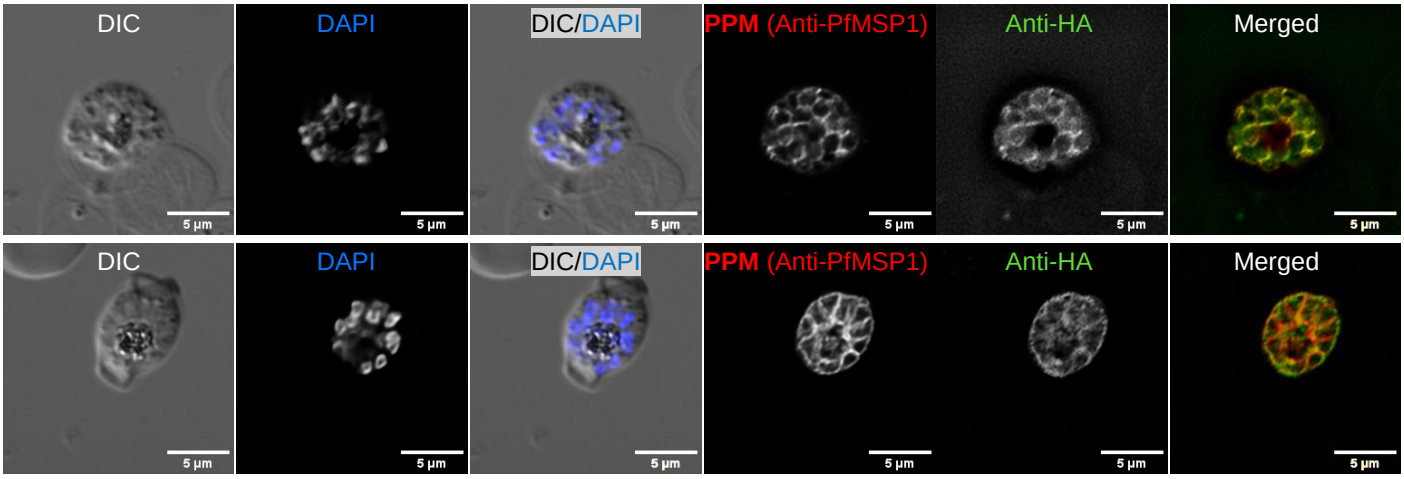
DIC
DAPI
DIC/DAPI
PPM (Anti-PfMSP1)
Anti-HA
Merged
5 µm

D.

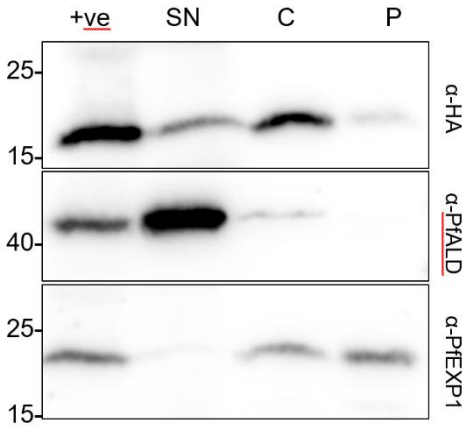
+ve
SN
C
P
25
15
40
25
15
α-HA
α-PfALD
α-PfEXP1

Fig. 25. IFA images and biochemical fractionation of PfEXP1-ΔC/ΔN (Group 2)

(A) Schematic representation of the PfEXP1-ΔC/ΔN plasmid design. Created in BioRender.com. **(B)** Trophozoite-stage immunofluorescence analysis of parasites expressing PfEXP1-ΔC/ΔN, co-stained with anti-HA and anti-PfEXP2 (PVM marker). The HA tag signal shows staining at the parasite boundary and overlaps with PfEXP2. DAPI stains parasite nuclei; DIC shows parasite morphology. **(C)** Schizont-stage immunofluorescence analysis of parasites expressing PfEXP1-ΔC/ΔN, co-stained with anti-HA and PfMSP1 (PPM marker). Slight overlap with PfMSP1 was observed in 26/30 schizonts (n = 30 schizonts). DAPI stains parasite nuclei; DIC shows parasite morphology. **(D)** Biochemical fractionation of PfEXP1-ΔC/ΔN analyzed by Western blot. Fractionation was performed twice; one representative experiment is shown. Samples were loaded as input (+ve; full cell lysate), supernatant (SN; soluble fraction), carbonate (C; carbonate-extractable fraction), and pellet (P; insoluble/membrane fraction). Anti-HA detects PfEXP1-ΔC/ΔN predominantly in C with a minor signal in SN. PfALD serves as a soluble control; anti-PfEXP1 detects endogenous PfEXP1 as a membrane-integrated positive control.

2.6 Transmembrane-domain replacement (Group 3)

2.6.1 PfETRAMP10.1-full (Group 3)

First member of transmembrane swapping group, PfETRAMP10.1-full, was analyzed by immunofluorescence microscopy in trophozoites and schizonts. In trophozoites, the HA tag signal showed staining at the parasite boundary and overlapped with the PVM marker PfEXP2 (Fig. 26, B). In schizonts, a PVM-like pattern was observed in 26 images, while 6 images showed a pattern with slight overlap with PfMSP1 (Fig. 26, C). Overall, these observations are consistent with PfETRAMP10.1-full being largely localized to the PVM.

A.

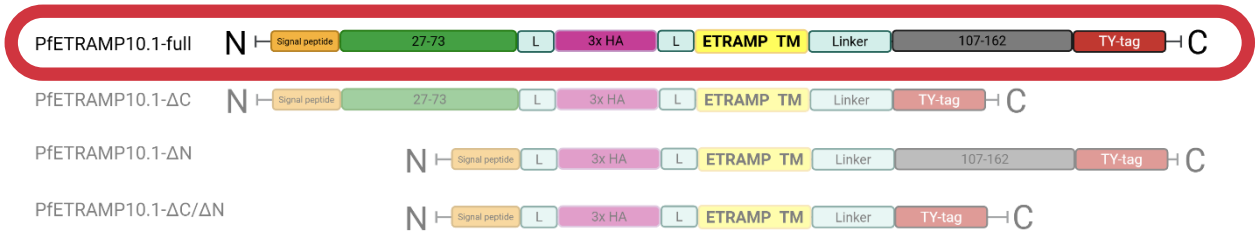

B.

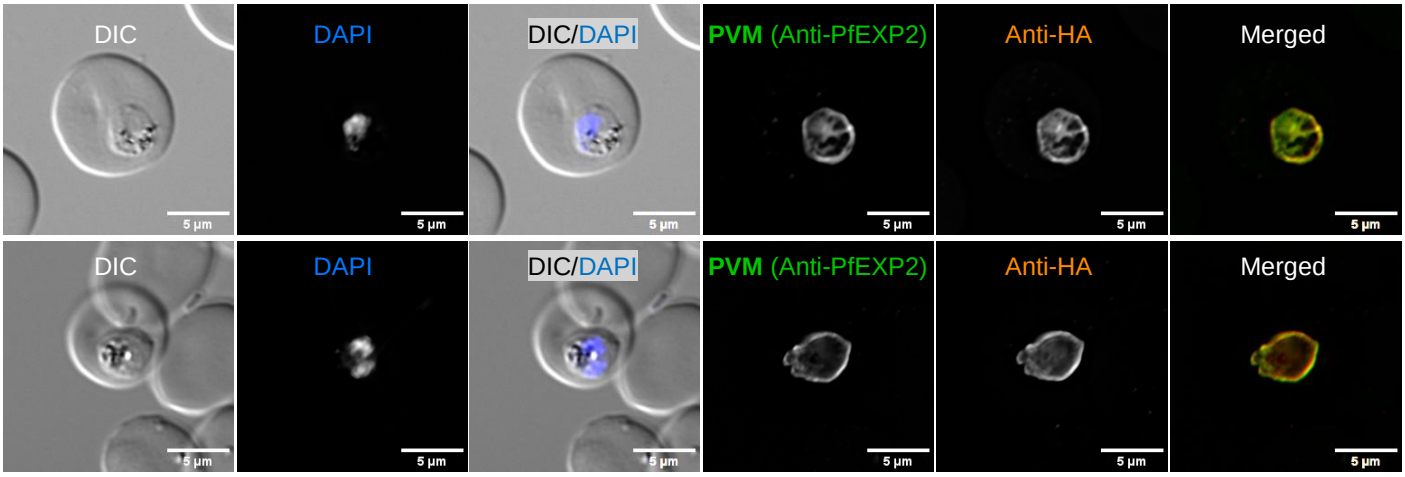

C.

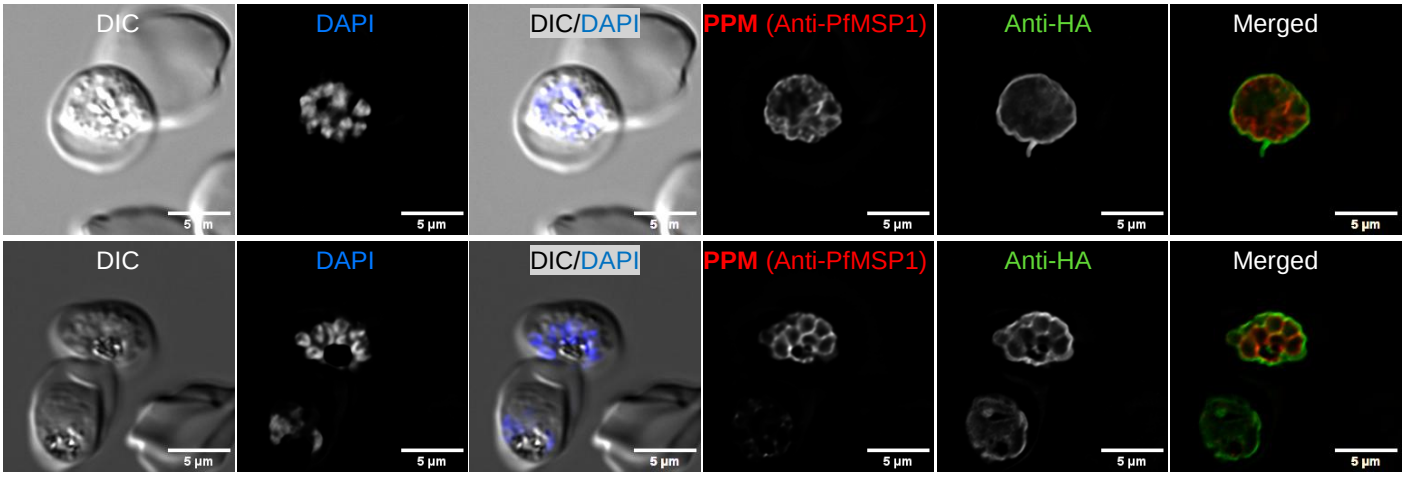

Fig. 26. IFA images of PfETRAMP10.1-full (Group 3)

(A) Schematic representation of the PfETRAMP10.1-full plasmid design. Created in BioRender.com. **(B)** Trophozoite-stage immunofluorescence analysis of parasites expressing PfETRAMP10.1-full, co-stained with anti-HA and anti-PfEXP2 (PVM marker). The HA signal shows staining at the parasite boundary and overlaps with PfEXP2. DAPI stains parasite nuclei; DIC shows parasite morphology. **(C)** Schizont-stage immunofluorescence analysis of parasites expressing PfETRAMP10.1-full, co-stained with anti-HA and PfMSP1 (PPM marker). A PVM-like pattern was observed in 26 images, whereas 6 images showed slight overlap with PfMSP1. DAPI stains parasite nuclei; DIC shows parasite morphology.

2.6.2 PfETRAMP10.1-ΔC (Group 3)

PfETRAMP10.1-ΔC was analyzed by immunofluorescence microscopy in trophozoites and schizonts. In trophozoites, the HA tag signal showed staining at the parasite boundary and overlapped with the PVM marker PfEXP2 (Fig. 27, B). In schizonts, a PVM-like pattern was observed in 33 images, while 14 images showed a pattern with slight overlap with PfMSP1 (Fig. 27, C). Taken together, the microscopy image data indicate that PfETRAMP10.1-ΔC shows a predominantly PVM-like localization.

A.

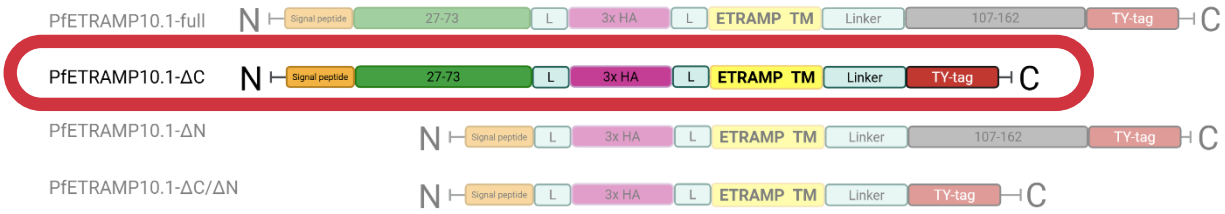

B.

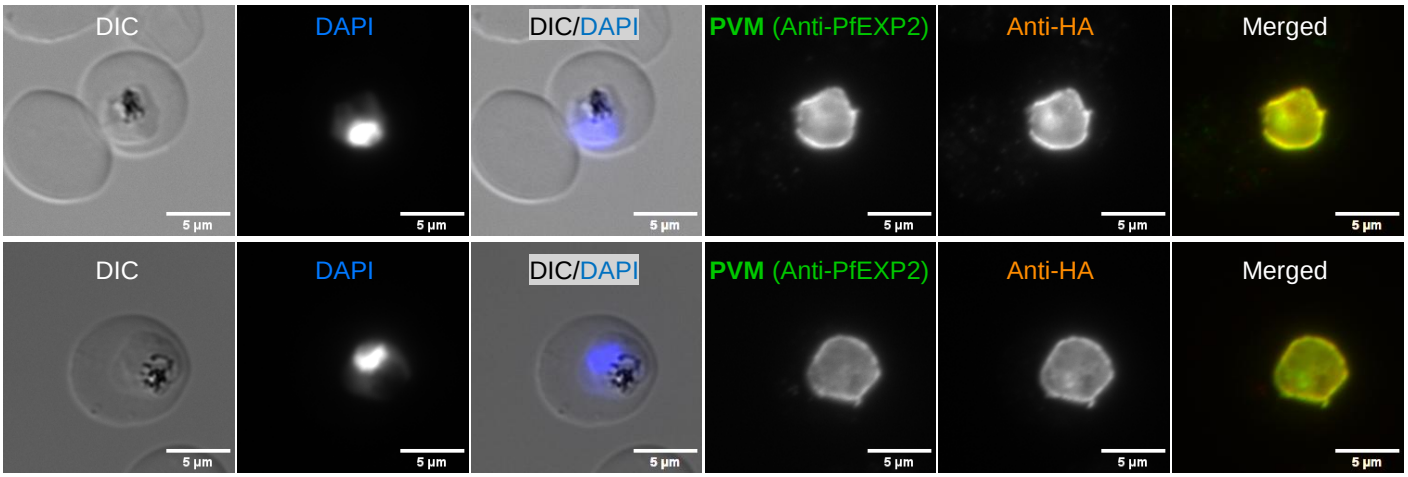

C.

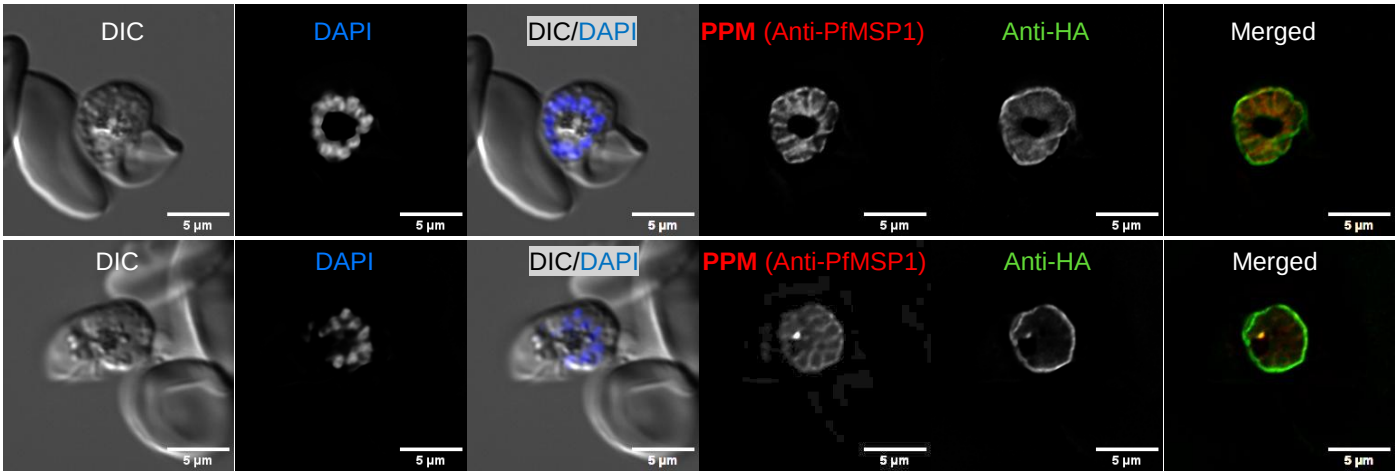

Fig. 27. IFA images of PfETRAMP10.1-ΔC (Group 3)

(A) Schematic representation of the PfETRAMP10.1-ΔC plasmid design. Created in BioRender.com. **(B)** Trophozoite-stage immunofluorescence analysis of parasites expressing PfETRAMP10.1-ΔC, co-stained with anti-HA and anti-PfEXP2 (PVM marker). The HA signal shows staining at the parasite boundary and overlaps with PfEXP2. DAPI stains parasite nuclei; DIC shows parasite morphology. **(C)** Schizont-stage immunofluorescence analysis of parasites expressing PfETRAMP10.1-ΔC, co-stained with anti-HA and PfMSP1 (PPM marker). A PVM-like pattern was observed in 33 images, whereas 14 images showed slight overlap with PfMSP1. DAPI stains parasite nuclei; DIC shows parasite morphology.

2.6.3 PfETRAMP10.1-ΔN (Group 3)

PfETRAMP10.1-ΔN was analyzed by immunofluorescence microscopy in trophozoites and mature schizonts. In trophozoites, the HA signal showed staining at the parasite boundary and overlapped with the PVM marker PfEXP2 (Fig. 28, B). In schizonts, 44 images were evaluated. Of these, 7/44 showed a PVM-like pattern, 11/44 showed slight overlap with PfMSP1, and 26/44 were not interpretable (Fig. 28, C). With the current dataset and no fractionation, we can only tentatively suggest localization at the PVM or the PPM.

A.

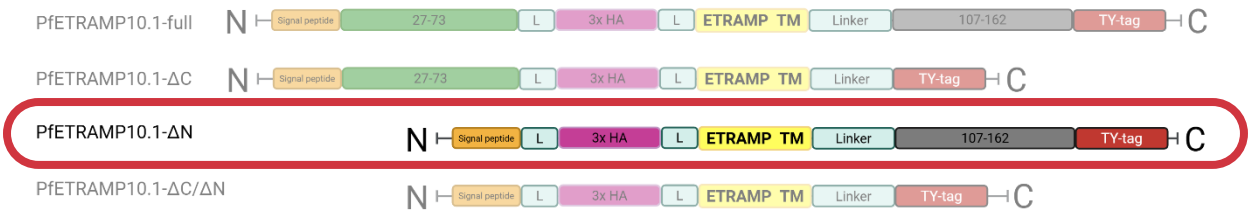

B.

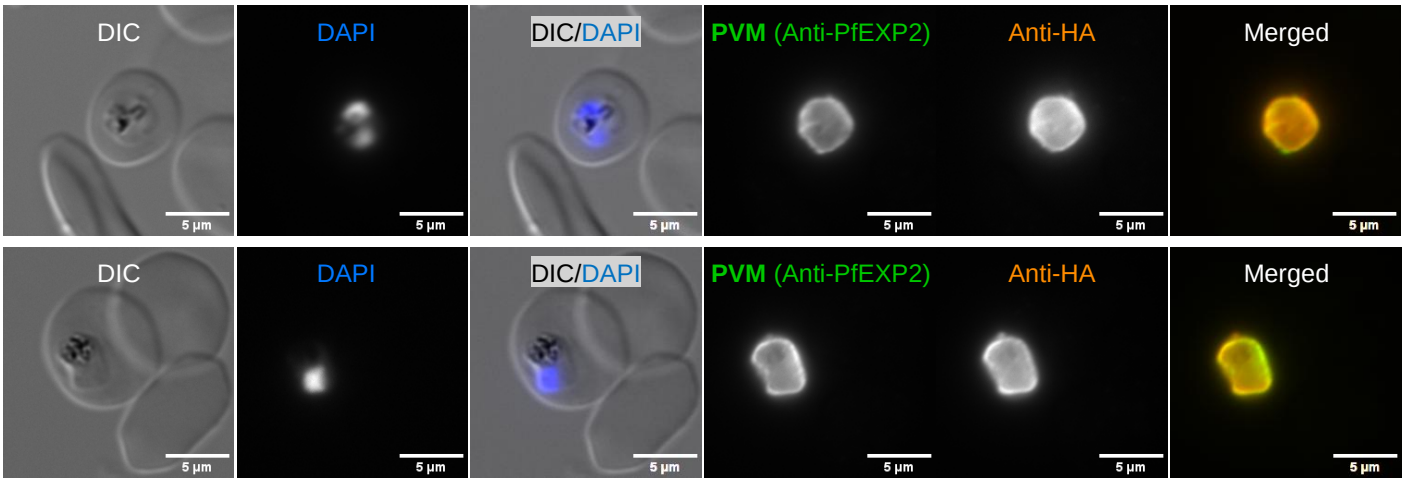

C.

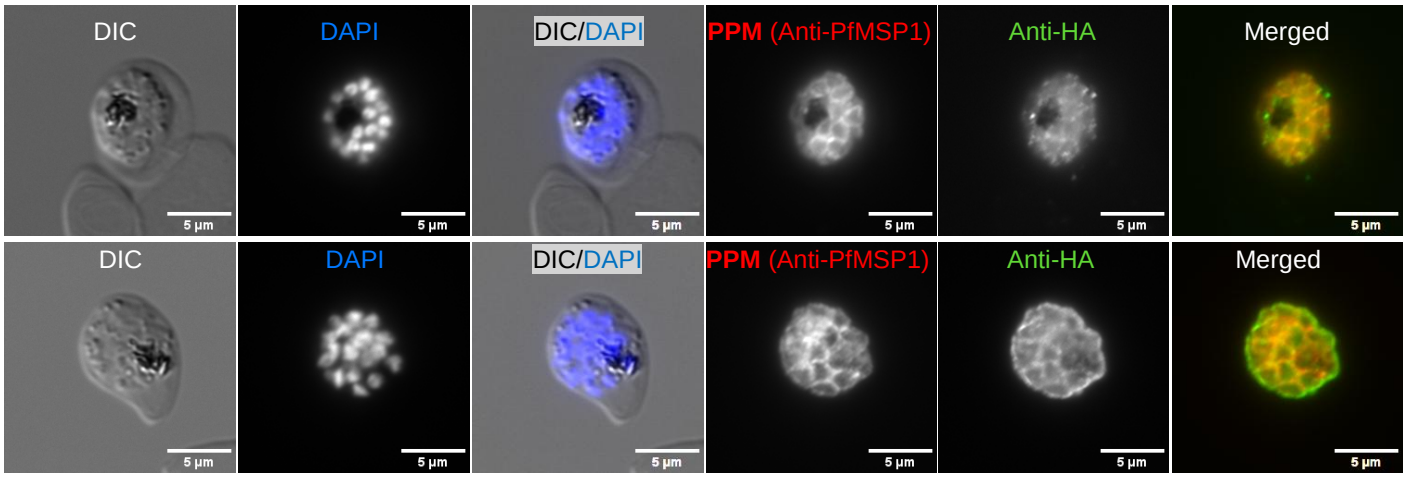

Fig. 28. IFA images of PfETRAMP10.1-ΔN (Group 3)

(A) Schematic of the PfETRAMP10.1-ΔN plasmid analyzed in this experiment. Created in BioRender.com. **(B)** Trophozoite-stage IFA of parasites expressing PfETRAMP10.1-ΔN-HA, co-stained with anti-HA and anti-PfEXP2 (PVM marker). The HA signal appears at the parasite boundary and overlaps with PfEXP2. DAPI stains parasite nuclei; DIC shows parasite morphology. **(C)** Schizont-stage IFA of parasites expressing PfETRAMP10.1-ΔN-HA, co-stained with anti-HA and anti-PfMSP1 (PPM marker). Across 44 schizont images, 7 showed a PVM-like outline, 11 showed slight overlap with the PfMSP1 signal, and 26 were not interpretable. DAPI stains parasite nuclei; DIC shows parasite morphology.

2.6.4 PfETRAMP10.1-ΔC/ΔN (Group 3)

PfETRAMP10.1-ΔC/ΔN was analyzed by immunofluorescence microscopy in trophozoites and schizonts. In trophozoites, the HA tag signal showed staining at the parasite boundary and overlapped with the PVM marker PfEXP2 (Fig. 29, B). In schizonts, 55 images were evaluated. 27/55 showed slight localization with PfMSP1, 8/55 showed clear localization with PfMSP1, 9/55 showed a PVM-like pattern, and 11/55 were not interpretable (Fig. 29, C). If the observed HA signal represents a membrane-integrated population rather than a soluble or peripheral pool, the schizont patterns are consistent with localization to either the PPM or the PVM.

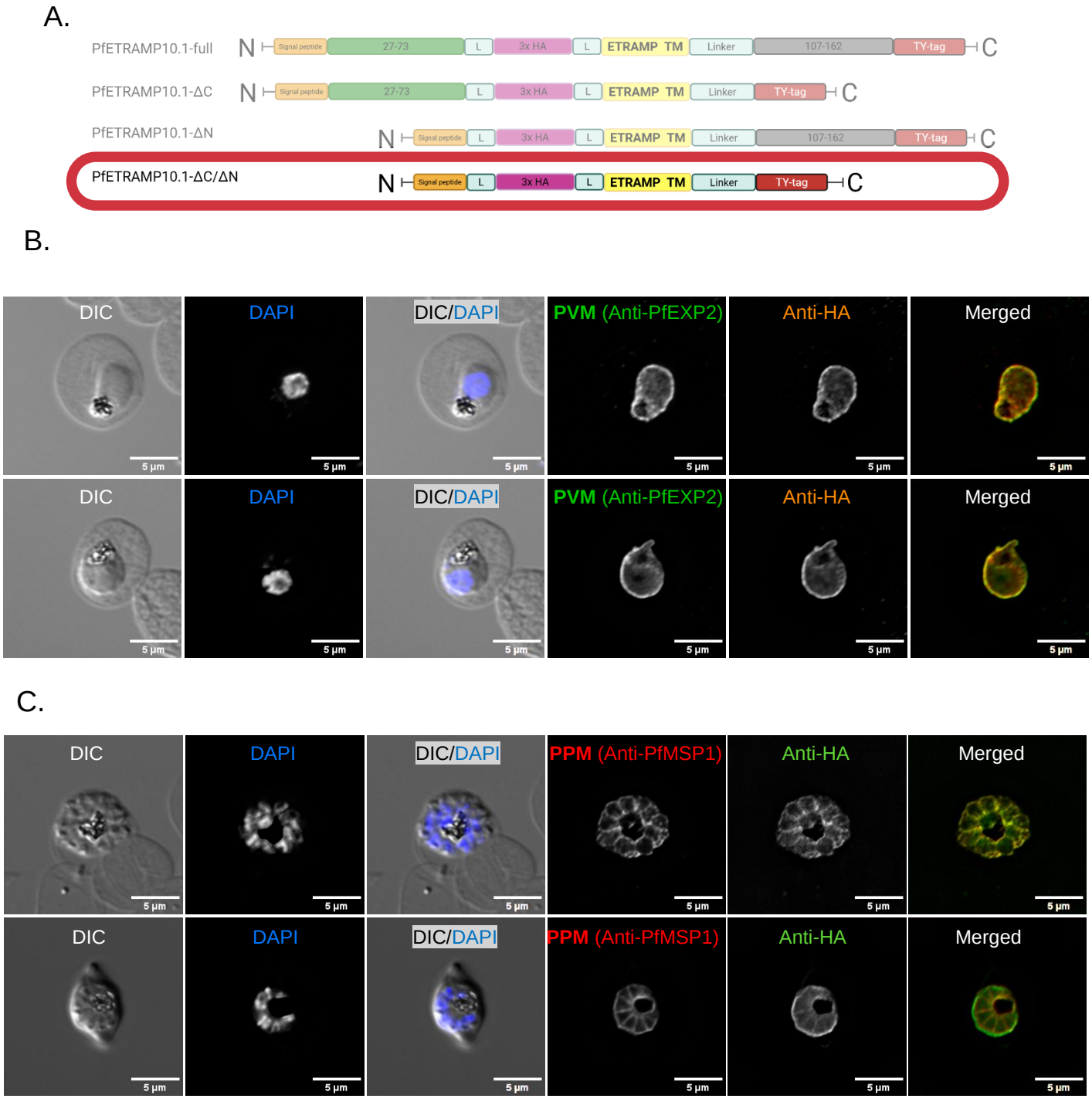

Fig. 29. IFA images of PfETRAMP10.1-ΔC/ΔN (Group 3)

(A) Schematic of the PfETRAMP10.1-ΔC/ΔN variant analyzed in this experiment. Created in BioRender.com. **(B)** Trophozoite-stage IFA of parasites expressing PfETRAMP10.1-ΔC/ΔN-HA, co-stained with anti-HA and anti-PfEXP2 (PVM marker). The HA signal is detected at the parasite boundary and overlaps with PfEXP2. DAPI stains parasite nuclei; DIC shows parasite morphology. **(C)** Schizont-stage IFA of parasites expressing PfETRAMP10.1-ΔC/ΔN-HA, co-stained with anti-HA and anti-PfMSP1 (PPM marker). Across 55 schizont images, 27 showed slight co-localization with PfMSP1, 8 showed clear co-localization with PfMSP1, 9 showed a clear PVM-like pattern, and 11 were not interpretable. DAPI stains parasite nuclei; DIC shows parasite morphology.

2.7 Synthetic transmembrane helices (Group 4)

2.7.1 Group 4: 23L-full

23L-full was analyzed by immunofluorescence microscopy in trophozoites and schizonts. In trophozoites, the HA tag signal showed staining at the parasite boundary and overlapped with the PVM marker PfEXP2 (Fig. 30, B). In schizonts, 25 images were evaluated. Of these, 18/25 showed slight localization with PfMSP1, whereas 7/25 were not interpretable (Fig. 30, C). A biochemical fractionation for solubility/membrane-association analysis was not performed for this parasite line because fractionation experiments were discontinued after the main positive-control line (PfEXP1-full) was found to be predominantly soluble. Based on these data alone, the schizont pattern is consistent with localization at the PPM.

A.

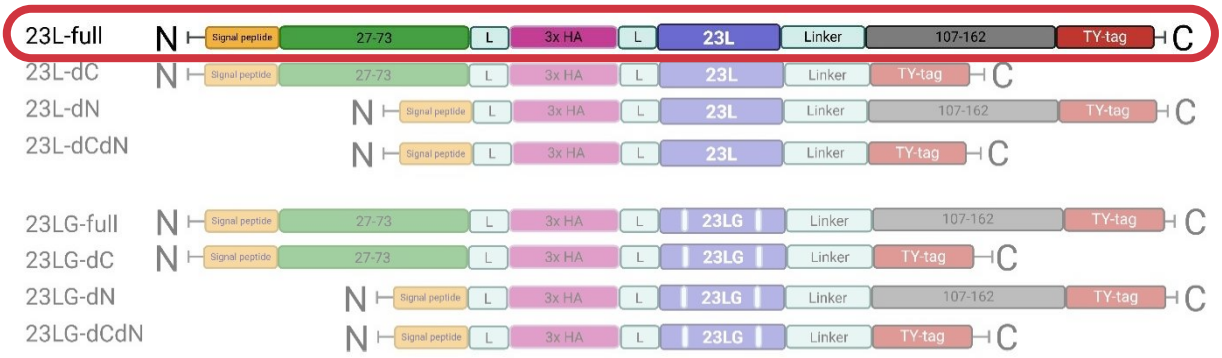

B.

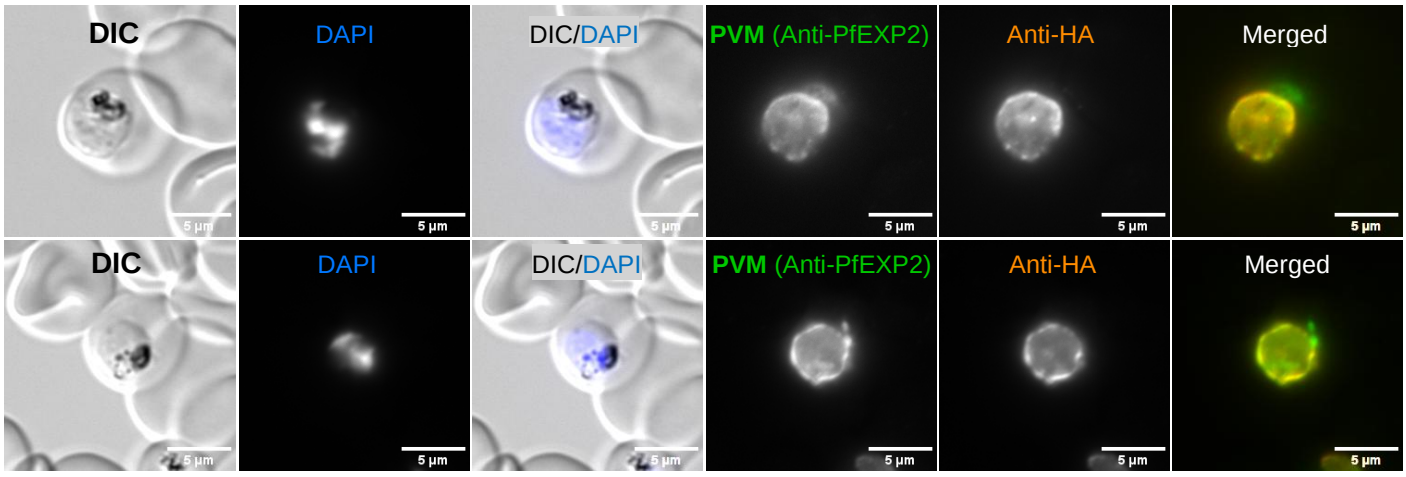

C.

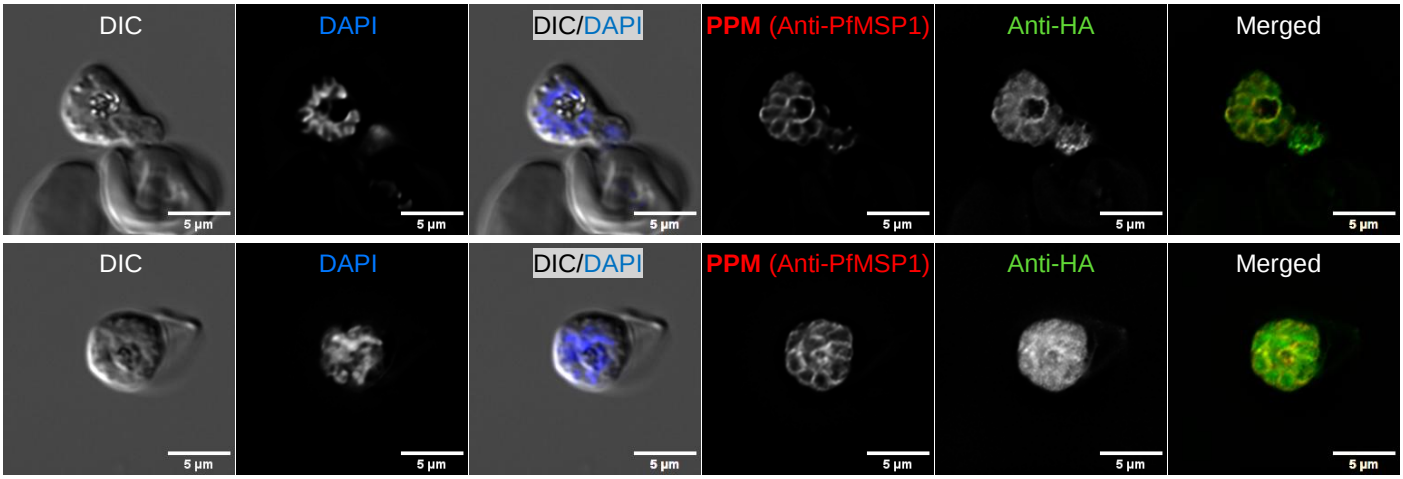

Fig. 30. IFA images of 23L-full (Group 4)

(A) Schematic of the 23L-full variant analyzed in this experiment. Created in BioRender.com. **(B)** Trophozoite-stage IFA of parasites expressing 23L-full-HA, co-stained with anti-HA and anti-PfEXP2 (PVM marker). The HA signal is detected at the parasite boundary and overlaps with PfEXP2. DAPI stains parasite nuclei; DIC shows parasite morphology. **(C)** Schizont-stage IFA of parasites expressing 23L-full-HA, co-stained with anti-HA and anti-PfMSP1 (PPM marker). Across 25 schizont images, 18 showed slight co-localization with PfMSP1 and 7 were not interpretable. DAPI stains parasite nuclei; DIC shows parasite morphology.

2.7.2 Group 4: 23L-ΔC

This variant was analyzed by immunofluorescence microscopy in trophozoites and schizonts. In trophozoites, the HA signal showed staining at the parasite boundary and overlapped with the PVM marker PfEXP2 (Fig. 31, B). In schizonts, 26 images were evaluated. The majority of images were of insufficient quality for confident interpretation (23/26) (Fig. 31, C). In the remaining images, the HA signal appeared weak and in some cases showed possible overlap with PfMSP1; however, this was not clear enough to classify the localization confidently. With these data alone, the staining could reflect localization at the PPM or a signal within the PV.

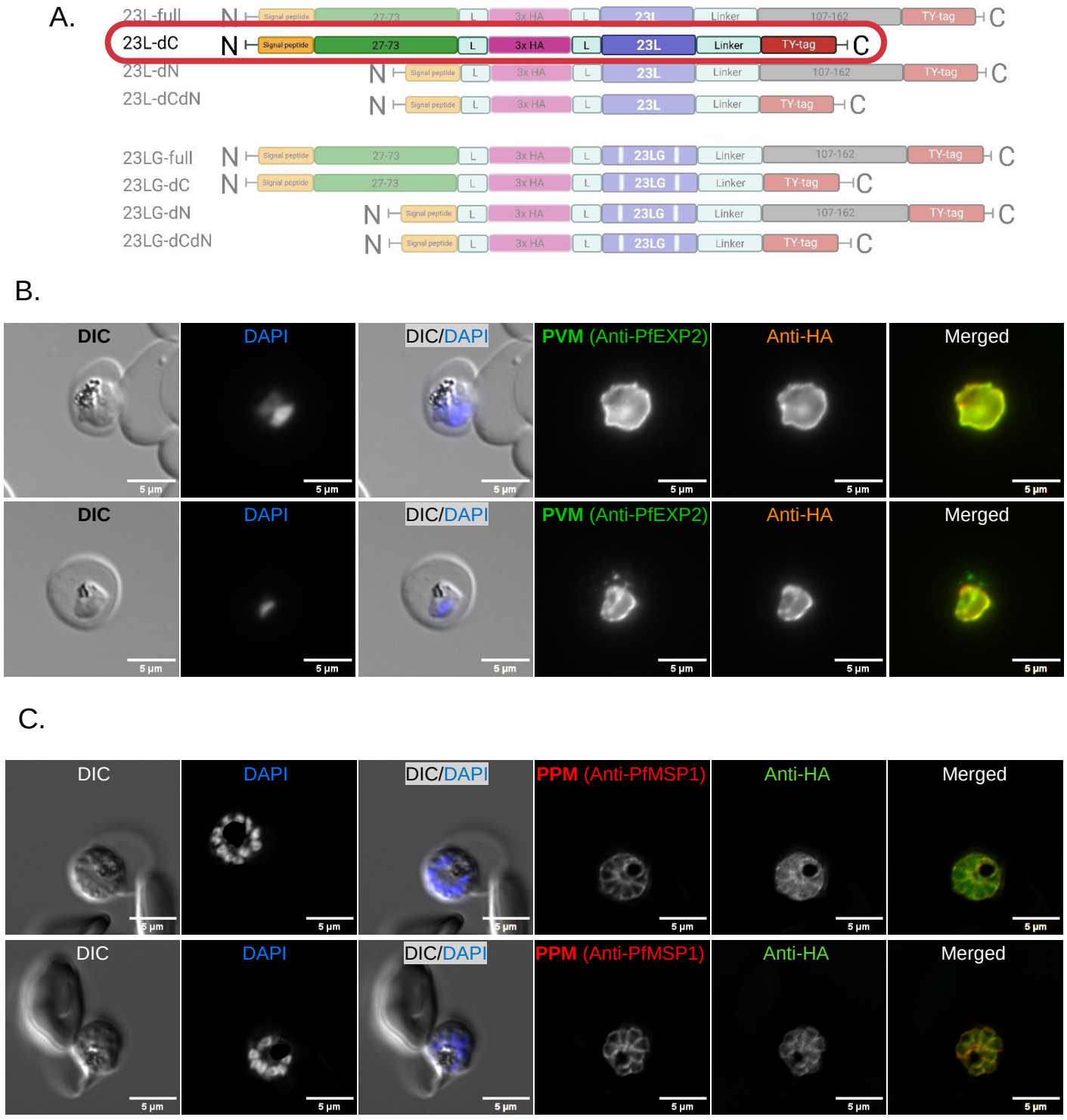

Fig. 31. IFA images of 23L-ΔC (Group 4)

(A) Schematic of the 23L-ΔC variant analyzed in this experiment. Created in BioRender.com. **(B)** Trophozoite-stage IFA of parasites expressing 23L-ΔC-HA, co-stained with anti-HA and anti-PfEXP2 (PVM marker). The HA signal is detected at the parasite boundary and overlaps with PfEXP2. DAPI stains parasite nuclei; DIC shows parasite morphology. **(C)** Schizont-stage IFA of parasites expressing 23L-ΔC-HA, co-stained with anti-HA and anti-PfMSP1 (PPM marker). Across 26 schizont images, 23 were not interpretable due to image quality; the remaining images showed weak HA signal with possible, but not definitive, overlap with PfMSP1. DAPI stains parasite nuclei; DIC shows parasite morphology.

2.7.3 Group 4: 23L-ΔN

This cell line also was analyzed by immunofluorescence microscopy in trophozoites and schizonts. In trophozoites, the HA signal was detected at the parasite boundary and was evaluated relative to PVM marker (Fig. 32, B). However, as described above, in trophozoites the PVM lies in very close apposition to the parasite plasma membrane (PPM), and conventional fluorescence microscopy cannot reliably distinguish PVM and PPM signals as separate structures. In schizonts, 17 images were evaluated. The HA-signal was not interpretable since it was too noisy, although in some images the HA signal appeared to show weak overlap with PfMSP1 (Fig. 32, C). With these data alone, the staining could reflect localization at the PPM or a signal associated with the PV lumen.

A.

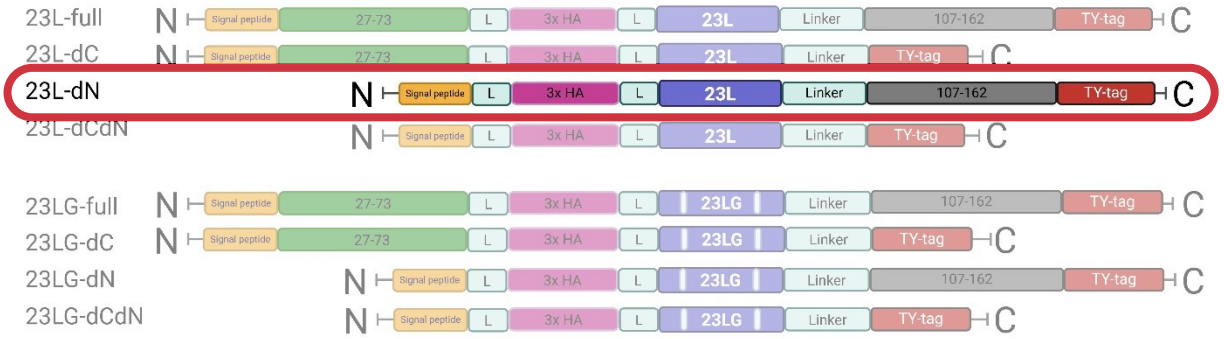

B.

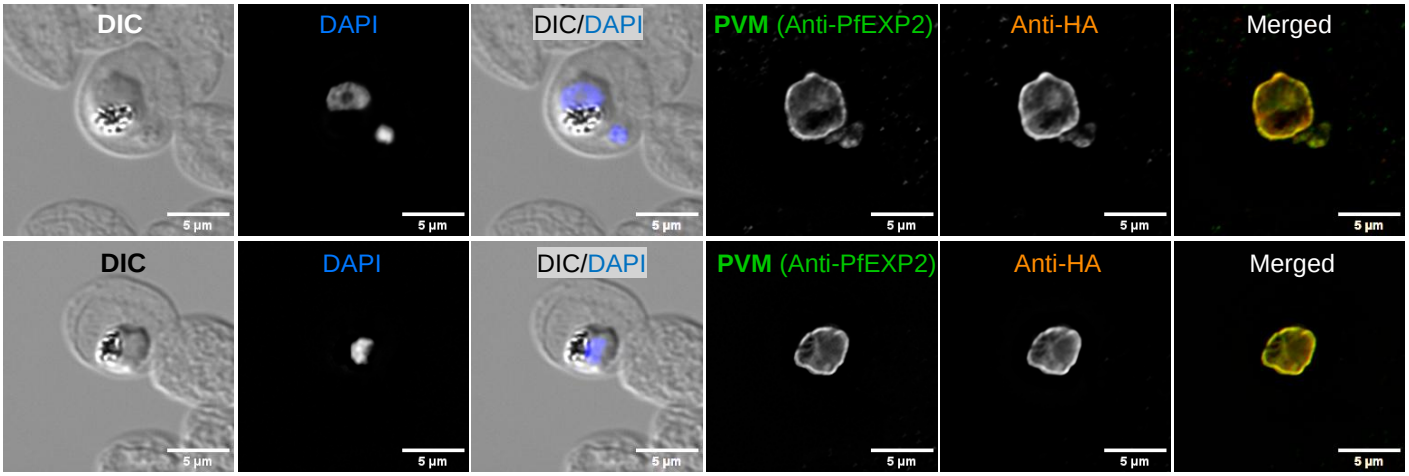

C.

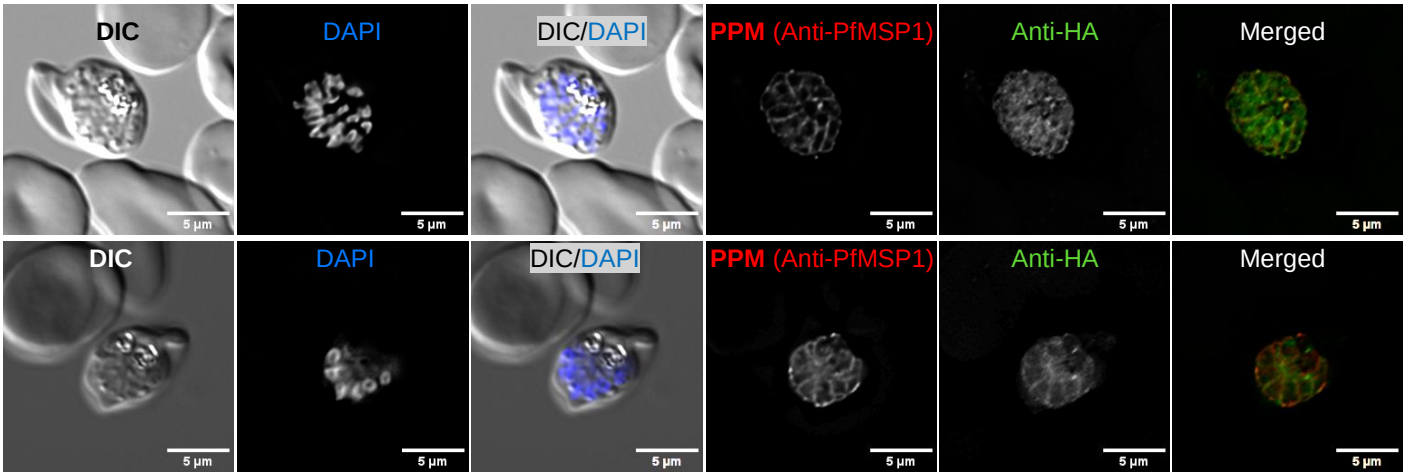

Fig. 32. IFA images of 23L-ΔN (Group 4)

(A) Schematic of the 23L-ΔN variant analyzed in this experiment. Created in BioRender.com. **(B)** Trophozoite-stage IFA of parasites expressing 23L-ΔN-HA, co-stained with anti-HA and anti-PfEXP2 (PVM marker). The HA signal is detected at the parasite boundary. DAPI stains parasite nuclei; DIC shows parasite morphology. **(C)** Schizont-stage IFA of parasites expressing 23L-ΔN-HA, co-stained with anti-HA and anti-PfMSP1 (PPM marker). Across 17 schizont images, the staining was not interpretable; weak overlap with PfMSP1 was observed in some images. DAPI stains parasite nuclei; DIC shows parasite morphology.

2.7.4 Group 4: 23L-ΔC/ΔN

This cell line was analyzed by immunofluorescence microscopy in trophozoites and schizonts and by biochemical fractionation. In trophozoites, the HA tag signal was detected at the parasite boundary and was evaluated relative to PVM marker (Fig. 33, B). In schizonts, 15 images were evaluated. 13 of 15 images were not interpretable, although in several of these the HA tag signal appeared to show weak overlap with PPM marker (Fig. 33, C). A biochemical fractionation analysis was performed once. The HA-tagged protein was detected predominantly in the pellet (P) fraction, with only minor signal in the supernatant (SN) and carbonate (C) fractions (Fig. 33, D). Taken together, the available data suggest localization at the PPM.

A.

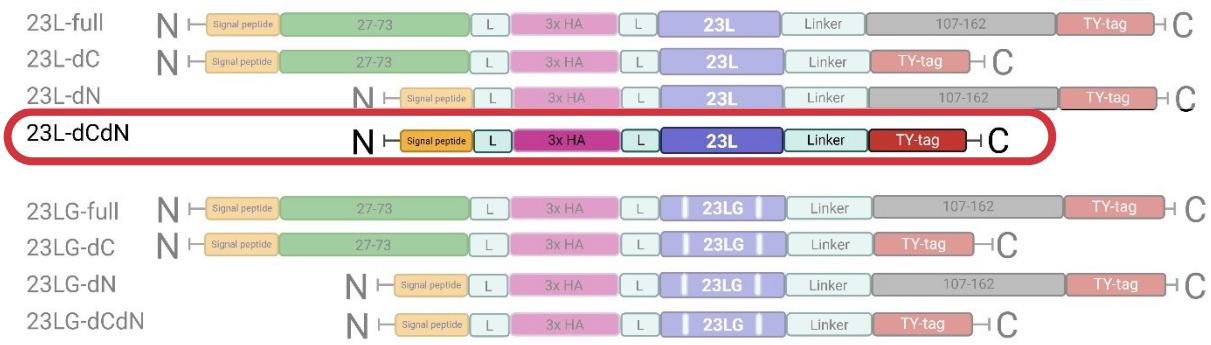
23L-full
23L-dC
23L-dN
23L-dCdN
23LG-full
23LG-dC
23LG-dN
23LG-dCdN
N
C
Signal peptide
27-73
L
3x HA
23L
23LG
Linker
107-162
TY-tag

B.

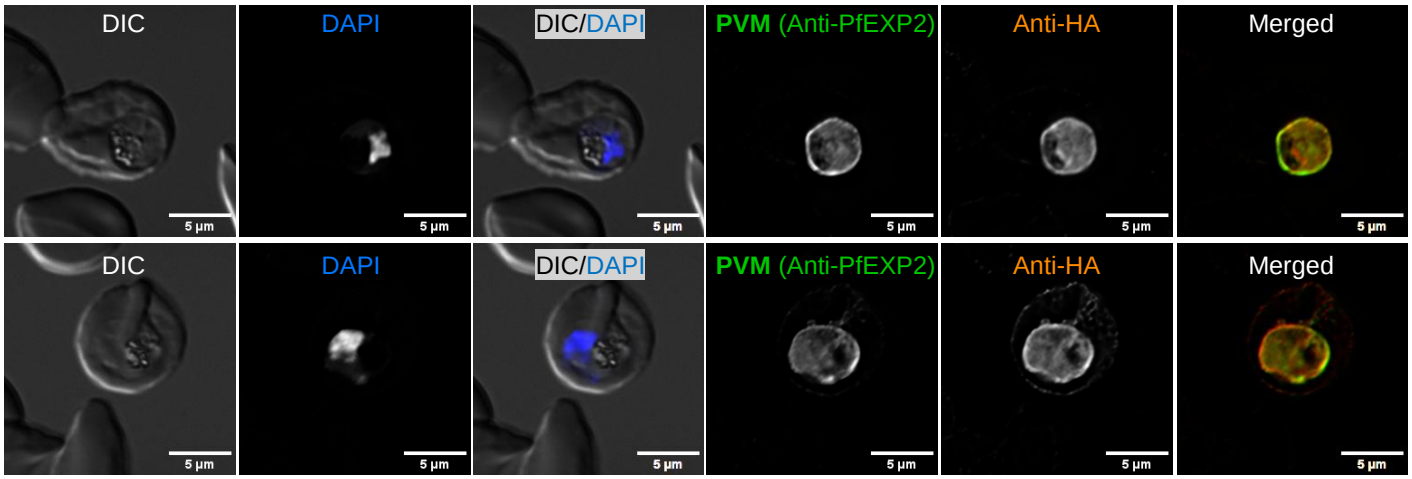
DIC
DAPI
DIC/DAPI
PVM (Anti-PfEXP2)
Anti-HA
Merged
5 µm

C.

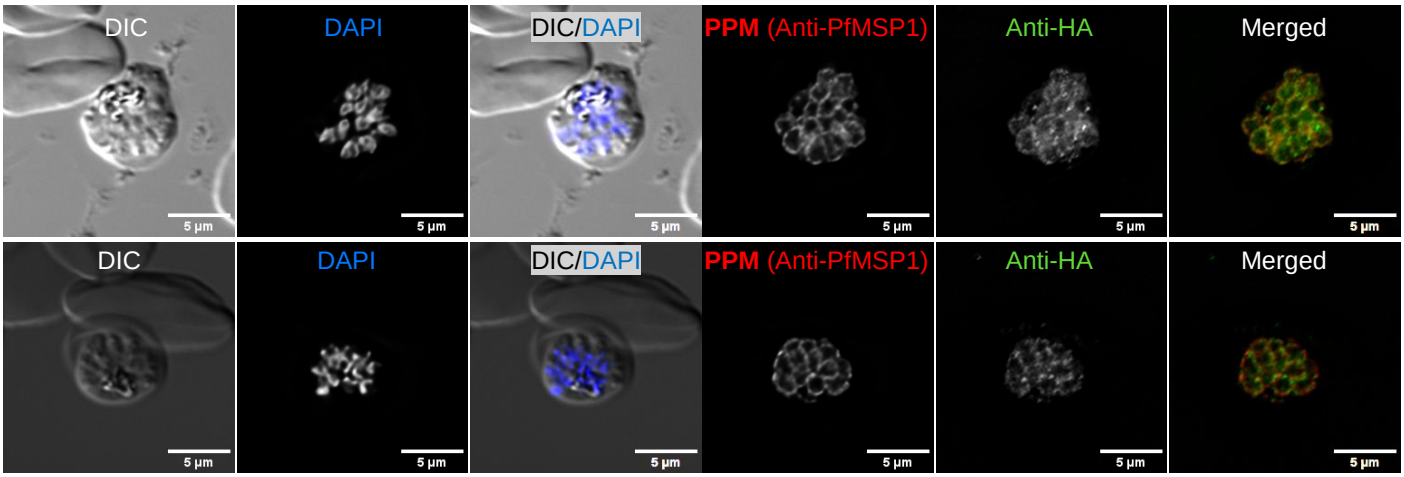
DIC
DAPI
DIC/DAPI
PPM (Anti-PfMSP1)
Anti-HA
Merged
5 µm

D.

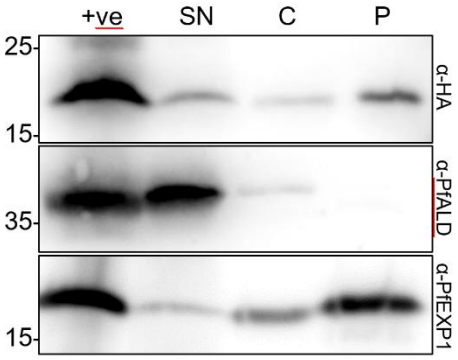
+ve
SN
C
P
25
15
35
15
α-HA
α-PfALD
α-PfEXP1

Fig. 33. IFA images and biochemical fractionation of 23L-ΔC/ΔN (Group 4)

(A) Schematic of the 23L-ΔC/ΔN variant analyzed in this experiment. Created in BioRender.com. **(B)** Trophozoite-stage IFA of parasites expressing 23L-ΔC/ΔN-HA, co-stained with anti-HA and anti-PfEXP2 (PVM marker). The HA signal is detected at the parasite boundary. DAPI stains parasite nuclei; DIC shows parasite morphology. **(C)** Schizont-stage IFA of parasites expressing 23L-ΔC/ΔN-HA, co-stained with anti-HA and anti-PfMSP1 (PPM marker). Across 15 schizont images, 13 were not interpretable; weak overlap with PfMSP1 was observed in some images. DAPI stains parasite nuclei; DIC shows parasite morphology. **(D)** Biochemical fractionation of 23L-ΔC/ΔN-HA analyzed by Western blot. Samples were loaded as input (+ve; full cell lysate), supernatant (SN), carbonate (C), and pellet (P) fractions. Anti-HA detects 23L-ΔC/ΔN-HA predominantly in the pellet (P) fraction, with minor signal in SN and C.

2.7.5 Group 4: 23LG-full

23LG-full was analyzed by immunofluorescence microscopy in trophozoites and schizonts and by biochemical fractionation. In trophozoites, the HA signal was detected at the parasite boundary and was evaluated relative to PVM marker (Fig. 34, B). However, as described above, in trophozoites the PVM lies in very close apposition to the parasite plasma membrane (PPM), and conventional fluorescence microscopy cannot reliably distinguish PVM and PPM signals as separate structures. In schizonts, 24 images were evaluated. 22 of 24 images were not interpretable, although in several of these the HA signal appeared to show weak overlap with PPM marker (Fig. 34, C). A biochemical fractionation analysis was performed once. The HA-tagged protein was detected predominantly in the pellet (P) fraction (Fig. 34, D). Taken together, the available data suggest localization at the PPM.

A.

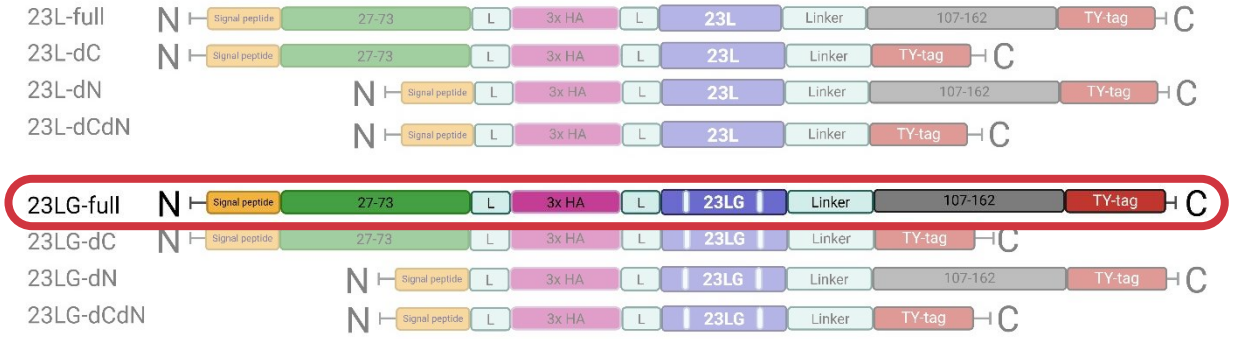
23L-full
23L-dC
23L-dN
23L-dCdN
23LG-full
23LG-dC
23LG-dN
23LG-dCdN
N
C
Signal peptide
27-73
L
3x HA
23L
23LG
Linker
107-162
TY-tag

B.

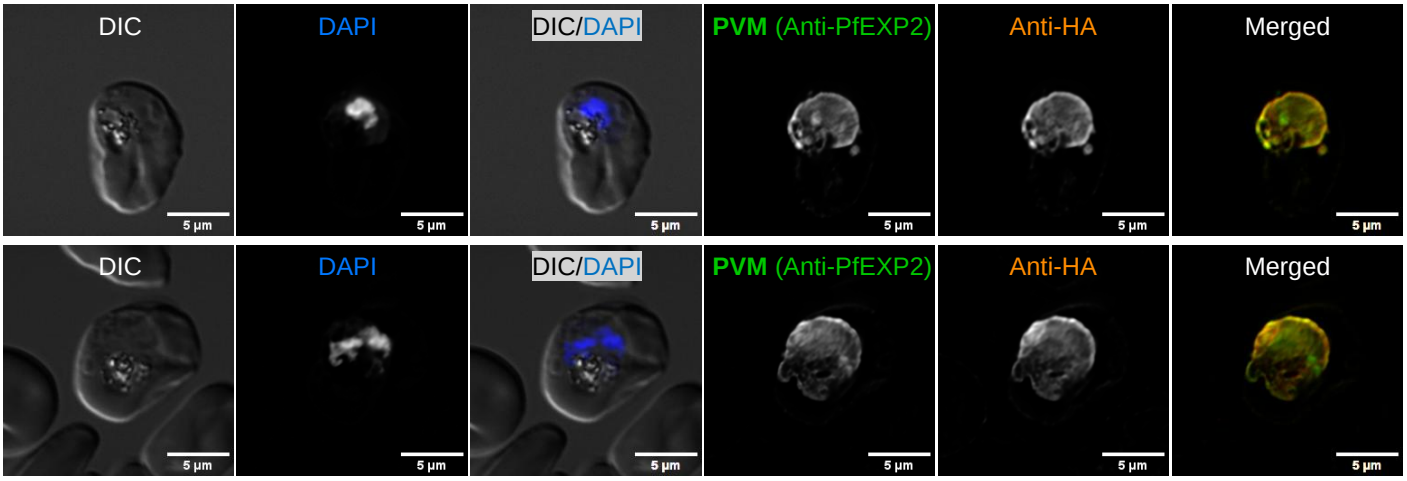
DIC
DAPI
DIC/DAPI
PVM (Anti-PfEXP2)
Anti-HA
Merged
5 µm

C.

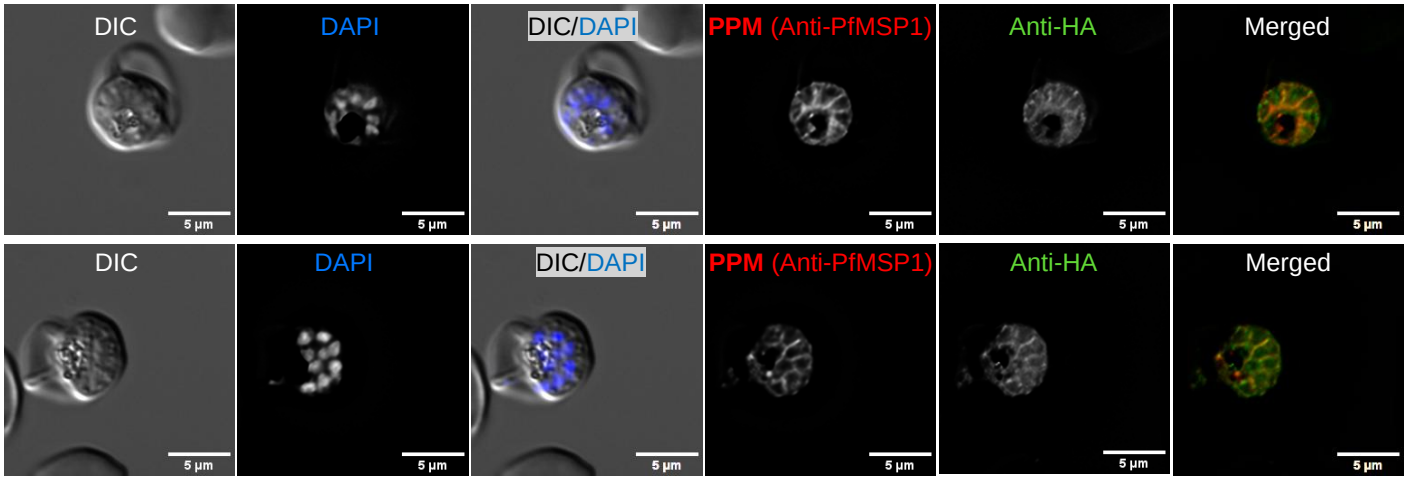
DIC
DAPI
DIC/DAPI
PPM (Anti-PfMSP1)
Anti-HA
Merged
5 µm

D.

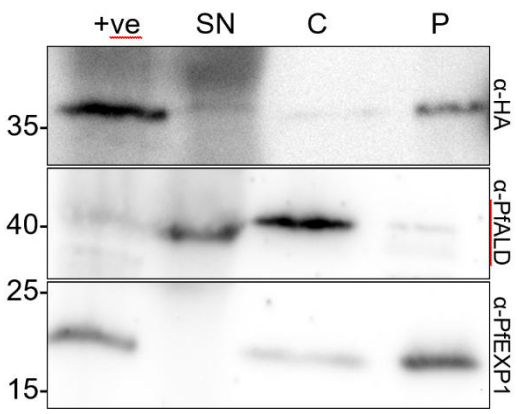
+ve
SN
C
P
35
40
25
15
α-HA
α-PfALD
α-PfEXP1

Fig. 34. IFA images and biochemical fractionation of 23LG-full (Group 4)

(A) Schematic of the 23LG-full variant analyzed in this experiment. Created in BioRender.com. **(B)** Trophozoite-stage IFA of parasites expressing 23LG-full-HA, co-stained with anti-HA and anti-PfEXP2 (PVM marker). The HA signal is detected at the parasite boundary. DAPI stains parasite nuclei; DIC shows parasite morphology. **(C)** Schizont-stage IFA of parasites expressing 23LG-full-HA, co-stained with anti-HA and anti-PfMSP1 (PPM marker). Across 24 schizont images, 22 were not interpretable; weak overlap with PfMSP1 was observed in some images. DAPI stains parasite nuclei; DIC shows parasite morphology. **(D)** Biochemical fractionation of 23LG-full-HA analyzed by Western blot (one experiment). Samples were loaded as input (+ve; full cell lysate), supernatant (SN), carbonate (C), and pellet (P) fractions. Anti-HA detects 23LG-full–HA predominantly in the pellet (P) fraction.

2.7.6 Group 4: 23LG-ΔC

23LG-ΔC cell line was analyzed by immunofluorescence microscopy in trophozoites and schizonts and by biochemical fractionation. In trophozoites, the HA tag signal was detected at the parasite boundary and was evaluated relative to PVM marker (Fig. 35, B). However, as described above, in trophozoites the PVM lies in very close apposition to the parasite plasma membrane (PPM), and conventional fluorescence microscopy cannot reliably distinguish PVM and PPM signals as separate structures. In schizonts, 18 images were evaluated. 16/18 images were not interpretable, although in several of these the HA tag signal appeared to show weak overlap with PPM marker (Fig. 35, C). A biochemical fractionation analysis was performed once. The HA-tagged protein was detected predominantly in the supernatant (SN) fraction (Fig. 35, D). Taken together, the available data are most consistent with a soluble pool, which could be located within the PV lumen.

A.

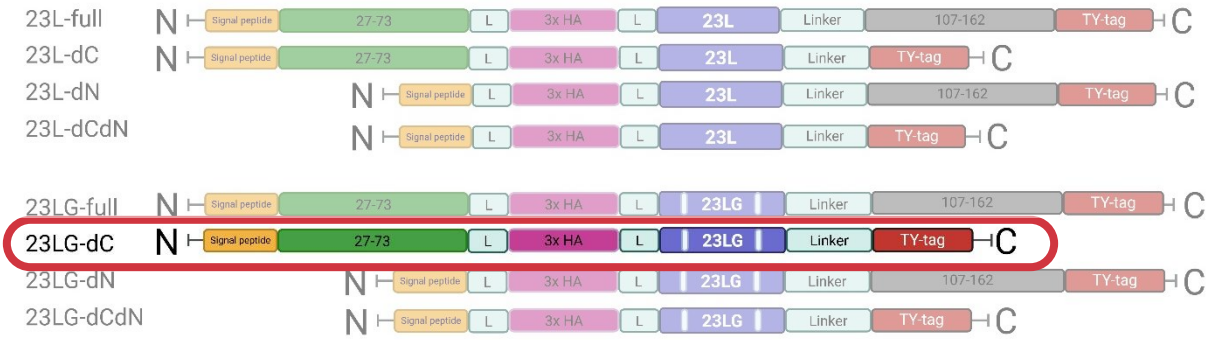
23L-full
23L-dC
23L-dN
23L-dCdN
23LG-full
23LG-dC
23LG-dN
23LG-dCdN
N
C
Signal peptide
27-73
L
3x HA
23L
23LG
Linker
107-162
TY-tag

B.

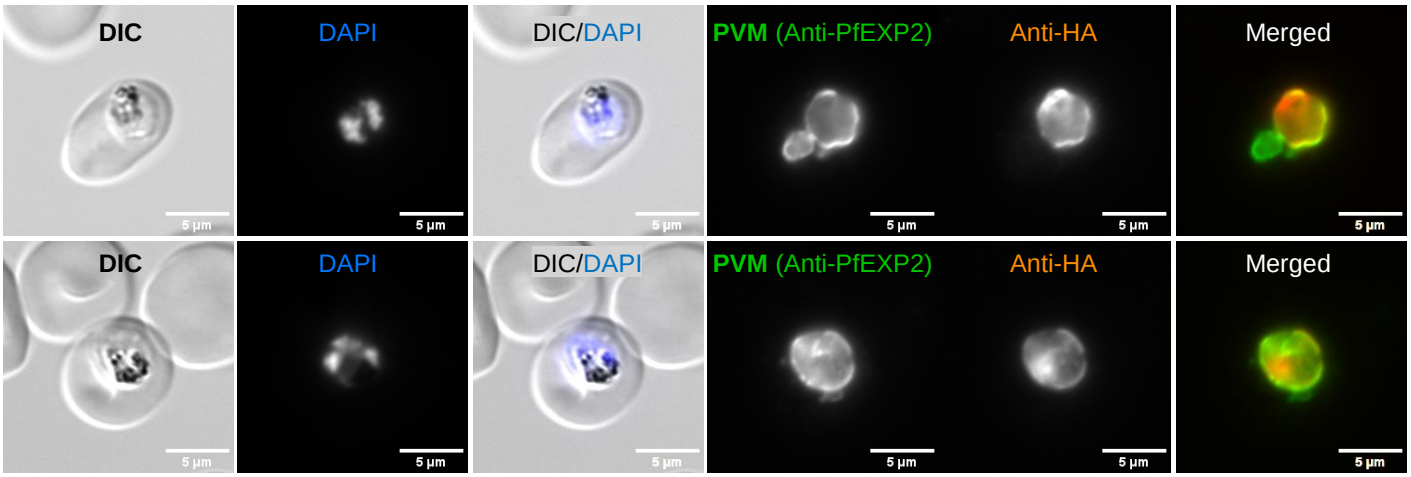
DIC
DAPI
DIC/DAPI
PVM (Anti-PfEXP2)
Anti-HA
Merged
5 µm

C.

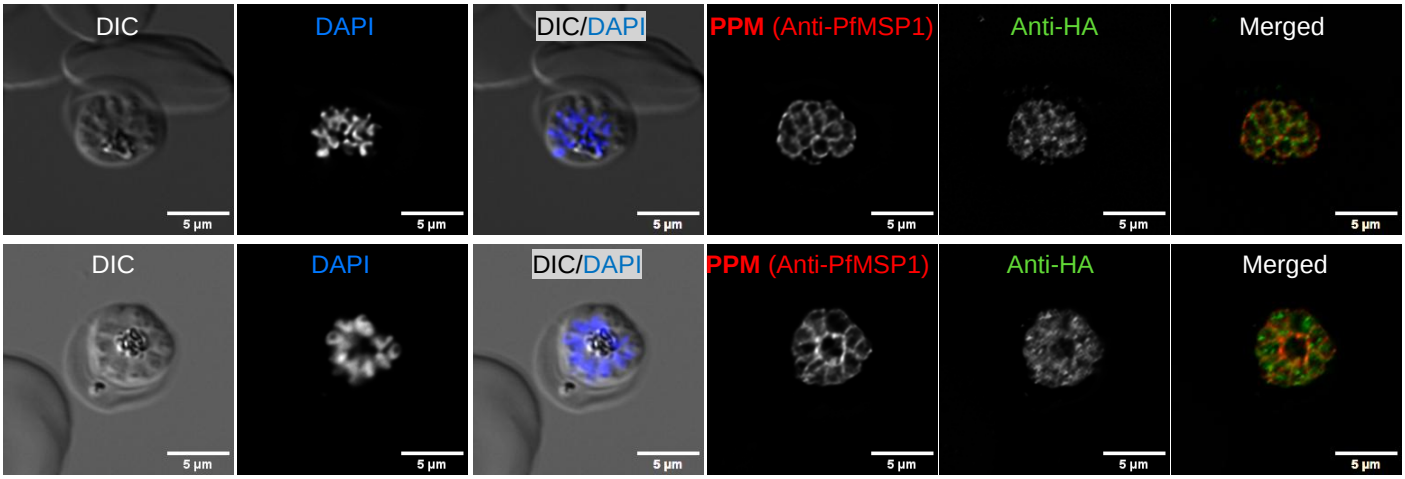
DIC
DAPI
DIC/DAPI
PPM (Anti-PfMSP1)
Anti-HA
Merged
5 µm

D.

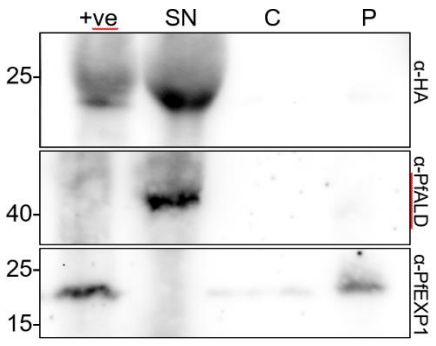
+ve
SN
C
P
25
40
25
15
α-HA
α-PfALD
α-PfEXP1

Fig. 35. IFA images and biochemical fractionation of 23LG-ΔC (Group 4)

(A) Schematic of the 23LG-ΔC variant analyzed in this experiment. Created in BioRender.com. **(B)** Trophozoite-stage IFA of parasites expressing 23LG-ΔC-HA, co-stained with anti-HA and anti-PfEXP2 (PVM marker). The HA signal is detected at the parasite boundary. DAPI stains parasite nuclei; DIC shows parasite morphology. **(C)** Schizont-stage IFA of parasites expressing 23LG-ΔC-HA, co-stained with anti-HA and anti-PfMSP1 (PPM marker). Across 18 schizont images, 16/18 were not interpretable; weak overlap with PfMSP1 was observed in some images. DAPI stains parasite nuclei; DIC shows parasite morphology. **(D)** Biochemical fractionation of 23LG-ΔC-HA analyzed by Western blot (one experiment). Samples were loaded as input (+ve; full cell lysate), supernatant (SN), carbonate (C), and pellet (P) fractions. Anti-HA detects 23LG-ΔC-HA predominantly in the SN fraction.

2.7.7 Group 4: 23LG-ΔN

23LG-ΔN was analyzed by immunofluorescence microscopy in trophozoites and schizonts and by biochemical fractionation. In trophozoites, the HA signal was detected at the parasite boundary and was evaluated relative to PVM marker (Fig. 36, B). In schizonts, 26 images were evaluated. 24/26 images were not interpretable, although in several of these the HA signal appeared to show weak overlap with PPM marker (Fig. 36, C). A biochemical fractionation analysis was performed once. The HA-tagged protein was detected in the supernatant (SN) fraction (Fig. 36, D). Taken together, the available data are most consistent with a soluble pool, which could be located within the PV lumen.

A.

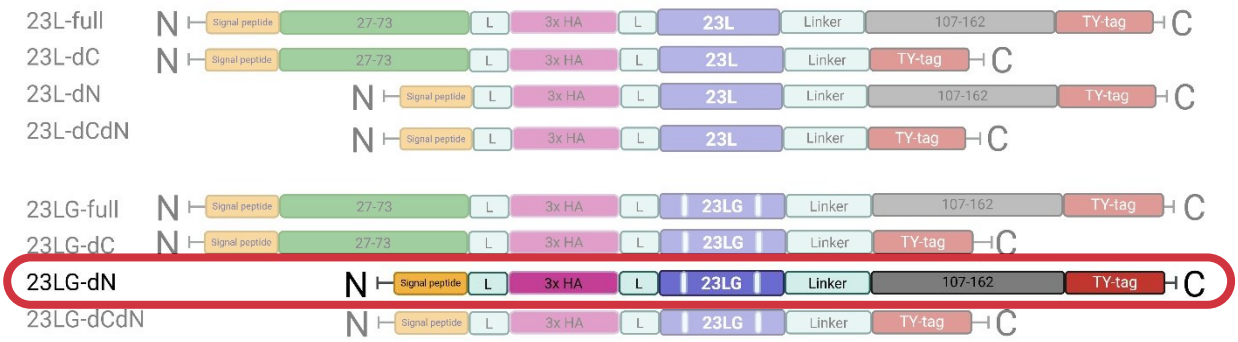
23L-full
23L-dC
23L-dN
23L-dCdN
23LG-full
23LG-dC
23LG-dN
23LG-dCdN
N
C
Signal peptide
27-73
L
3x HA
23L
23LG
Linker
107-162
TY-tag

B.

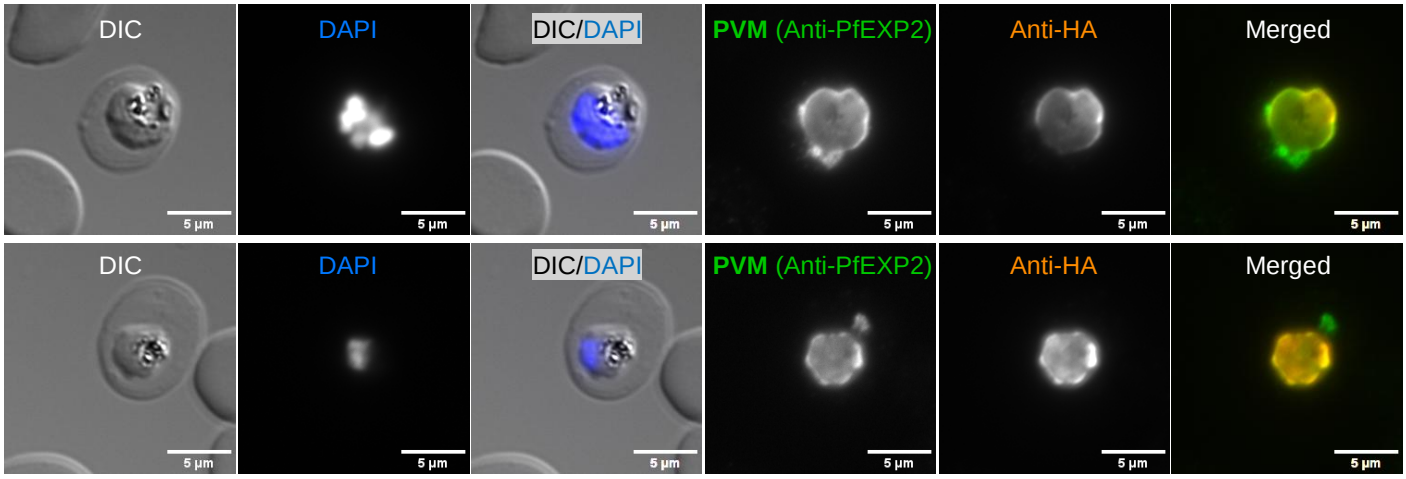
DIC
DAPI
DIC/DAPI
PVM (Anti-PfEXP2)
Anti-HA
Merged
5 µm

C.

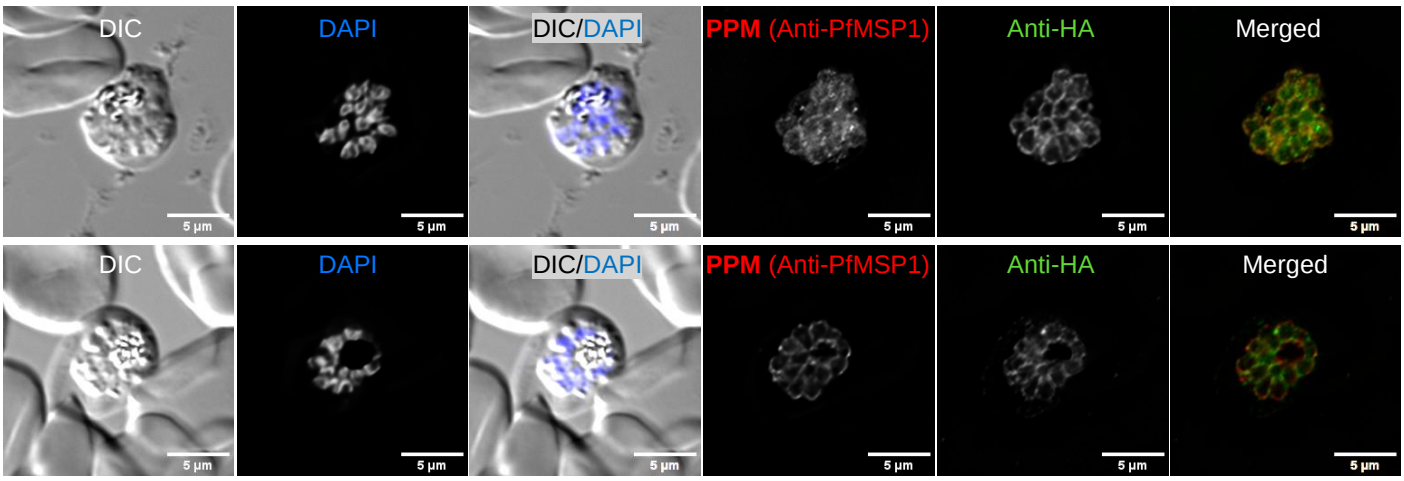
DIC
DAPI
DIC/DAPI
PPM (Anti-PfMSP1)
Anti-HA
Merged
5 µm

D.

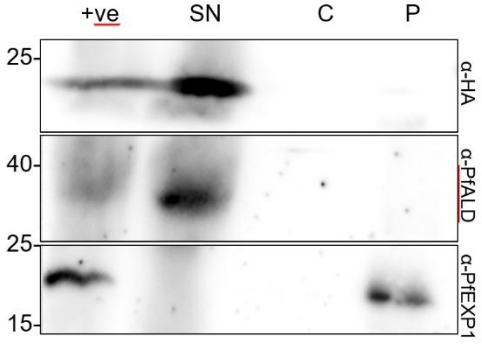
+ve
SN
C
P
25
40
25
15
α-HA
α-PfALD
α-PfEXP1

Fig. 36. IFA images and biochemical fractionation of 23LG-ΔN (Group 4)

(A) Schematic of the 23LG-ΔN variant analyzed in this experiment. Created in BioRender.com. **(B)** Trophozoite-stage IFA of parasites expressing 23LG-ΔN-HA, co-stained with anti-HA and anti-PfEXP2 (PVM marker). The HA signal is detected at the parasite boundary. DAPI stains parasite nuclei; DIC shows parasite morphology. **(C)** Schizont-stage IFA of parasites expressing 23LG-ΔN-HA, co-stained with anti-HA and anti-PfMSP1 (PPM marker). Across 26 schizont images, 24/26 were not interpretable; weak overlap with PfMSP1 was observed in some images. DAPI stains parasite nuclei; DIC shows parasite morphology. **(D)** Biochemical fractionation of 23LG-ΔN-HA analyzed by Western blot (one experiment). Samples were loaded as input (+ve; full cell lysate), supernatant (SN), carbonate (C), and pellet (P) fractions. Anti-HA detects 23LG-ΔN-HA in the SN fraction.

2.7.8 Group 4: 23LG-ΔC/ΔN

23LG-ΔC/ΔN was analyzed by immunofluorescence microscopy in trophozoites and schizonts and by biochemical fractionation. In trophozoites, the HA tag signal was detected at the parasite boundary and was evaluated relative to PfEXP2 (PVM marker) (Fig. 37, B). In schizonts, 30 images were evaluated. All images (30/30) were not interpretable, although the HA signal appeared to show weak overlap with PfMSP1 (PPM marker) in several images (Fig. 37, C). A biochemical fractionation analysis was performed once. The HA-tagged protein was detected predominantly in the pellet (P) fraction, with only minor signal in the supernatant (SN) fraction (Fig. 37, D). With these data, the available evidence suggests localization at the PPM.

A.


23L-full
23L-dC
23L-dN
23L-dCdN
23LG-full
23LG-dC
23LG-dN
23LG-dCdN
N
C
Signal peptide
27-73
L
3x HA
23L
23LG
Linker
107-162
TY-tag

B.

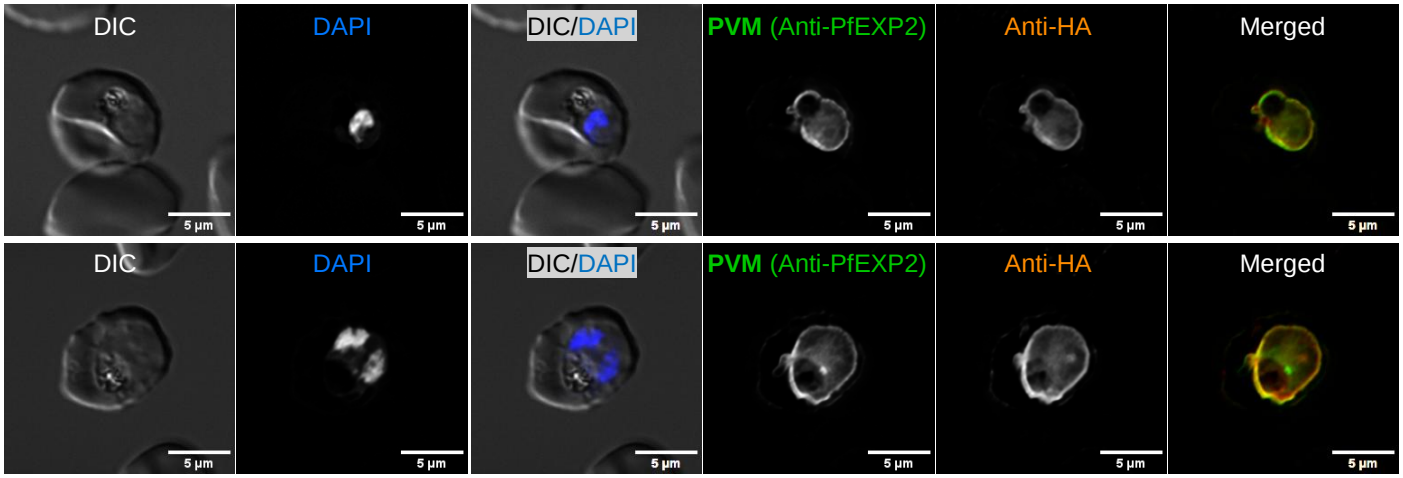
DIC
DAPI
DIC/DAPI
PVM (Anti-PfEXP2)
Anti-HA
Merged
5 µm

C.

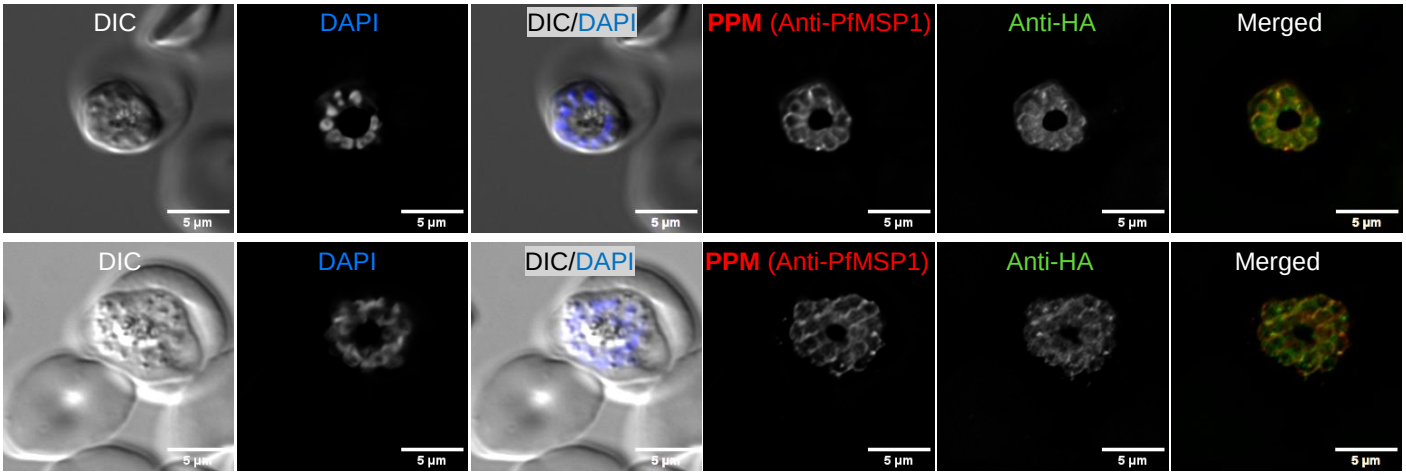
DIC
DAPI
DIC/DAPI
PPM (Anti-PfMSP1)
Anti-HA
Merged
5 µm

D.

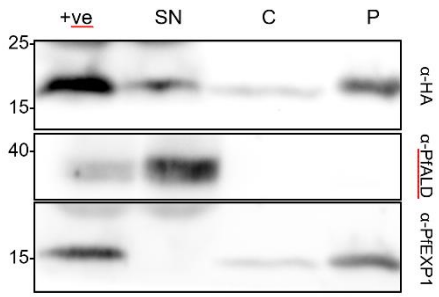
+ve
SN
C
P
25
15
40
15
α-HA
α-PfALD
α-PfEXP1

Fig. 37. IFA images and biochemical fractionation of 23LG-ΔC/ΔN (Group 4)

(A) Schematic of the 23LG-ΔC/ΔN variant analyzed in this experiment. Created in BioRender.com. **(B)** Trophozoite-stage IFA of parasites expressing 23LG-ΔC/ΔN-HA, co-stained with anti-HA and anti-PfEXP2 (PVM marker). The HA signal is detected at the parasite boundary. DAPI stains parasite nuclei; DIC shows parasite morphology. **(C)** Schizont-stage IFA of parasites expressing 23LG-ΔC/ΔN-HA, co-stained with anti-HA and anti-PfMSP1 (PPM marker). Across 30 schizont images, all were not interpretable; weak overlap with PfMSP1 was observed in some images. DAPI stains parasite nuclei; DIC shows parasite morphology. **(D)** Biochemical fractionation of 23LG-ΔC/ΔN-HA analyzed by Western blot (one experiment). Samples were loaded as input (+ve; full cell lysate), supernatant (SN), carbonate (C), and pellet (P) fractions. Anti-HA detects 23LG-ΔC/ΔN–HA predominantly in the pellet (P) fraction, with minor signal in SN.

3 Discussion

After invasion of the erythrocyte, *Plasmodium falciparum* resides within a parasitophorous vacuole (PV) bounded by the parasitophorous vacuolar membrane (PVM), a host-parasite interface that is rapidly remodeled by parasite-derived proteins and supports essential transport processes (Goldberg and Zimmerberg 2020; Beck and Ho 2021). The PVM must accommodate nutrient exchange and protein traffic while remaining closely apposed to the parasite plasma membrane (PPM) (Garten et al., 2018).

PfEXP1 is among the earliest described parasite-encoded proteins associated with the PVM and has long served as a reference marker for this compartment. Classic biochemical and *in vitro* translation studies demonstrated that PfEXP1 is synthesized as an integral membrane protein and supported a defined topology with an N-terminus on the PV-luminal side and a C-terminus exposed to the cytosolic side (Simmons et al., 1987; Günther et al., 1991). Despite this established topology, the signals and rules that ensure selective delivery of PfEXP1 (and other single-pass PVM proteins) to the PVM rather than the PPM remain unresolved; notably, PfEXP1 trafficking to the PVM continues upon PTEX inactivation and is independent of cargo folding, arguing for a pathway distinct from canonical protein export (Tribensky et al., 2017).

This thesis aimed to identify which sequence features of PfEXP1 are required for robust localization to the PVM region and stable membrane insertion. To do this, PfEXP1 variants were engineered in four construct groups (progressive terminal deletions; full-length and domain-removed controls; transmembrane-domain (TMD) swaps with ETRAMP10.1; and synthetic TMD swaps). Localization was assessed primarily by immunofluorescence assay (IFA) and microscopy, alongside sequential extraction as a biochemical readout of membrane association.

A key outcome that shapes interpretation of the entire dataset was that the intended exogenous reference construct (PfEXP1-full) was recovered predominantly in supernatant fractions in sequential extraction, even though endogenous PfEXP1 is an integral membrane protein. This single observation changed the meaning of the entire dataset: it indicates that construct architecture (including tag/linker context) can dominate the readout, so each interpretive claim must be matched to the resolution of the assay.

In summary, across the construct panel, distal C-terminal truncation had broadly PVM-like localization: ΔC50 and PfEXP1-ΔC remained consistent with PVM-like localization in mature schizonts and were pellet-enriched in sequential extraction. In contrast, removal of N-terminal context more often coincided with reduced biochemical evidence for stable membrane association and with less robust localization readouts. Group 4 further showed that strong hydrophobic helices can support membrane association in some architectures but do not reproduce robust PVM localization, indicating that membrane insertion alone is insufficient.

3.1 Group 1: progressive deletion constructs

Group 1 tested whether terminal sequences contain essential information for PfEXP1 delivery to the PVM region. Because parallel work on the full variant series was discontinued after the unexpected behavior of the main control (Group 2), three deletion constructs had sufficient data for interpretation: ΔC50, ΔN50, and ΔN10.

ΔC50 was the most interpretable construct in this group. In trophozoites it showed parasite-boundary signal overlapping with the PVM marker PfEXP2, and in schizonts it produced a clear PVM-like outline distinct from PfMSP1-labeled merozoites. Crucially, sequential extraction detected ΔC50 predominantly in the pellet fraction. Together, these observations support the conservative conclusion that the distal 50 amino acids of the C-terminus are not essential for PVM localization and membrane-associated behavior under the conditions used.

In contrast, ΔN50 was not resolved by microscopy. Trophozoites showed parasite-boundary signal, but schizont-stage imaging was too noisy to be interpreted.

ΔN10 was analyzed next to test whether short (10 aa) N-terminal sequence elements, rather than the larger N-terminal region as a whole, contribute to PfEXP1 targeting. Trophozoite IFA again showed parasite-boundary signal close to PfEXP2, but schizont IFA remained non-diagnostic. Importantly, fractionation performed twice detected ΔN10 predominantly in the supernatant, and no clear pellet enrichment, indicating that this construct does not behave as a stably membrane-integrated species. Since endogenous PfEXP1 is an integral membrane protein, this predominantly soluble/carbonate-extractable behavior was unexpected. In contrast to PfEXP1-full, this result (soluble behavior) is less likely to reflect the same linker/tag architecture effect, because ΔN10 belongs to the simpler deletion series, lacks the linker-containing Group 2 construct format, and carries only a one-sided tag. This supports the interpretation that loss of N-terminal sequence itself may contribute to the observed defect in stable membrane association and/or PVM targeting. This point is discussed further in the Conclusions.

3.1.1 Take-home (Group 1)

C-terminal truncation (ΔC50) did not prevent PVM localization and pellet enrichment in this assay context. Evidence for a specific N-terminal targeting element is weaker in the incomplete Group-1 dataset, but the ΔN10 fractionation behavior is consistent with an N-terminal contribution to stable membrane association and/or robust targeting.

3.2 Group 2: controls reveal the central interpretation problem

Group 2 provided the baseline needed to interpret all deletion and swap constructs by testing whether the tagged expression format yields a well-behaved full-length reference and whether removal of major regions (ΔC, ΔN, ΔC/ΔN) alters localization or membrane association in predictable ways.

3.2.1 PfEXP1-full: the reference construct is predominantly soluble

Anti-HA signal in trophozoite IFA appeared at the parasite boundary, but mature schizont IFA was largely non-diagnostic. Most importantly, biochemical fractionation (four repeats) detected PfEXP1-full predominantly in supernatant. Thus, in this expression format the intended full-length reference does not behave as a robust membrane-integrated positive control. This most likely reflects a construct-dependent effect of the engineered tag/linker context on membrane insertion and/or topology, which limits the use of PfEXP1-full as an architectural control.

3.2.2 PfEXP1-ΔC: strongest PVM-insertion behavior among Group 2 controls

PfEXP1-ΔC gave the most consistent membrane-associated profile among Group-2 controls. It showed a PVM-like signal in schizonts in the majority of interpretable images and was predominantly pellet-enriched in two independent biochemical fractionations. These data support the conclusion that removal of the C-terminal region does not prevent PVM-like localization and membrane association under the conditions used.

3.2.3 PfEXP1-ΔN and PfEXP1-ΔC/ΔN: soluble behavior

PfEXP1-ΔN produced trophozoite IFA similar to other controls, but fractionation performed twice detected PfEXP1-ΔN predominantly in carbonate with minor supernatant signal. The most conservative interpretation is that PfEXP1-ΔN is present mainly as a soluble or loosely associated pool in the PV lumen rather than a PVM-integrated species under these conditions. Similarly, PfEXP1-ΔC/ΔN showed parasite-boundary signal in trophozoites (overlap with PfEXP2), and fractionation twice again detected predominantly carbonate with minor supernatant. This pattern also fits better with a soluble/weakly associated pool in the PV lumen rather than a clearly membrane-integrated PVM protein.

3.2.4 Take-home from Group 2

(1) The full-length exogenous reference construct (PfEXP1-full) is not a robust membrane-integrated architectural control in this format, imposing a major caution on interpretation;
(2) PfEXP1-ΔC is the most consistent membrane-associated construct in Group 2
(3) ΔN and ΔC/ΔN show carbonate/SN-enriched behavior consistent with solubility or weak integration.

3.2.5 Group 2 conclusion

A simplistic interpretation would be that constructs lacking the C-terminus but retaining the N-terminus "go to the PVM," whereas constructs that retain the C-terminus or lack the N-terminus become problematic. The most defensible conclusions from Groups 1 and 2 are therefore: (1) ΔC50 supports that the distal C-terminal 50 amino acids are not essential for PVM localization; (2) the solubility of PfEXP1-full indicates a construct-dependent issue that likely influences membrane insertion and/or topology; and (3) differences among Group 2 variants are best interpreted as architecture-dependent effects on membrane insertion behavior, rather than evidence for a simple biological model in which the C-terminus "blocks" trafficking.

3.2.6 Synthesis of Groups 1-2

Taken together, Groups 1-2 support a conservative but consistent message: removal of distal C-terminal sequence did not prevent PVM-like localization in our assays (ΔC50 and PfEXP1-ΔC), whereas removal of N-terminal context was more often associated with reduced biochemical evidence for membrane insertion and less robust localization readouts.

3.3 Group 3: PfETRAMP10.1 transmembrane-domain replacement

Group 3 was designed to test whether swapping the TMD of PfEXP1 with the TMD from another PVM-resident ETRAMP protein (PfETRAMP10.1) preserves PVM-like localization.

PfETRAMP10.1-full and PfETRAMP10.1-ΔC: predominantly PVM-like patterns in schizonts

Both PfETRAMP10.1-full and PfETRAMP10.1-ΔC showed parasite-boundary signal in trophozoites with overlap to PfEXP2, and in schizonts they were predominantly scored as PVM-like, consistent with localization to the PVM region. This supports the view that replacing the PfEXP1 TMD with the PfETRAMP10.1 TMD does not disrupt a PVM-like schizont pattern, at least when the PfEXP1 N-terminal region is retained.

3.3.1 PfETRAMP10.1-ΔN and PfETRAMP10.1-ΔC/ΔN: more PPM-like patterns

When the PfEXP1 N-terminus was removed (PfETRAMP10.1-ΔN and PfETRAMP10.1-ΔC/ΔN), schizont images became substantially more difficult to interpret, and the evaluable subset more often showed overlap consistent with the PPM marker PfMSP1 rather than a clear PVM-like outline. This shift suggests that, within this construct architecture, the PfEXP1 N-terminal context contributes to the clearest PVM-like outcomes.

Because biochemical fractionation was not performed for Group 3, these conclusions are limited to the microscopy readout.

3.3.2 Working conclusion from Group 3

A PVM-protein-derived TMD can support PVM-like localization patterns in schizonts, and the PfEXP1 N-terminal context contributes to the clearest outcomes in this construct architecture; however, biochemical validation is required to link these patterns to membrane association and topology.

3.3.3 Combined interpretation of Groups 1–3

Based on the deletion series and control constructs (Groups 1–2), and supported by the TMD-swap patterns in Group 3, removal of distal C-terminal sequence did not prevent PVM-like localization, whereas removal of the N-terminal region tended to produce less robust localization readouts. At this stage, this trend is best interpreted as an N-terminal contribution to robust PVM localization. This conclusion is reassessed in light of Group 4, which tests whether PVM-like localization can be supported by artificial TMD architectures in the absence of native PfEXP1 sequence context.

3.4 Group 4: synthetic transmembrane helices (23L / 23LG)

Group 4 was designed to test TMD sufficiency. Instead of swapping the PfEXP1 TMD for another parasite-derived TMD (Group 3), we replaced it with artificial helices: a purely hydrophobic poly-leucine (23L) segment as a “neutral” membrane anchor, and a modified version (23LG) containing glycine residues. These designs were motivated by the reported functional importance of small residues within the native PfEXP1 TMD and by the broader idea that glycine-containing motifs can influence helix packing (Zhao et al., 2012; Teese and Langosch, 2015; Bugge et al., 2016). Importantly, these constructs used the same general architecture as Groups 2–3 (linkers/tags), allowing the effect of TMD composition to be tested within a shared design context.

3.4.1 23L variants: PVM targeting not supported

For 23L-full, trophozoites showed signal at the parasite boundary; in schizonts, the evaluable images most often showed overlap consistent with the PPM region. The 23L-ΔC and 23L-ΔN were largely non-diagnostic by schizont IFA (noisy signal). For 23L-ΔC/ΔN, one fractionation experiment detected the HA-tagged protein predominantly in the pellet, indicating membrane insertion; however, schizont IFA was again largely not interpretable, and the available evidence was judged most consistent with localization at the PPM rather than the PVM.

3.4.2 23LG variants: mixed behavior, either membrane-associated or soluble

For 23LG-full, one fractionation experiment detected the protein predominantly in the pellet, again consistent with membrane association; schizont IFA was mostly not interpretable, and the available evidence was interpreted as most consistent with localization at the PPM. In contrast, 23LG-ΔC and 23LG-ΔN each showed a clear biochemical shift toward the supernatant (SN) fraction in fractionation experiments, consistent with a predominantly soluble pool, plausibly within the PV lumen. Finally, 23LG-ΔC/ΔN was detected predominantly in the pellet (with minor SN), but schizont IFA remained not interpretable; the available evidence was again interpreted as most consistent with PPM localization.

3.4.3 Working conclusion from Group 4

Across Group 4, a strongly hydrophobic synthetic helix could support pellet enrichment in some constructs, demonstrating that membrane association can be achieved within this format. However, a generic hydrophobic anchor did not reproduce robust PVM localization: where anti-HA signal in schizont IFA was interpretable, localization more often supported the PPM region, and in other variants fractionation indicated predominantly soluble in the PV.

3.5 Determinants of PVM localization in this dataset

Across the complete construct panel, the clearest supported conclusion is that the distal C-terminal cytosolic tail is not strictly required for PVM-like localization and membrane-associated fractionation in our assay context. This is most strongly supported by ΔC50 and PfEXP1-ΔC, which show clear PVM-like schizont outlines and are pellet-enriched in fractionation. In the independent construct panel of Mesén-Ramírez et al. (2019), multiple C-terminal deletion variants - including PfEXP1ΔC105–162 (and also PfEXP1ΔC131–162 and PfEXP1ΔC145–162) - show a peripheral schizont signal and partition predominantly with the parasite pellet in a saponin-based supernatant/pellet (SN/P) assay (Fig. 38). Taken together, both studies support the conclusion that the distal C-terminal region is not a dominant determinant for PVM targeting.

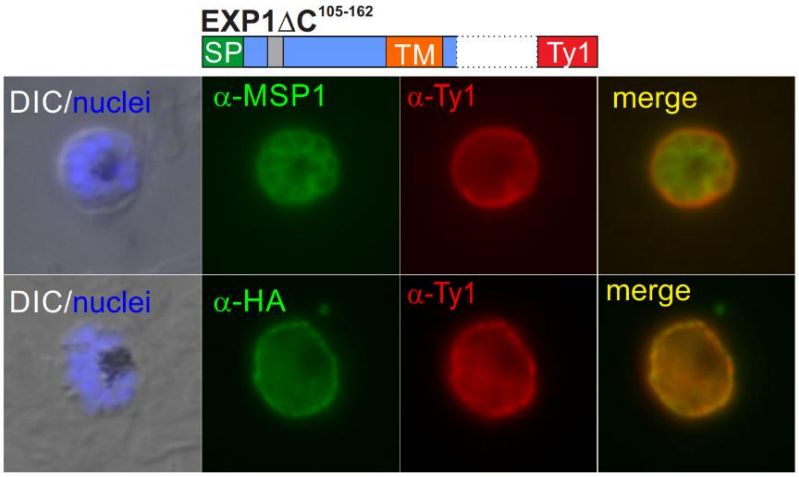

Fig. 38. C-terminal deletion of PfEXP1 construct in Mesén-Ramírez et al. study

Schizont IFA (2019; Suppl. Fig. S3) showing that the C-terminal deletion variant (e.g., EXP1ΔC105–162) shows a peripheral schizont signal consistent with PVM localization in that study. Adapted from Mesén-Ramírez et al. (2019), PLOS Biology.

In contrast, removal of N-terminal context was repeatedly associated with less robust outcomes and reduced biochemical evidence for stable membrane association. ΔN10 is predominantly supernatant/carbonate in two fractionations, and Group 2 PfEXP1-ΔN and PfEXP1-ΔC/ΔN constructs are carbonate/SN-enriched, consistent with soluble in the PV lumen. In Group 3, N-deleted TMD-swap constructs were also substantially more ambiguous by schizont IFA than their N-retaining counterparts. Mesén-Ramírez et al. (2019) also include an N-truncated PfEXP1 variant ("EXP1ΔN$^{\text{short}}$") and interpret the schizont IFA as PVM localization (fig. 39). However, the representative image is not diagnostic: the PfEXP1ΔN$^{\text{short}}$ signal is weak/discontinuous and does not form a convincing continuous boundary/rim around the schizont, making it difficult to assign PVM insertion based on microscopy alone. Therefore, we treat this specific "PVM localization" call as supportive at best, and emphasize that membrane identity and orientation require additional biochemical/topology-resolving validation (as also discussed throughout our dataset).

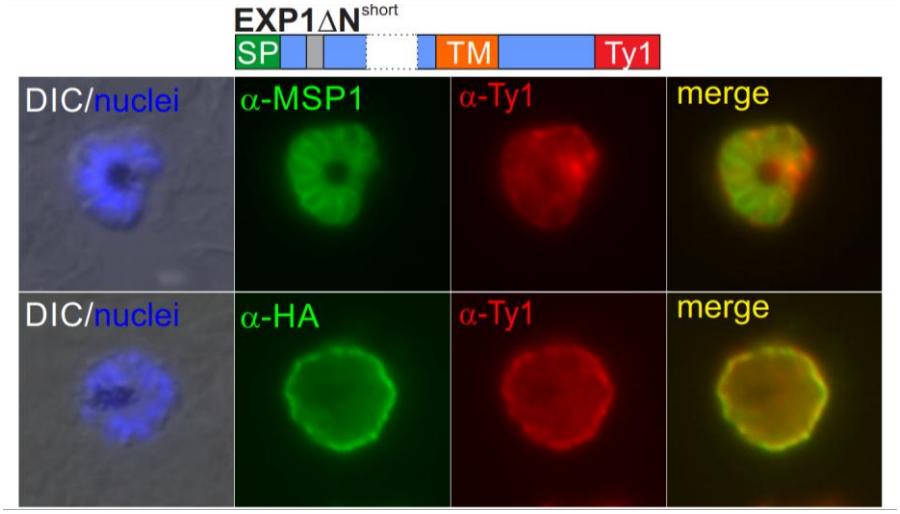

Fig. 39. Mesén-Ramírez et al. "EXP1ΔNshort" schizont IFA

Representative schizont IFA image for the PfEXP1ΔN^{short} variant from Mesén-Ramírez et al. (2019; Suppl. Fig. S3A), referenced here as an example where the signal is not diagnostic for confident PVM insertion by IFA alone. Adapted from Mesén-Ramírez et al. (2019), PLOS Biology.

An important directly relevant observation in Mesén-Ramírez et al. (2019) is that the C-terminal PfEXP1wt–mScarlet fusion shows an unusually large soluble pool: in their saponin-based partitioning assay (where SN contains PV/host soluble proteins and P contains parasite-associated material), PfEXP1wt–mScarlet produces a strong α-RFP signal in the supernatant as well as the pellet (Fig. 40), indicating substantial release into the PV/host soluble fraction. This provides an external precedent for our central interpretive issue: our episomally expressed PfEXP1-full reference construct likewise fails to behave as a robust membrane-integrated control and is recovered predominantly in supernatant fractions. These observations support the conclusion that tags and linkers identity/placement and overall construct architecture can strongly influence PfEXP1's PVM insertion and therefore must be validated biochemically before a tagged construct is used as the reference for mapping targeting determinants.

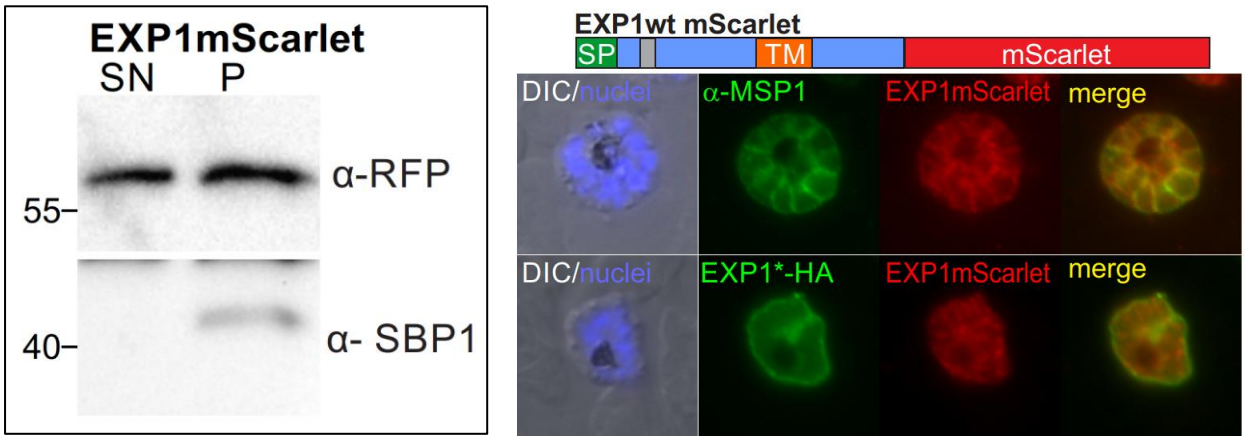

Fig. 40. PfEXP1wt-mScarlet shows a substantial soluble pool in SN/P partitioning

Left: Immunoblot excerpt from Mesén-Ramírez et al. (2019; Suppl. Fig. S3B) showing PfEXP1wt–mScarlet detected in both SN and pellet (P) fractions, providing an external precedent for construct-context–dependent solubility. **Right:** Representative schizont IFA image for the PfEXP1wt–mScarlet variant from Mesén-Ramírez et al. (2019; Suppl. Fig. S3A). Adapted from Mesén-Ramírez et al. (2019), PLOS Biology.

Taken together, these findings are most consistent with a combinatorial contribution to PVM localization: distal C-terminal sequence is broadly dispensable, while N-terminal context together with an appropriate PVM-protein-derived transmembrane domain most often yields the clearest PVM-like outcomes. Group 4 further shows that strong hydrophobicity can support membrane association but is not sufficient to reproduce robust PVM localization, indicating that determinants beyond generic hydrophobicity are required.

Because the exogenously expressed PfEXP1-full reference behaved unexpectedly in fractionation, we interpret these conclusions as trends in this expression format rather than as a precise map of targeting signals.

3.6 Assay and construct design considerations

3.6.1 Why IFA was used as a first screen (and what it cannot decide)

We started with IFA mainly because it is fast and allows rapid screening. As a first pass, this is useful to see whether a variant remains within the parasite, accumulates at the parasite boundary, or shows an obviously aberrant pattern (for example, ER-like staining). However, IFA is not a definitive decision assay especially in trophozoites because the PPM and PVM are extremely closely apposed, so a boundary signal cannot reliably distinguish the two membranes. In schizonts, interpretation is typically stronger because the PVM can form a single outline around the mature schizont while PfMSP1 highlights individual merozoites' PPM; accordingly, many studies rely primarily on schizont IFA for PVM assignment.

Nevertheless, even schizont IFA is not fully definitive, and PV-lumen pools positioned close to the boundary can complicate interpretation. In addition, localization can vary between individual parasites within the same line, and IFA typically involves scoring only tens of selected cells, so borderline cases can become observer-dependent and sensitive to image quality. For these reasons, biochemical-based assays provide a stronger complement: they report on large parasite populations and can deliver clearer yes/no answers about membrane identity and topology. For example, selective permeabilization combined with protease protection provides a direct readout of accessibility and orientation that microscopy alone cannot provide (Tribensky et al. 2017).

3.6.2 What sequential extraction adds

To address the specific limitation that IFA cannot distinguish membrane-integrated from soluble or weakly associated pools, we complemented IFA with sequential extraction/fractionation. This allowed constructs to be classified based on enrichment in supernatant (SN), carbonate-extractable (C), or pellet (P) fractions, providing information that microscopy alone cannot deliver. In practice, this biochemical readout became essential once PfEXP1-full construct was found to be predominantly soluble: without fractionation, several constructs would have appeared ‘reasonable’ by IFA but could not be interpreted in terms of membrane association.

3.6.3 Topogenesis: why PfEXP1-full solubility is surprising

From a membrane-insertion (topogenesis) perspective, PfEXP1-full behaving mainly soluble was genuinely unexpected. In the canonical pathway, the N-terminal signal peptide is recognized early during translation, recruits the ribosome to the ER via signal recognition particle (SRP), and engages the Sec61 translocon. Once the nascent chain is feeding into Sec61, a true stop-transfer helix is normally inserted laterally into the membrane as it emerges through the translocon’s lateral gate, producing a stable single-pass membrane protein. In that logic, the TMD is synthesized only after ER targeting has already happened, so “never integrating at all” should not be the default outcome for a construct that still carries a signal peptide and a hydrophobic helix. Therefore, the PfEXP1-full fractionation profile suggests either (i) inefficient recognition/integration of the membrane-anchor module in its engineered tag/linker context, or (ii) an initially integrated protein that later loses stable membrane association. The current readouts cannot distinguish these possibilities, but the key point for the Discussion is that construct design can change the biology you think you are reading out; not just the microscopy aesthetics.

3.6.4 Brefeldin A as a practical diagnostic follow-up

Brefeldin A (BFA) is a classical tool to block ER-to-Golgi trafficking and to collapse early Golgi compartments back into the ER, thereby trapping newly synthesized secretory and membrane proteins in an ER-enriched state (Fujiwara et al. 1988; Lippincott-Schwartz et al. 1989). In *P. falciparum*, BFA was shown to reversibly block secretion of newly synthesized proteins and impair parasite maturation, supporting the presence of a conserved secretory step in the parasite (Crary and Haldar 1992). In the context of this thesis, BFA would be useful as a diagnostic follow-up to clarify at which stage the PfEXP1-full 'solubility/weak association' phenotype arises. If PfEXP1-full is already soluble or weakly associated at the ER stage, then trapping it with BFA would not be expected to show pellet enrichment. By contrast, if the construct integrates into membranes initially but becomes destabilized at a later stage after leaving the ER, then blocking ER exit with BFA could show the distribution toward a more membrane-integrated pool (pellet). Even though this would still not resolve membrane identity or orientation, it would help localize the likely failure point (early insertion versus later destabilization) and guide rational redesign of tags/linkers.

3.6.5 Tag and linker context can change the readout

A major take-home message from this work is the sensitivity of membrane-protein localization readouts to construct design. Protein tags, for example, are invaluable tools, but they can also alter localization or behavior in localization studies, and this caution has been discussed explicitly in the broader literature (Schneider and Hackenberger 2017). In our dataset, the unexpected solubility of PfEXP1-full highlights that even modest design features (tags and/or linkers) can affect membrane insertion and/or stability. This is not just a technical inconvenience: if a tag or linker changes the way the TMD is read during insertion, then "mapping targeting signals" becomes confounded by topogenesis effects.

3.6.6 DeepTMHMM as a supportive check

As a supportive in silico check, we used DeepTMHMM to inspect whether engineered sequences retained a confidently predicted transmembrane helix and topology. In several designs, inclusion of tags/linkers reduced the confidence of transmembrane predictions relative to the native sequence, consistent with the idea that construct context can influence apparent topogenesis. These predictions are not proof of behavior *in vivo*, but they served as a useful warning sign while interpreting difficult constructs.

3.6.7 Charge bias and the positive-inside rule

A further design consideration is charge. For many single-pass membrane proteins, positively charged residues are enriched on the cytosolic side of transmembrane helices, and this charge bias contributes to both topology choice and insertion efficiency (the 'positive-inside rule') (Von Heijne 1986; Lerch-Bader et al. 2008). Quantitative insertion studies also show that Lys/Arg residues placed near the cytosolic end of a helix can measurably promote membrane insertion and influence orientation, particularly for segments that are near the threshold of hydrophobicity (Lerch-Bader et al. 2008; Virkki et al. 2014). In our construct series, tags, linkers and terminal deletions alter the distribution of charged residues flanking the helix. A plausible consequence is that some variants may insert with an altered orientation ('flip') compared with native PfEXP1, or insert less efficiently, increasing the fraction that is released into the PV as a soluble pool. This matters for signal mapping: if a determinant required for PVM delivery is normally presented on the PV lumen side, a flipped construct would present that determinant to the parasite cytosol instead, where it may be invisible to the relevant machinery. In that scenario, the protein could fail to be delivered or retained at the PVM and instead accumulate at non-PVM locations or populate soluble in the PV lumen, even though the primary sequence 'determinant' is still present. Therefore, differences among variants should be interpreted not only as loss of a targeting determinant, but also as a potential topology/insertion effect driven by altered flanking-charge context.

3.6.8 Protease protection: the missing topology-resolving assay

Ultimately, the decisive way to distinguish membrane identity (PPM versus PVM versus PV lumen) and determine orientation is protease protection combined with selective permeabilization, as exemplified for PfEXP1 reporters by Tribensky et al. (2017). In brief, streptolysin O (SLO) selectively permeabilizes the erythrocyte membrane while leaving the PVM intact, so that an exogenous protease (for example, proteinase K) can digest domains exposed to the host cytosol while protected luminal domains remain intact. Subsequent treatment with saponin permeabilizes the PVM and releases PV contents while leaving the parasite plasma membrane largely intact, enabling discrimination between domains that were protected behind the PVM/PPM and those located in the PV lumen. Applied to dual-tagged PfEXP1 constructs, this strategy can distinguish four key outcomes (two possible orientations in the PVM and two in the PPM). This matters because a construct can appear boundary-localized by IFA yet be inserted into the PPM instead of the PVM, or inserted with the wrong orientation; and fractionation alone will not resolve either membrane identity or topology. An analogous strategy was planned for key constructs in this thesis, but was not completed, leaving orientation and definitive membrane identity unresolved for variants.

3.7 Limitations and decisive next experiments

A key limitation throughout is that microscopy alone cannot resolve PVM versus PPM at the parasite boundary, cannot distinguish membrane integration from soluble inside the PV lumen, and cannot determine orientation. Not all planned variant series were completed, and Group 3 lacks biochemical fractionation, limiting conclusions from that group to the microscopy readout.

3.8 Priority follow-up experiments

1. **Protease protection with selective permeabilization.** This is the highest-priority follow-up experiment to resolve membrane identity (PPM versus PVM versus PV lumen) and determine orientation, following published workflows for PfEXP1 reporters (Tribensky et al., 2017).
2. **Re-establishment of a robust reference construct.** Tag and linker placement should be redesigned, or an endogenously tagged PfEXP1 reference should be validated, and membrane association should be confirmed biochemically before additional variants are interpreted.

3.9 Conclusions

This thesis used systematic construct engineering to identify sequence features that support PfEXP1 targeting to the parasitophorous vacuolar membrane (PVM) region and, where measured, stable membrane association. Across the complete construct panel, the most consistent supported conclusion is that the distal C-terminal region is not the dominant determinant of PVM-like localization in the assay systems used here. This is best supported by ΔC50 and PfEXP1-ΔC, both of which showed a schizont pattern consistent with PVM-like localization and were enriched in the pellet fraction during sequential extraction. PfETRAMP10.1-ΔC provided additional microscopy-only support for this trend. Together, these data indicate that removal of distal C-terminal sequence does not by itself prevent membrane-associated behavior or PVM-like localization under these experimental conditions. In contrast, disruption of N-terminal context was more often associated with loss of robust biochemical evidence for membrane insertion and with less conclusive localization readouts. The clearest example is ΔN10, which remained predominantly in the supernatant and carbonate fractions and did not show a convincing PVM-like schizont pattern. A similar trend was observed in the Group 2 control constructs lacking N-terminal context, which were not pellet-enriched and more often behaved like soluble or only weakly associated species. Although the present dataset does not define a precise linear targeting motif, it supports the conclusion that N-terminal context contributes importantly to correct PfEXP1 targeting and/or stable insertion at the PVM.

The transmembrane-domain replacement experiments further showed that not all hydrophobic segments behave equivalently. When the native PfEXP1 transmembrane domain was replaced with the transmembrane domain of the related PVM protein PfETRAMP10.1, constructs retaining PfEXP1 N-terminal context still frequently showed a PVM-like schizont pattern. In contrast, synthetic hydrophobic helices did not reproduce robust PVM-like localization, even when combined with both PfEXP1-derived terminal regions. These findings argue against a model in which hydrophobicity alone is sufficient for correct targeting. Instead, they support the view that a compatible parasite-derived transmembrane domain and the PfEXP1 N-terminal context act together more effectively than artificial TMDs in promoting correct localization behavior.

Based on the complete dataset, the results are most consistent with a working model involving three separable signals. First, the signal peptide directs entry into the parasite secretory pathway and initial membrane insertion. Second, the transmembrane domain must be compatible with a further trafficking step beyond the parasite plasma membrane, namely a step that permits removal from the PPM, passage through the PV lumen, and reinsertion into the PVM. Third, the N-terminal region appears to provide a luminal determinant required for this transport system. In this model, the relevant machinery would act from the PV lumen side. This interpretation is consistent with the established PV-luminal position of the PfEXP1 N-terminus and with the unresolved post-PPM trafficking step highlighted by Tribensky et al. (2017). This working model is summarized in Fig. 41.

This model provides a possible explanation for the main trends observed in this thesis. Constructs containing artificial hydrophobic TMDs may fail at the second requirement and therefore remain at or near the PPM instead of reaching the PVM. By contrast, when a more compatible parasite-derived TMD is present but the N-terminal luminal determinant is missing, the system may still be able to remove the protein from the PPM, but cannot complete productive reinsertion into the PVM. In that case, the protein would be expected to accumulate as a soluble or weakly associated pool in the PV lumen. In this sense, the data support a model in which correct PfEXP1 localization depends not only on entering the membrane, but on successfully completing a second, selective transfer step from the PPM to the PVM.

This model remains hypothetical and should be interpreted cautiously. An important limitation of this study is that the exogenous full-length PfEXP1 reference construct behaved unexpectedly in the sequential extraction assay and was recovered predominantly in soluble and/or carbonate-extractable fractions.

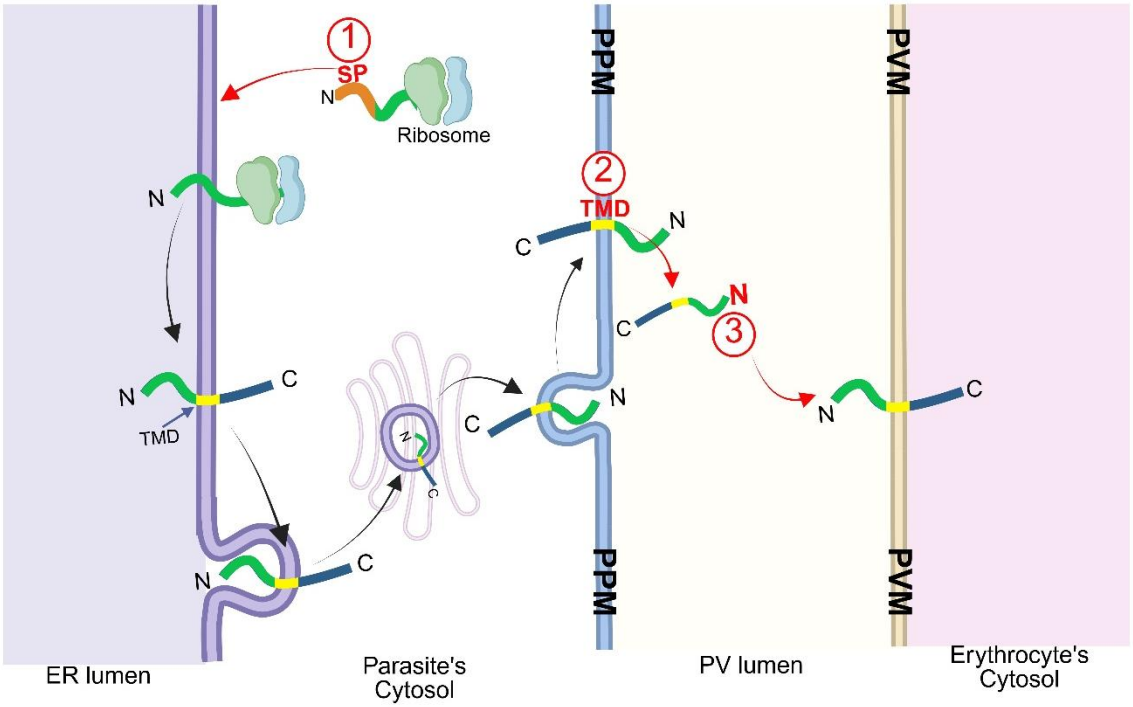

Fig. 41. Hypothetical model for PfEXP1 targeting from the PPM to the PVM

Schematic model proposing that PfEXP1 localization to the PVM depends on three separable signals:

1- **Signal peptide (SP)** for entry into the secretory pathway

2- **Transmembrane domain (TMD)** for removal from the PPM and transfer toward the PVM

3- **N-terminal luminal determinant** required for successful transport and reinsertion at the PVM.

In this model, failure of the TMD-dependent step favors retention at or near the PPM, whereas loss of the N-terminal luminal determinant allows removal from the PPM but prevents productive reinsertion, leading to accumulation as a soluble or weakly associated pool in the PV lumen. The model is hypothetical and is consistent with previous work showing that PfEXP1 trafficking to the PVM is independent of PTEX and protein unfolding (Tribensky et al. 2017). Created in BioRender.com

Because endogenous PfEXP1 is a well-established integral membrane protein, this result indicates that construct architecture itself, including tag and linker context, can substantially influence the readout. For this reason, the conclusions drawn here should be interpreted as trends within the present expression system rather than as a definitive map of PfEXP1 targeting information. Nevertheless, the internal consistency of several construct classes supports the relevance of the patterns observed here.

Overall, this study supports a model in which correct PfEXP1 targeting to the PVM depends on more than simple membrane insertion. The distal C-terminal region appears broadly dispensable in this assay context, whereas N-terminal context and a compatible parasite-derived transmembrane domain most often correlate with the clearest PVM-like outcomes. The decisive next step is now to test this model directly with topology-resolving assays, particularly protease protection combined with selective permeabilization, in order to determine whether the proposed N-terminal contribution acts during removal from the PPM, during transfer through the PV lumen, or during reinsertion and stabilization at the PVM itself.

4 Materials and Methods

4.1 Materials

4.1.1 Organisms and Cell Lines

Table 2. Organisms and cell lines

Strain/Cell Line	Description	Source
E. coli TOP10	Electro-competent Strain. Genotype: F–mcrA Δ(mrr-hsdRMS-mcrBC) φ80lacZΔM15 ΔlacX74 recA1 araD139 Δ(ara-leu)7697 galU galK λ– rpsL(Str^R) endA1 nupG	Life Technologies, Carlsbad, USA
E. coli XL1-Blue	Chemically Competent Strain. Genotype: recA1 endA1 gyrA96 thi-1 hsdR17 supE44 relA1 lac [F proAB laclqZΔM15 Tn10 (Tetr)]	Agilent Technologies, Waldbronn, Germany
P. falciparum 3D7	Wild-type parasite	Walliker et al., 1987
P. falciparum CS2	Wild-type parasite	Beeson et al., 2000
CL-22.0025 (3D7)	pVP1-**ETRAMP10.1**-Full-PF3D7-22.0025 transfected into *P. falciparum* 3D7	Generated during the project
CL-22.0026 (3D7)	pVP1-**PfEXP1-Full**-PF3D7-22.0026 transfected into *P. falciparum* 3D7	Generated during the project
CL-23.0001 (3D7)	pVP1-**ETRAMP10.1-ΔN**-PF3D7-23.0001 transfected into *P. falciparum* 3D7	Generated during the project
CL-23.0002 (3D7)	pVP1-**ETRAMP10.1-ΔC**-PF3D7-23.0002 transfected into *P. falciparum* 3D7	Generated during the project
CL-23.0003 (3D7)	pVP1-**ETRAMP10.1-ΔC/ΔN**-PF3D7-23.0003 transfected into *P. falciparum* 3D7	Generated during the project
CL-23.0004 (3D7)	pVP1-**PfEXP1-ΔN**-PF3D7-23.0004 transfected into *P. falciparum* 3D7	Generated during the project

Strain/Cell Line	Description	Source
CL-23.0005 (3D7)	pVP1-**PfEXP1-ΔC**-PF3D7-23.0005 transfected into *P. falciparum* 3D7	Generated during the project
CL-23.0006 (3D7)	pVP1-**PfEXP1-ΔC/ΔN**-PF3D7-23.0006 transfected into *P. falciparum* 3D7	Generated during the project
CL-23.0007 (3D7)	pVP1-**23L**-PfEXP1_TMD-PF3D7-22.0007 transfected into *P. falciparum* 3D7	Generated during the project
CL-23.0008 (3D7)	pVP1-**23L**-PfEXP1_TMD-ΔN-PF3D7-22.0008 transfected into *P. falciparum* 3D7	Generated during the project
CL-23.0009 (3D7)	pVP1-**23L**-PfEXP1_TMD-ΔC-PF3D7-22.0009 transfected into *P. falciparum* 3D7	Generated during the project
CL-23.0010 (3D7)	pVP1-**23L**-PfEXP1_TMD-ΔN/ΔC-PF3D7-22.00010 transfected into *P. falciparum* 3D7	Generated during the project
CL-23.0011 (3D7)	pVP1-**23LG**-PfEXP1_TMD-PF3D7-22.00011 transfected into *P. falciparum* 3D7	Generated during the project
CL-23.0012 (3D7)	pVP1-**23LG**-PfEXP1_TMD-ΔN-PF3D7-22.00012 transfected into *P. falciparum* 3D7	Generated during the project
CL-23.0013 (3D7)	pVP1-**23LG**-PfEXP1_TMD-ΔC-PF3D7-22.00013 transfected into *P. falciparum* 3D7	Generated during the project
CL-23.0014 (3D7)	pVP1-**23LG**-PfEXP1_TMD-ΔN/ΔC-PF3D7-22.00014 transfected into *P. falciparum* 3D7	Generated during the project

4.1.2 Gene IDs

Table 3. Gene IDs

Name	Gene ID *P. falciparum* 3D7	Gene annotation
PfEXP1	PF3D7_1121600	*P. falciparum* exported protein 1, an integrated PVM protein
PfETRAMP10.1	PF3D7_1001500	*P. falciparum* early transcribed membrane protein family member, an integrated PVM protein

4.1.3 Plasmids

Table 4. Plasmids

SysID	Name	*E. coli* Selection Marker	*P. falciparum* Selection Marker	Source
PL-19.0049	5'_PfExp1_Cd3	AmpR	hDHFR	Generated by Violeta Pancakova
PL-19.0042	5'_PfExp1_N-term-3xHA	AmpR	hDHFR	Generated by Violeta Pancakova
PL-19.0044	5'_PfExp1-C-term-3xHA	AmpR	hDHFR	Generated by Violeta Pancakova
PL-19.0045	pARL2_5'_G1	AmpR	hDHFR	Generated by Violeta Pancakova
PL-19.0047	5'_PfExp1_Cd1	AmpR	hDHFR	Generated by Violeta Pancakova
PL-19.0048	5'_PfExp1_Cd2	AmpR	hDHFR	Generated by Violeta Pancakova
PL-19.0050	5'_PfExp1_Cd4	AmpR	hDHFR	Generated by Violeta Pancakova
PL-19.0051	5’_PfExp1_Cd5	AmpR	hDHFR	Generated by Violeta Pancakova
PL-19.0052	5'_PfExp1_Nd2	AmpR	hDHFR	Generated by Violeta Pancakova
PL-19.0053	5’_PfExp1_Nd3	AmpR	hDHFR	Generated by Violeta Pancakova
PL-19.0054	5’_PfExp1_Nd4	AmpR	hDHFR	Generated by Violeta Pancakova
PL-19.0055	5’_PfExp1_Nd5	AmpR	hDHFR	Generated by Violeta Pancakova

SysID	Name	*E. coli* Selection Marker	*P. falciparum* Selection Marker	Source
PL-19.0056	5'_PfExp1_Nd6	AmpR	hDHFR	Generated by Violeta Pancakova
PL-20.0018	Exp1FULL_ETRAMP10.1 TM_XhoI-XmaI_pUC57	AmpR	hDHFR	GenScript Biotech
PL-20.0019	Exp1FULL_ETRAMP10.1 TM_XhoI-XmaI_pVP1	AmpR	hDHFR	Generated by Violeta Pancakova
PL-20.0022	23LG GenScript	AmpR	hDHFR	GenScript Biotech
PL-22.0001	pVP1_Exp1full_Exp1-TMD	AmpR	hDHFR	Generated during this project
PL-22.0002	pVP1_Exp1full_Exp1-TMD_ΔN-term	AmpR	hDHFR	Generated during this project
PL-22.0003	pVP1_Exp1full_ETRAMP10.1-TMD_ΔN-term	AmpR	hDHFR	Generated during this project
PL-22.0076	pVP1_Exp1full_ETRAMP10.1-TMD_ΔC-term	AmpR	hDHFR	Generated during this project
PL-22.0077	pVP1_Exp1full_Exp1-TMD_ΔC-term	AmpR	hDHFR	Generated during this project
PL-22.0078	pVP1-Exp1full_ETRAMP10.1-TMD_ΔN/ΔC-term	AmpR	hDHFR	Generated during this project
PL-22.0079	pVP1_Exp1full_ETRAMP10.1-TMD_ΔN/ΔC-term	AmpR	hDHFR	Generated during this project
PL-22.0080	pVP1_Exp1full_23L-TMD	AmpR	hDHFR	Generated during this project
PL-22.0081	pVP1_Exp1full_23LG-TMD	AmpR	hDHFR	Generated during this project

SysID	Name	*E. coli* Selection Marker	*P. falciparum* Selection Marker	Source
PL-22.0082	pVP1_Exp1full_23L-TMD_ΔN-term	AmpR	hDHFR	Generated during this project
PL-22.0083	pVP1_Exp1full_23LG-TMD_ΔN-term	AmpR	hDHFR	Generated during this project
PL-22.0084	pVP1_Exp1full_23L-TMD_ΔC-term	AmpR	hDHFR	Generated during this project
PL-22.0085	pVP1_Exp1full_23LG-TMD_ΔC-term	AmpR	hDHFR	Generated during this project
PL-22.0086	pVP1_Exp1full_23L-TMD_ΔC/ΔN-term	AmpR	hDHFR	Generated during this project
PL-22.0087	pVP1_Exp1full_23LG-TMD_ΔC/ΔN-term	AmpR	hDHFR	Generated during this project
PL-23.0011	pVP1-Exp1full-Exp1TM+SDEL_C-term	AmpR	hDHFR	Generated during this project

4.1.4 Oligonucleotides

Table 5. Oligonucleotides

Oligonucleotide	Sequence (5'-3')	Usage
23L_R	CCATGGTCTTGGTGGAGGTGGATTTTCCTCGTTATTGTTTTCTTCGTTATTGTTATTATTTTCTTC	Cloning
3xTy_gDNA-PCR_R	GGACTTCAGAACCATCAAGT	PCR control
Exp1_5_Xh_R	TACTCGAGTTTGAATATATTAAATAAATTAAAAATCTACAAAC	Cloning
Exp1_C_3xHA_F	ATCCCTATGATGTGCCCGATTATGCGTATCCTTACGATGTTCCAGATTATGCCGAGCTCATAGGATCAAGCGACCCAG	Cloning

Oligonucleotide	Sequence (5'-3')	Usage
Exp1_C_3xHA_R	ACGCATAATCGGGCACATCATAGGGATAGCCAGC GTAGTCCGGGACGTCGTACGGGTATTTGAATGGGT GTCTTCCTTTTTC	Cloning
Exp1_CodM_F	CAGCAAGAAAAAGAACAAGAAAGGATCAGGTGAAC CATTAATAG	Integration PCR
Exp1_CodM_R	CCTTTCTTGTTCTTTTTCTTGCTGCTAACACCACTT CC	Integration PCR
Exp1_N_3xHA_F	ATCCCTATGATGTGCCCGATTATGCGTATCCTTAC GATGTTCCAGATTATGCCGAGCTCGTTAACAAAAG AAAATCCAAATATAAACTTG	Integration PCR
Exp1_N_3xHA_R	ACGCATAATCGGGCACATCATAGGGATAGCCAGC GTAGTCCGGGACGTCGTACGGGTATTCAACAAGTT CTTCTTCTTTTTTGATC	Integration PCR
Exp1_SP29_FRB_F	CatctcatgccagaggattctagaagcAGTTCCTTTGTTTGTTT TTT	Cloning
Exp1_SP29_FRB_R	AAAAAACAAACAAAGGAACTgcttctagaatcctctggcatga gatG	Cloning
Exp1_SP40_FRB_F	AAGAAAAAGAACAAGgcttctagaatcctctggcatgagatG	Cloning
Exp1_SP40_FRB_R	CatctcatgccagaggattctagaagcCTTGTTCTTTTTCTT	Cloning
Exp1_Start_Hind_F	TaagcttATGAAAATCTTATCAGTATTTTTTCTTGC	Cloning
Exp1_Start_Xh_F	TACTCGAGATGAAAATCTTATCAGTATTTTTTCTTG C	Cloning
Exp1_Stop_Pac_R	taTTAATTAAggttagtgttcagtgccacttacg	Cloning
Exp1_Stop_Xm_R	TACCCGGGTTAGTGTTCAGTGCCACTTACG	Cloning
Exp1TM_BssHII_F2	ATGCGCGCTATAAACTTGCCACTTCAGTACTTGC	Cloning
Exp1TM_KpnI_R	ATGGTACCTCCTTTTTCAGTATTGTATAATAC	Cloning
FRB_Exp1-29-_N_R	TTGCTGCTAACACCACTTCCctttgagattcgtcggaacac	Cloning

Oligonucleotide	Sequence (5'-3')	Usage
FRB_Exp1-40-_N_F	gtgttccgacgaatctcaaagAAAGGATCAGGTGAACCATTAATA	Integration PCR
FRB_Exp1-40-_N_R	TATTAATGGTTCACCTGATCCTTTctttgagattcgtcggaacac	Integration PCR
New 23L_F	GCGCGCGGTGGTGGAGGAAGTTTGTTGCTCCTCCTGCTTTTGTTGCTTCTTTTATTATTGTTATTG	Integration PCR
pVP1_XhoI-67_F	AAGCATGTATAACAATTTTAATCAATTTTC	Cloning
SDEL- F	GAATCAGGACCCACTTGATG	Cloning
SDEL- R	TCGACCCGGGTTAAAGCTCA	Cloning
SDEL-Overlap 1	AGGACCCACTTGATGGTTCTGAAGTCCATACAAATCAAGATCCTT	Integration PCR
SDEL-Overlap 2	CCCGGGTTAAAGCTCATCAGAATCTAAAGGATCTTGATTTGTATGG	Integration PCR

4.1.5 Chemicals

Table 6. Chemicals

Chemical	Supplier
Acetate	Merck, Darmstadt, Germany
Acetone	Merck, Darmstadt, Germany
Agar-Agar	Roth, Karlsruhe, Germany
Agarose	Peqlab (VWR), Radnor, USA
AlbuMAX II	Gibco (Thermo Fisher Scientific), Waltham, USA
APS	Roth, Karlsruhe, Germany
Bromophenol blue	Sigma-Aldrich, Taufkirchen, Germany
BSA (Albumin Fraction V)	Roth, Karlsruhe, Germany
$CaCl_2$	Roth, Karlsruhe, Germany

Chemical	Supplier
Cacodylate sodium salt	Roth, Karlsruhe, Germany
Carbenicillin	Roth, Karlsruhe, Germany
DAPI	Thermo Fisher Scientific
DMSO	Roth, Karlsruhe, Germany
DNA-Dye NonTox	Applichem, Darmstadt, Germany
DTT	Roth, Karlsruhe, Germany
EDTA	Roth, Karlsruhe, Germany
EGTA	Roth, Karlsruhe, Germany
Ethanol	Roth, Karlsruhe, Germany
Fluoromount-G	SouthernBiotech, Birmingham, USA
Gelafundin ISO 40 mg/ml	B Braun, Melsungen, Germany
Geneticin (G418)	Gibco (Thermo Fisher Scientific), Waltham, USA
Giemsa	Sigma-Aldrich, Taufkirchen, Germany
Glucosamine	Sigma-Aldrich, Taufkirchen, Germany
Glucose	Merck, Darmstadt, Germany
Glutaraldehyde	Roth, Karlsruhe, Germany
Glycerol	Roth, Karlsruhe, Germany
Glycine	Roth, Karlsruhe, Germany
H_2O_2 (25%)	Merck, Darmstadt, Germany
HCl	Roth, Karlsruhe, Germany
HEPES	Roth, Karlsruhe, Germany
Hypoxanthine	Roth, Karlsruhe, Germany
Immersion oil	Sigma-Aldrich, Taufkirchen, Germany

Chemical	Supplier
K_2HPO_4	Roth, Karlsruhe, Germany
KCl	Roth, Karlsruhe, Germany
KH_2PO_4	Roth, Karlsruhe, Germany
KOH	Roth, Karlsruhe, Germany
Luminol	Applichem, Darmstadt, Germany
Methanol	Roth, Karlsruhe, Germany
$MgCl_2$	Roth, Karlsruhe, Germany
Milk powder	Roth, Karlsruhe, Germany
Na_2HPO_4	Roth, Karlsruhe, Germany
NaCl	Roth, Karlsruhe, Germany
NaOH	Roth, Karlsruhe, Germany
Neomycin	Sigma-Aldrich, Taufkirchen, Germany
P-coumaric acid	Sigma-Aldrich, Taufkirchen, Germany
Paraformaldehyde	Roth, Karlsruhe, Germany
PBS (pH 7.2)	Gibco (Thermo Fisher Scientific), Waltham, USA
Peptone/Tryptone	Roth, Karlsruhe, Germany
PIC (protease inhibitor cocktail)	Calbiochem (Merck), Darmstadt, Germany
PMSF	Merck, Darmstadt, Germany
Poly-L-lysine solution (0.01%)	Sigma-Aldrich, Taufkirchen, Germany
Ponceau S	Roth, Karlsruhe, Germany
Rotiphorese Gel30 (37;5:1)	Roth, Karlsruhe, Germany
RPMI 1640 (+HEPES, +L-Glutamine)	Gibco (Thermo Fisher Scientific), Waltham, USA
RPMI powder	Sigma-Aldrich, Taufkirchen, Germany

Chemical	Supplier
SDS	Roth, Karlsruhe, Germany
SOB Broth	Roth, Karlsruhe, Germany
Sorbitol	Roth, Karlsruhe, Germany
TCA	Sigma-Aldrich, Taufkirchen, Germany
TEMED	Roth, Karlsruhe, Germany
Tris	Roth, Karlsruhe, Germany
Triton-X-100	Sigma-Aldrich, Taufkirchen, Germany
WR99210	Jacobus Pharmaceutical, Princeton, USA
Yeast extract	Oxioid (Thermo Fisher Scientific), Waltham, USA

4.1.6 Buffers and Solutions

Table 7. Buffers and Solutions

Buffer/Solution	Composition
100 mM PMSF	0.174 g PMSF; total volume up to 10 ml of Isopropyl alcohol
10X PBS (pH 7.4)	80 g NaCl (fc: ~1.37 M) 2 g KCl (fc: ~27 mM) 14.4 g Na_2HPO_4 (fc: ~88 mM) 2.4 g KH_2PO_4 (fc: ~18 mM) Ad 1 L ddH_2O
10x Taq-buffer	200 mM Tris-HCl, 100 mM KCl, 100 mM $(NH_4)_2SO_4$, 20 mM $MgSO_4$, 1% (w/v) Triton-X-100 in ddH_2O

Buffer/Solution	Composition
10x Transfer buffer	250 mM Tris, 1.92 M Glycine, pH 8.3 in ddH_2O
2x SDS loading buffer (pH 6.8)	100 mM Tris, 0.2% (w/v) Bromophenol blue, 20% (v/v) Glycerol, 4% SDS, 200 mM DTT in ddH_2O
5% Sorbitol solution	5% (w/v) D-sorbitol in ddH_2O
50x TAE buffer	2 M Tris 50 mM EDTA (pH 8) in ddH_2O
Albumax solution	500 ml RPMI1640 (+HEPES, +L-glutamine) 5% (w/v) AlbuMAXII
Blocking solution IFA	3% (w/v) BSA in PBS (pH 7.4)
Carbenicillin solution	50 mg/ml Carbenicillin in 50% ethanol
Cytomix solution	120 mM KCl, 0.15 mM $CaCl_2$, 1 ml Stock solution I pH 7.6 (fc: 10 mM), 10 ml Stock solution II pH 7.6 (fc: 25 mM HEPES, 2 mM EGTA), 5 mM $MgCl_2$, Ad 100 ml ddH_2O
Cytomix Stock solution I (1M Phosphate buffer)	86.6 mM K_2HPO_4 13.4 mM KH_2PO_4 pH 7.6 in ddH_2O

Buffer/Solution	Composition
Cytomix Stock solution II (HEPES, EGTA)	250 mM $C_8H_{12}N_2O_4S$ (HEPES), 20 mM $C_{14}H_{24}N_2O_{10}$ (EGTA), pH 7.6 (with KOH) in ddH_2O
ECL solution	160 ml ddH_2O 32 ml 1 M Tris/HCl (pH 8.5) 3.2 ml 250 mM Luminol (in DMSO) 1.424 ml 90 mM P-coumaric acid (in DMSO)
Fixation solution IFA	4% (w/v) PFA, 0.0075% GA, in PBS (pH 7.4)
Permeabilisation solution IFA	0.1% Triton-X-100 (v/v), 125 mM Glycine, in PBS (pH 7.4)
Ponceau S solution	0.2% Ponceau S, 0.3% TCA, in ddH_2O
Separation gel buffer	28% (v/v) Glycerol, 3% (w/v) D-sorbitol, 0.65% (w/v) NaCl, in ddH_2O
Stacking gel buffer	0.5 M Tris pH 6.8 in ddH_2O
Taq reaction mix	600 µl Taq-buffer (10x), 120 µl dNTP Mix (10 mM each), Ad 6 ml ddH_2O
TE buffer	10 mM Tris (pH 8), 1 mM EDTA (pH 8), in ddH_2O

Buffer/Solution	Composition
Thawing solutions	I: 12% (w/v) NaCl II: 1.6% (w/v) NaCl III: 0.9% (w/v) NaCl + 0.2% (w/v) glucose in ddH_2O

4.1.7 Cell culture media

Table 8. Cell culture media

Medium	Composition
P. falciparum human plasma culture medium	500 ml RPMI1640 (+HEPES, +L-glutamine) Supernatant of 50 ml human plasma (A^+) 10 ml 10 mM Hypoxanthine (fc: 0.2 mM) 5 ml 10 mg/ml Neomycin (fc: 0.1 mg/ml)
P. falciparum transfection culture medium	500 ml RPMI1640 (+HEPES, +L-glutamine), 25 ml supernatant of human plasma (A^+), 25 ml Albumax solution, 10 ml 10 mM Hypoxanthine (fc: 0.2 mM), 5 ml 10 mg/ml Neomycin (fc: 0.1 mg/ml)
LB_{Carb} medium	1% (w/v) Pepton/Trypton, 0.5% (w/v) Yeast extract, 170 mM NaCl, Ad 1 L ddH_2O, + 50 µg/ml Carbenicillin
LB_{Carb} agar	1% (w/v) Pepton/Trypton, 0.5% (w/v) Yeast extract, 170 mM NaCl, 15 g Agar, Ad 1 L ddH_2O, + 100 µg/ml Carbenicillin
SOC medium	20 mM glucose in SOB medium
SOB medium	10.66 g SOB 400 ml ddH_2O

4.1.8 Antibodies

Table 9. Antibodies

Antibody	Origin	Dilution for IFA	Dilution for WB	Supplier
α-HA (12CA5)	Mouse	1:200	1:1000	Roche, Basel, Switzerland
α-PfAldolase	Rabbit	-	1:5000	Prof. Jude Przyborski
α-PfEXP1	Rabbit	-	1:500	Prof. Jude Przyborski
α-PfEXP2	Rabbit	1:500	-	Prof. Jude Przyborski
α-PfMSP1	Mouse	1:500	-	Prof. Jude Przyborski
α-Mouse-Cy3	Goat	1:1000	-	Jackson ImmunoResearch, West Grove, USA
α-Mouse-Cy2	Goat	1:1000	-	Jackson ImmunoResearch, West Grove, USA
α-Rabbit-Cy2	Goat	1:1000	-	Jackson ImmunoResearch, West Grove, USA
α-Rabbit-Cy3	Goat	1:1000	-	Jackson ImmunoResearch, West Grove, USA
α-Mouse-HRP	Goat	-	1:2000	Dako, Glostrup, Denmark
α-Rabbit-HRP	Goat	-	1:2000	Dako, Glostrup, Denmark

4.1.9 Enzymes

Table 10. Enzymes

Enzyme	Supplier
Taq DNA Polymerase	Made in Prof. Jude Przyborski's lab
KOD DNA Polymerase	Merck, Darmstadt, Germany
Antarctic Phosphatase	NEB, Ipswich, USA
T4 DNA Ligase	Thermo Fisher Scientific, Waltham, USA
Restriction enzymes (AluI, AvrII, BssHII, EcoRV, HindIII, KpnI, MluI, NdeI, NotI, PstI, XhoI, XmaI)	NEB, Ipswich, USA

4.1.10 PCR and WB Markers

On an agarose gel for analyzing DNA fragments, 5 µl of 1 kb Plus DNA Ladder was used as a molecular weight marker. For Western blot analysis, 4 µl of PageRuler™ Prestained Protein Ladder was loaded onto an SDS-PAGE gel to serve as a protein size marker in the 10–180 kDa range (Fig. 42)

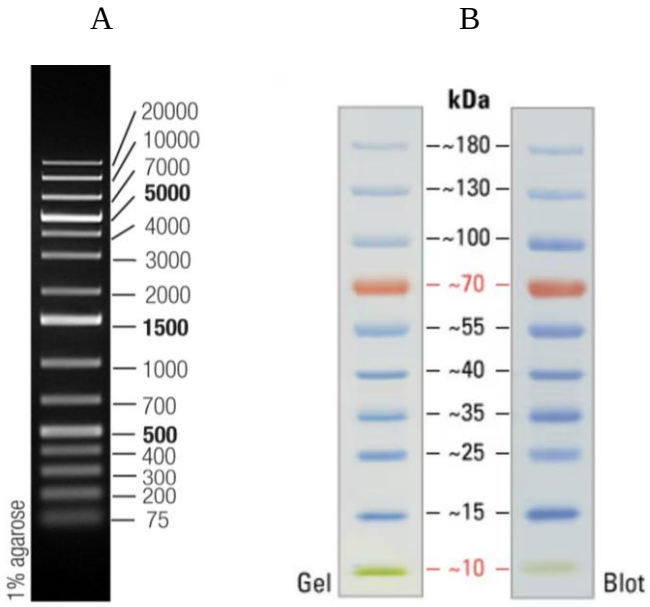

Fig. 42. DNA marker and Protein Molecular Weight Marker.

(A) 1 kb Plus DNA Ladder (Thermo Fisher Scientific, Waltham, USA). **(B)** PageRuler™ Prestained Protein Ladder (Thermo Fisher Scientific, Waltham, USA).

4.1.11 Kits

Table 11. Kits

Kit	Supplier
QIAquick® PCR Purification Kit	Qiagen, Venlo, Netherlands
QIAquick® Gel Extraction Kit	Qiagen, Venlo, Netherlands
QIAprep® Spin Miniprep Kit	Qiagen, Venlo, Netherlands
QIAGEN® Plasmid Maxi Kit	Qiagen, Venlo, Netherlands
QIAamp® DNA Blood Mini Kit	Qiagen, Venlo, Netherlands

4.1.12 Equipment

Table 12. Equipment

Equipment	Supplier
Agarose gel electrophoresis: Power supply, Agarose gel electrophoresis chambers, Gel imaging system	 Amersham EPS 301, Owl separation systems B1A and B2, FastGene FAS-DIGI Compact with camera, Pentax MX-1
Biospectrometer	Eppendorf BioSpectrometer basic
Centrifuges	Sorvall LYNX 4000 centrifuge Hettich Centrifuge Mikro 220R Megafuge 1.0R centrifuge Eppendorf centrifuge 5415R
Cuvette (Biospectrometer)	Eppendorf µCuvette G1.0
Incubator (*P. falciparum*)	Labotect C200
Heat bath	PolyScience heat bath
Heat block, mixer	IKA Dry Block Heater 2 Neolab neoBlock II Eppendorf Thermomixer comfort
Ice machine	Icematic F80C

Equipment	Supplier
Microscopes: A: Light microscope B: Inverse microscope C: Fluorescence microscope	A: Zeiss Axio Lab.A1 microscope, B: Kern Inverted microscope OCM 161 with microscope camera ODC 832, C: Zeiss Axio Observer Z1 fluorescence microscope
Incubator shaker (*E. coli*)	Innova 44 Incubator shaker series, Max Q 6000 (Thermo Fisher Scientific)
Magnetic cell sorter stand (MACS)	Miltenyi Biotec Magnetic cell sorter
Orbital shaker	Heidolph unimax 2010 orbital shaker
PCR machines	FastGene FG-TC01 Eppendorf Mastercycler® nexus gradient
pH meter	Knick pH-Meter 766 Calimatic
Pipettes: Single-channel pipettes, Multipipette Electric Pipette 12-channel pipette	Eppendorf Research, Gilson Pipetman Eppendorf M4 Brand AccuJet pro Eppendorf Research plus
Plate reader	Clariostar plate reader
Roller	CAT RM5 roller
Scales	Kern ABT 120-5DM, Kern 474, Kern 440-47N
Sterile work bench	HERA-Safe HS
Transfection Electroporation system	BioRad Capacitance Extender II, BioRad Pulse Controller Plus, BioRad Gene Pulser II

Equipment	Supplier
Ultra pure water system	membraPure Astacus
Vacuum pump	MAGV
Vortexer	Phoenix RS-VA10
Western blot: SDS Gel system Power supply Transfer machine Developing machine	 BioRad Mini-PROTEAN Tetra cell system, BioRad Power Pac 300, BioRad TransBlot Turbo, Intas ECL Chemostar

4.1.13 Consumables

Table 13. Consumables

Consumable	Supplier
1.5 ml, 2 ml SafeSeal tubes	Sarstedt, Nümbrecht, Germany
15 ml and 50 ml tube	Greiner, Kremsmünster, Austria
2 ml, 5 ml, 10 ml, 25 ml pipette	Sarstedt, Nümbrecht, Germany Greiner, Kremsmünster, Austria
20 ml syringe	BD, Franclin Lakes, USA
20 µl, 200 µl, 1000 µl filter tips	Nerbe plus, Winsen, Germany
96-well plate (black; T bottom)	Greiner, Kremsmünster, Austria
Blunt cannula (0.8 x 22 mm)	B Braun, Melsungen, Germany
Cellstar cell culture flask T74	Greiner, Kremsmünster, Austria
Cryo.S tubes	Greiner, Kremsmünster, Austria
CS column	Miltenyi Biotec, Bergisch Gladbach, Germany
Gene Pulser Cuvette (0.2 cm)	BioRad, Hercules, USA
Microscope slides ISO 8037/1	Epredia (Thermo Fisher Scientific, USA)

Consumable	Supplier
Nitrocellulose membrane 0.22 µm	Neolab, Heidelberg, Germany
PCR tube strips	Nippon Genetics, Düren, Germany
Petri dish (100x 15 mm) for binding assay	Falcon (Corning, Corning, USA)
Steritop 0.22 µm	Merck, Darmstadt, Germany
TC 6-well und 12-well plate	Sarstedt, Nümbrecht, Germany
TC Petri dish for cell culture	Sarstedt, Nümbrecht, Germany
Three-way stopcock	B Braun, Melsungen, Germany

4.1.14 Software and online tools

Table 14. Software and online tools

Software/Online tool	Supplier
BioRender	BioRender Inc., Toronto, ON M5V 2J1, Canada
Labguru	BioData Inc. (Labguru), Cambridge, MA 02141, USA
ImageJ 2.3.0	National Institutes of Health (NIH), Bethesda, MD, USA
PlasmoDB	EuPathDB Consortium (hosted by University of Pennsylvania), Philadelphia, PA, USA
SnapGene Premium	Dotmatics Ltd. (formerly GSL Biotech), Burlington, MA, USA
UniProt	UniProt Consortium (EMBL-EBI, SIB, PIR), Hinxton, Cambridge, UK / Geneva, Switzerland
ZEN 3.2	Carl Zeiss Microscopy GmbH, Carl-Zeiss-Promenade 10, 07745 Jena, Germany

4.2 Molecular Methods

4.2.1 Genomic DNA Extraction from *P. falciparum*

Genomic DNA was isolated from *P. falciparum* cultures to serve as a template for PCR amplification of inserts used in the construction of transfection plasmids, as well as for verifying successful transfection. DNA was extracted from 200 µL of packed, infected red blood cells collected from synchronized trophozoite-stage cultures with parasitemia exceeding 10%. The extraction was performed using the QIAamp DNA Blood Mini Kit (Qiagen, Venlo, Netherlands) according to the manufacturer's instructions and eluted in 100 µl of nuclease-free water.

4.2.2 PCR (Polymerase Chain Reaction)

The polymerase chain reaction (PCR) is a method for the targeted amplification of DNA fragments using a thermostable DNA polymerase and specific oligonucleotides (primers). A typical PCR program consists of three temperature-dependent steps that are repeated for up to 35 cycles. In the first step, double-stranded DNA is denatured into single strands at 92-98 °C. This is followed by an annealing step at 50–60 °C, during which the primers bind to complementary sequences on the single-stranded DNA. The exact annealing temperature depends on the melting temperatures of the oligonucleotides used. In the final elongation step, the DNA polymerase synthesizes the new DNA strand by extending from the primers along the template strand. Although the optimal elongation temperature for most DNA polymerases is 72 °C, a reduced temperature of 68 °C was used to accommodate the AT-rich and repetitive nature of *P. falciparum* DNA, thereby slowing down the polymerase and improving the fidelity of elongation.

A self-made Taq polymerase was used for colony PCRs to screen for positively transformed and ligated *E. coli* colonies, as well as for verifying transfected parasite lines. For cloning purposes, and in cases where Taq polymerase did not yield specific bands, the proofreading KOD Hot Start DNA polymerase (Merck, Darmstadt, Germany) was employed to amplify inserts for all PfExp1, PfETRAMP10.1, 23L, and 23LG constructs.

KOD reaction	KOD PCR program
34 µl ddH_2O 5 µl 10x KOD buffer 5 µl 2 mM dNTPs 3 µl 25 mM $MgSO_4$ 1 µl template DNA 25 pmol forward/reverse primer 1 µl KOD polymerase	1) Initial denaturation: 95 °C, 10 min 2) Denaturation step: 95 °C, 1 min 3) Annealing step: 50-60 °C, 1 min 4) Elongation step: 68 °C, 30 s/kb + 10 sec - Repeat steps 2-4 for 35 cycles 5) Final elongation: 68 °C, 10 min 6) Hold at 4 °C

Taq reaction	Taq PCR program
25 µl Taq reaction mix (master mix) 25 pmol forward/reverse primer 0.5 µl Taq polymerase	1) Initial denaturation: 95 °C, 10 min 2) Denaturation step: 95 °C, 1 min 3) Annealing step: 50-60 °C, 1 min 4) Elongation step: 68 °C, 1 min/kb +10 sec - Repeat steps 2-4 for 35 cycles 5) Final elongation: 68 °C, 1 min 6) Hold at 4 °C

4.2.3 Standard Agarose Gel Electrophoresis for DNA Fragment Separation

DNA fragments are separated by agarose gel electrophoresis based on their size and conformation. Due to the negatively charged phosphate backbone of DNA, the fragments migrate through the gel matrix when subjected to an electric field. Smaller DNA fragments move faster through the agarose gel than larger fragments, and varying agarose concentrations can improve resolution. Depending on the expected fragment sizes, a 0.75% to 1.5% agarose gel was prepared. All samples were mixed with 6x DNA Dye Non-Tox (AppliChem GmbH, Darmstadt, Germany), which binds to double-stranded DNA and can be visualized in an LED chamber at 470 nm (blue light). Compared to the toxic ethidium bromide, DNA Dye Non-Tox is a non-hazardous alternative that does not intercalate into DNA and does not require UV light for visualization, thereby avoiding potential mutagenic effects. To assess fragment sizes, a 1 kb Plus marker (Thermo Fisher Scientific, Waltham, USA) was loaded onto the gel. The samples were separated at 100-120 V for 30-45 min in TAE buffer and visualized at 470 nm.

4.2.4 DNA Isolation and Purification

Intermediate products (e.g., PCR products and restriction digests) were purified to eliminate contaminants that could interfere with subsequent reactions. The QIAquick PCR Purification Kit (Qiagen, Venlo, Netherlands) was used for purification, with elution in 30 µl of ddH_2O. To isolate restriction-digested vector DNA from an agarose gel, the QIAquick Gel Extraction Kit (Qiagen, Venlo, Netherlands) was applied according to the manufacturer's instructions, and the DNA was eluted in 30 µl of ddH_2O.

4.2.5 Photometric Determination of DNA Concentration

The concentration of DNA was determined using an Eppendorf BioSpectrometer by measuring absorbance at 260 nm, which corresponds to the absorption maximum of nucleic acids. Accurate quantification was essential for setting up ligation reactions, preparing samples for sequencing, and producing plasmid DNA for transfection. In addition, the absorbance ratio at 260 nm and 280 nm was used to assess DNA purity and detect possible contamination with proteins.

4.2.6 Restriction Enzyme Digestion of Vectors and DNA Fragments

PCR products and plasmid vectors were digested with the appropriate restriction enzymes from New England Biolabs (NEB, Ipswich, USA) according to the manufacturer's instructions. Restriction sites had been incorporated into the primers during the cloning design phase. The enzymes BssHII and KpnI were used to generate sticky ends with compatible overhangs, allowing directional ligation. Digestion was performed at 37 °C: PCR products were incubated for 2-3 hours, plasmid vectors for 6 hours, and test digestions for 1 hour.

Insert restriction digest/test digest	Vector digest
3 µl 10x CutSmart buffer 2.5 U per restriction enzyme ~1 µg insert / ~300 ng vector for test digestion Ad 30 µl ddH_2O	3 µl 10x CutSmart buffer 7.5 U per restriction enzyme ~2 µg vector Ad 30 µl ddH_2O

The vector was first incubated with Antarctic Phosphatase (NEB, Ipswich, USA) for 1 hour to remove phosphate groups, thereby preventing re-ligation. After this dephosphorylation step, the purification and ligation process was carried out.

4.2.7 DNA Ligation

To prepare for ligation, the respective inserts and vectors were first digested with restriction enzymes. The resulting DNA fragments were then incubated overnight at 16 °C with T4 DNA ligase (Invitrogen, Waltham, USA), following the manufacturer's instructions. This enzyme catalyses the formation of phosphodiester bonds by joining 3′ hydroxyl and 5′ phosphate termini of nucleic acids. A total of 100 ng of vector DNA was used in each reaction, with the corresponding amount of insert DNA calculated to maintain a 3:1 molar excess over the vector. Before ligation, DNA concentrations were confirmed by agarose gel electrophoresis.

$$Insert\ DNA\ (ng) = \frac{Vektor\ DNA\ (ng) * Insert\ DNA\ (bp)}{Vektor\ DNA\ (bp)} * \frac{3}{1}$$

Ligation reaction
100 ng Vector DNA x ng Insert DNA 2 µl 5x Ligase buffer 1 U T4 DNA Ligase Ad 10 µl ddH_2O

4.2.8 Competent *E. coli* Transformation

Two types of *E. coli* strains were employed for transformation: chemically competent XL1-Blue and electrocompetent TOP10 cells. To introduce plasmid DNA into XL1-Blue cells, 5 µl of the ligation reaction was gently mixed with 50 µl of competent cells and incubated on ice for 30 minutes. The cells were then subjected to heat shock at 42 °C for 90 seconds and promptly returned to ice for 2 minutes. Following this, 300 µl of SOC medium was added, and the mixture was incubated at 37 °C for one hour to allow recovery. The culture was then plated on LB agar containing 100 µg/ml carbenicillin and incubated overnight at 37 °C for colony formation. Before the transformation of TOP10 cells via electroporation, the ligation mixture underwent ethanol precipitation to eliminate inhibitory salts. Specifically, 20 µl of cold 100% ethanol (−20 °C) and 1 µl of 3 M sodium acetate (pH 5.3) were added to 10 µl of the ligation product. After thorough mixing, the solution was centrifuged at 13,000 ×g for 15 minutes at 4 °C. The resulting pellet was washed with 500 µl of 70% ethanol, followed by complete removal of the supernatant. The pellet was dried at 50 °C to eliminate residual ethanol and then resuspended in 10 µl of ddH_2O. Vortexing and a 10-minute incubation at 50 °C ensured full resuspension, and the DNA was cooled on ice before use.

Electroporation involved combining 5 µl of the prepared DNA with 50 µl of TOP10 electrocompetent cells. This mixture was transferred into a sterile electroporation cuvette (0.2 cm gap) and pulsed under the following conditions: 2 kV, 25 µF, and 200 Ω. Immediately after pulsing, 1 ml of SOC medium was added, and the cells were incubated at 37 °C for one hour. The culture was then plated on LB agar supplemented with 100 µg/ml carbenicillin and incubated overnight at 37 °C.

4.2.9 Plasmid DNA Extraction and Purification from *E. coli*

Plasmid DNA was extracted and purified from *E. coli* cultures grown overnight in LB medium (37 °C, 120 rpm), using either 5 ml or 400 ml culture volumes. For the 5 ml cultures, the QIAprep Spin Miniprep Kit (Qiagen, Venlo, Netherlands) was used following the manufacturer's protocol. Cells were lysed using an alkaline buffer to release plasmid DNA, which was subsequently bound to a silica membrane, washed, and eluted in 30 µl of double-distilled water.

For larger-scale preparations from 400 ml cultures, a slightly modified version of the QIAGEN Plasmid Maxi Kit protocol (Qiagen, Venlo, Netherlands) was applied. Cells were pelleted (3000 × g, 15 min, 4 °C) and resuspended in 20 ml of resuspension buffer. Lysis was carried out by adding 20 ml of alkaline lysis buffer for 5 min, followed by neutralization with 20 ml of neutralization buffer and incubation on ice for 20 min. The lysate was clarified by centrifugation (3600 × g, 30 min, 4 °C), and the supernatant was filtered and applied to the column. Plasmid DNA was then washed, eluted, precipitated according to the manufacturer's instructions, and finally resuspended in 1.5 ml of TE buffer for storage at −20 °C.

4.2.10 Sequencing of DNA

To confirm proper integration and ensure that no mutations were introduced during the cloning process, the isolated plasmids were subjected to Sanger sequencing. For this, 10 µl of plasmid DNA (at 100 ng/µl) was combined with 4 µl of primer (5 µM) and submitted to LGC Genomics (Berlin, Germany) for sequencing.

4.2.11 Biochemical protocols

SDS-PAGE (sodium dodecyl sulfate–polyacrylamide gel electrophoresis)

SDS-PAGE was performed to separate proteins based on their molecular weight under denaturing conditions. In this method, the anionic detergent SDS masks the native charge of proteins and imparts a uniform negative charge proportional to their size, allowing separation in an electric field. Smaller proteins migrate more rapidly through the gel matrix than larger ones. To prepare the samples, protein lysates were mixed with 4X SDS loading buffer containing 100 mM dithiothreitol (DTT) and denatured by heating at 95 °C for 15 minutes. DTT serves as a reducing agent, breaking disulfide bonds and facilitating complete protein denaturation. Electrophoresis was carried out on a 15% polyacrylamide resolving gel overlaid with a 4% stacking gel. A volume equivalent to 1×10^7 cells was loaded per lane, along with 5 µl of a pre-stained protein molecular weight marker (Thermo Fisher Scientific, Waltham, USA). The gel was run in SDS running buffer at 80 V for 20 minutes to allow proper stacking, followed by 120 V for the remaining separation phase.

Following electrophoresis, the proteins were transferred for Western blot analysis.

4% Stacking gel	12% Separation gel
5 ml 4% Stacking gel solution 5 µl TEMED 25 µl 10% APS	10 ml 12% Separation gel solution 5 µl TEMED 50 µl 10% APS

4% Stacking gel solution (100 ml)	12% Separation gel solution (100 ml)
61 ml ddH_2O 25 ml Stacking gel buffer (0.5 M Tris-HCl) pH 6.8 13 ml 30% Acrylamide 1 ml 10% SDS	34 ml ddH2O 25 ml Separation gel buffer (1.5 M Tris-HCl) pH 8.8 40 ml 30% Acrylamide 1 ml 10% SDS

4.2.12 Western blot

Western blotting was performed to detect specific proteins using antibody-based recognition. Initially, proteins were separated by SDS-PAGE and subsequently transferred onto a nitrocellulose membrane. For the transfer, the gel, nitrocellulose membrane, and twelve blotting papers were equilibrated in transfer buffer and assembled into a Trans-Blot Turbo cassette (Bio-Rad, Hercules, USA) in the following sequence: six blotting papers, nitrocellulose membrane, gel, and six additional blotting papers. Protein transfer was carried out using the Trans-Blot Turbo system at 25 V and 1 A for 30 minutes, allowing the negatively charged proteins to migrate toward the anode and bind to the membrane.

Following transfer, the membrane was briefly stained with Ponceau S solution (2 minutes), then rinsed with 1% acetic acid to visualize protein bands and confirm successful transfer. The stain was removed by washing the membrane using 1x PBS buffer (pH 7.4).

For samples with high hemoglobin content, such as MACS-purified parasites, the membrane was incubated in enhanced chemiluminescence (ECL) solution supplemented with 1:1000 diluted 30% H_2O_2 for 20–30 minutes to minimize background signals caused by hemoglobin.

To block nonspecific binding, the membrane was incubated in 5% (w/v) non-fat milk in 1x PBS buffer (pH 7.4) for 1 hour at room temperature. The primary antibody, specific to the target protein, was diluted in 5% milk/PBS and applied to the membrane overnight at 4 °C with gentle agitation.

The following day, the membrane was washed three times for 10 minutes each with 1x PBS buffer (pH 7.4) and incubated for 2 hours with an HRP-conjugated secondary antibody (Dako, Glostrup, Denmark), diluted 1:2000 in 5% milk/PBS. After incubation, the membrane was rewashed three times for 10 minutes with 1x PBS buffer and incubated in ECL solution containing 1:1000 diluted 30% H_2O_2. Chemiluminescent signals were immediately detected using an Intas ECL ChemoStar imaging system.

4.3 Methods in cellular biology

4.3.1 Culturing *P. falciparum in vitro*

The *P. falciparum* parasites were cultured in Petri dishes with cell culture medium and A^+ red blood cells from the blood bank of the University Hospital in Giessen, maintaining a hematocrit of 4%. The cultures were incubated at 37°C in a gas atmosphere of 90% N_2, 3-5% CO_2, and 5% O_2, following the method of Trager and Jensen (1976).

The standard cell culture medium consisted of 500 ml of RPMI 1640 with HEPES and L-glutamine, supplemented with 10 ml of hypoxanthine solution (resulting in a concentration of 0.2 mM), a final concentration of 0.1 mg/mL of neomycin solution, and 50 ml of human plasma (A^+). For transfected parasites, the medium was modified to include 500 mL of RPMI 1640 with HEPES and L-glutamine, hypoxanthine (0.2 mM), neomycin (0.1 mg/mL), 25 mL of human plasma (A^+), and 25 mL of sterile-filtered Albumax solution until parasite growth was reestablished. The Albumax solution was prepared by dissolving 25 g of AlbuMAX II in 500 ml of RPMI 1640 with HEPES and L-glutamine. Human plasma (A^+) was sourced from the blood banks in Giessen and stored at -20°C. Four plasma bags were thawed, pooled, aliquoted into 50 ml tubes, and heat-inactivated at 56°C for 2 hours. Before adding the supernatant to the culture medium, the plasma was centrifuged (1600 × g for 20 minutes) to remove cellular debris.

4.3.2 Giemsa Staining of Blood Smears

Blood smears were made at least three times a week to check on the parasites and reduce stress from high parasitemia. Five microliters of parasite culture were spread evenly on a slide and left to air dry. The cells were fixed with methanol for a few seconds, then stained with Giemsa for about 10 minutes. After rinsing the slides with water, they were examined under a light microscope at 1000x magnification with an oil-immersion lens. The culture was diluted according to the level of parasitemia seen.

4.3.3 Cryogenic preservation of *P. falciparum*

To cryopreserve parasites, 0.5 ml of *P. falciparum* ring-stage infected red blood cells with a parasitemia of 2% or higher was resuspended in 0.5 ml of freezing solution and transferred into cryotubes. After snap-freezing in liquid nitrogen for 10 minutes, samples were stored in liquid nitrogen tanks at −196 °C until needed.

4.3.4 Thawing of parasites

To re-establish cryopreserved *P. falciparum* cultures into continuous cell culture, cryotubes were thawed at 37°C for a few minutes. Subsequently, 200 µl of a 12% NaCl solution was added drop-wise, and the diluted cell suspension was transferred into a 15 ml tube. After 3 minutes, 5 ml of a 1.2% NaCl solution was added drop-wise while gently agitating the tube. This step was followed by the addition of 5 ml of a 0.9% NaCl solution containing 0.2% glucose, after which the cells were pelleted by centrifugation (1600 × g for 2 minutes). The cell pellet was then washed once with culture medium. Finally, the washed cells were reseeded with 0.5 ml of A^+ red blood cells and culture medium and cultivated as previously described.

4.3.5 Sorbitol-Based Synchronization of Asexual *P. falciparum* Stages

Due to the formation of new permeability pathways by the parasite, infected red blood cells (iRBCs) exhibit increased membrane permeability to solutes (Ginsburg and Stein 1987). As a result, treatment with d-sorbitol induces osmotic lysis of RBCs harboring mature parasite stages, such as trophozoites and schizonts, while ring-stage parasites survive (Lambros and Vanderberg 1979). This selective lysis promotes a more synchronous parasite development, which can be further enhanced by administering d-sorbitol twice daily at 4–6 hour intervals.
To synchronize the culture, 500 µl of infected blood was pelleted via centrifugation (1600 × g, 2 minutes), then resuspended in 5 ml of a 5% d-sorbitol solution and incubated for 10–15 minutes at 37°C. Following incubation, the cell pellet was washed once with 10 ml of complete media and re-seeded for further cultivation.

4.3.6 ML10-Based Synchronization of Asexual *P. falciparum* Stages

To obtain tightly staged mature schizonts for immunofluorescence analyses, parasite egress was reversibly blocked using the PKG inhibitor ML10, which arrests parasites shortly before egress and can be washed out to resume development. ML10 is a potent derivative of the previously used PKG inhibitor Compound 2. Mature schizonts were incubated with 50 nM ML10 under standard culture conditions, harvested at the arrested stage, and processed for fixation and immunostaining (Ressurreição et al. 2020).

4.3.7 Purification of parasite via Magnetic Activated Cell Sorting (MACS)

Hemozoin, which accumulates in mature *P. falciparum* stages such as trophozoites and schizonts (Francis et al. 1997), has paramagnetic properties that allow for the selective enrichment of infected red blood cells (iRBCs) using Magnetic Activated Cell Sorting (MACS). A MACS CS-column was prepared by connecting it to a 20-ml syringe via a three-way stopcock and mounting it on a VarioMACS separator. The column was washed with 20 ml of PBS (pH 7.4) before loading the parasite culture. A synchronized culture, containing 5-10% trophozoites and/or schizonts, was gently pipetted onto the column at a flow rate of 1-2 drops per second. After the first flow-through, the column was washed with an additional volume of PBS, which was then reapplied to improve recovery. The column was then washed with PBS to remove uninfected RBCs and ring-stage parasites that did not bind to the column.

Once the flow-through appeared clear, the column was then removed from the magnetic field, and the bound hemozoin-containing iRBCs were eluted with PBS (pH 7.4). The eluate was then centrifuged (1600 × g, 2 min) to pellet the cells. The resulting cell pellet was washed twice more with PBS to remove residual unbound components.

After the final wash, 10 µL of the packed iRBC pellet was resuspended in 40 µL of PBS. To this suspension, 1 mM PMSF and protease inhibitor cocktail (PIC; 1:200, Calbiochem) were added. Then, 50 µl of 4× protein sample buffer was added to the mixture. The sample was denatured at 95°C for 10 minutes.

For SDS-PAGE analysis, 10 µl of the sample was loaded per lane. This volume corresponds to approximately 1 × 10^7 cells, based on the assumption that 1 µl of packed iRBCs contains roughly 10^7 cells, and the sample was diluted 1:10 during processing.

4.3.8 Electroporation-based transfection of *P. falciparum*

Transgenic parasite lines were generated via electroporation as previously described (Wu et al., 1995). A total of 150 µg of plasmid DNA was first precipitated by adding two volumes of 100% ethanol (−20 °C) and 1/10 volume of 3 M sodium acetate (pH 5.3). The mixture was centrifuged (13,000 × g, 20 min, 4 °C), and the supernatant was discarded. The DNA pellet was stored in 70% ethanol at −20 °C until use.

On the day of transfection, the DNA was re-pelleted (13,000 × g, 20 min, 4 °C), air-dried under sterile conditions, and resuspended in 30 µl of TE buffer by incubation at 50 °C with shaking. Just before electroporation, 370 µl of cytomix buffer was added to the DNA and vortexed thoroughly.

In parallel, a synchronized *P. falciparum* culture containing 5–10% ring-stage parasites was centrifuged (1600 × g, 2 min), and 200 µl of the packed infected erythrocytes was added to the DNA-cytomix solution. The mixture was transferred into a 0.2 cm-gap electroporation cuvette.

Electroporation was performed using the following parameters: 950 µF and 310 V (Fidock and Wellems, 1997).

Immediately following electroporation, the parasites were transferred into pre-warmed transfection medium in a Petri dish containing 400 µl of fresh O^+ erythrocytes. After a 6-hour incubation period, drug selection was initiated by adding 2.5 nM WR99210 to the culture. The medium was replaced daily, and 20 µl of fresh blood was added regularly until no viable parasites were observed by Giemsa-stained blood smears.

To maintain the culture during the drug selection phase, medium changes were reduced to twice weekly until transgenic parasites reappeared.

4.3.9 Microscopy-Based Methods

Immunofluorescence Assay (IFA)

Immunofluorescence assays (IFA) were employed to study the expression and subcellular localization of specific proteins in the blood stages of *P. falciparum*. This technique relies on the binding of a primary antibody to the target protein, followed by detection using a fluorophore-conjugated secondary antibody. Upon excitation, the attached fluorophores (e.g., Cy2, Cy3) emit light at distinct wavelengths, allowing visualization of the protein of interest.

Depending on the target protein and the properties of the primary antibody, two different IFA protocols were applied to optimize fluorescence signal and resolution. Both protocols were adapted from Tonkin et al., 2004.

4.3.10 PFA fixation (IFA in solution)

This protocol allows visualization of protein localization in *P. falciparum*-infected red blood cells (iRBCs) while maintaining their three-dimensional morphology. Fixation with paraformaldehyde (PFA), combined with a low concentration of glutaraldehyde (0.0075%), stabilizes cellular structures through covalent cross-linking (Tonkin et al., 2004).

A total of 10 µl of iRBCsF from a ~5% trophozoite-stage culture was resuspended in 1 ml of fixation buffer (4% PFA, 0.0075% glutaraldehyde in PBS, pH 7.4) and incubated for 30 minutes at 37°C with gentle shaking. After centrifugation (1000 × g, 1 min, room temperature), the pellet was resuspended in 1 ml of permeabilization/quench buffer (125 mM glycine, 0.1% Triton X-100 in PBS) and incubated for 15 minutes at room temperature. The cells were then pelleted again under the same conditions and incubated in 1 ml of blocking buffer (5% milk in PBS) for 1 hour at room temperature to minimize nonspecific antibody binding.

Following blocking, the cells were incubated overnight at 4 °C with gentle rolling in primary antibody diluted in blocking buffer. The next day, they were washed three times for 15 minutes each with PBS (pH 7.4) and subsequently incubated with the appropriate fluorophore-conjugated secondary antibody (diluted in blocking buffer) for 2 hours at room temperature, protected from light and with continuous rolling.

After staining, the cells were washed three times in PBS, with DAPI (1:10,000; stock 10 mg/ml) included in the final wash to stain nuclei. The samples were then resuspended in PBS and stored at 4 °C until imaging. Fluorescence microscopy was performed using a Zeiss Observer Z1 microscope equipped with ZEN 3.7 software.

4.3.11 IFA on Slides (Acetone–Methanol Fixation)

Fixation with a chilled acetone–methanol mixture causes cellular dehydration and protein denaturation, leading to precipitation of intracellular components. While this method disrupts the three-dimensional structure of the cells, it may be more effective for visualizing proteins (Tonkin et al. 2004).

Thin blood smears were prepared from a ~5% trophozoite-stage *P. falciparum* culture and fixed in a solution of 90% acetone and 10% methanol at −20 °C for 10 minutes. Following fixation, slides were incubated in blocking buffer for 1 hour at room temperature with gentle shaking. Primary antibodies, diluted in blocking buffer, were pipetted onto parafilm, and slides were placed face-down onto the droplets. Incubation was carried out overnight at 4 °C in a humidified chamber.

The next day, slides were washed three times in PBS (pH 7.4), followed by a 2-hour incubation at room temperature in the dark with the appropriate secondary antibody diluted in blocking buffer, applied similarly using parafilm. After staining, the slides were washed three more times in PBS (pH 7.4), with DAPI (1:10,000; stock 10 mg/ml) included in the final wash step. A final rinse with ddH_2O was performed before mounting.

Slides were mounted using Fluoromount-G® (Southern Biotech, Birmingham, USA) and covered with a coverslip. The mounting medium was allowed to solidify for a minimum of 2 hours at 4 °C. Imaging was performed using a Zeiss Observer Z1 microscope equipped with ZEN 3.7 software.

4.3.12 Sequential Membrane Extraction

At least 1 × 10^8 MACS-purified *P. falciparum*-infected erythrocytes (corresponding to approximately 10 µl packed cells) were washed twice in PBS and resuspended in 20 µl 10 mM Tris-HCl, pH 7.4, supplemented with protease inhibitor cocktail and 1 mM PMSF. Hypotonic lysis was achieved by three cycles of rapid freezing in liquid nitrogen followed by thawing in a warm water bath. An aliquot of the total lysate was mixed 1:1 with SDS sample buffer and heated at 95°C for 10 min to generate the input control **(+ve)**.

The remaining lysate was centrifuged at 18,000 rpm (~36,000 × g) for 20 min at 4°C. The soluble supernatant fraction (**SN**) was collected, while the pellet was resuspended in 10 mM Tris-HCl, pH 7.4, and centrifuged again under the same conditions to improve recovery of the soluble fraction. The resulting supernatant was combined and prepared in SDS sample buffer. The pellet was then washed with PBS until the membrane fraction was largely cleared of residual hemoglobin and subsequently extracted with 500 µl 100 mM sodium carbonate (Na2CO3), pH 11, for 30 min on ice, with mixing every 10 min. After centrifugation, the carbonate supernatant (**C**) was collected and clarified by an additional centrifugation step. Proteins in this fraction were precipitated by addition of trichloroacetic acid (TCA) to a final concentration of 20% and incubated on ice for 1 h. The precipitated proteins were pelleted by centrifugation, the supernatant was removed, and the pellet was resuspended in SDS sample buffer. Residual acidity was neutralized with a small amount of Tris base before heating at 95°C for 10 min.

The final pellet fraction (**P**) was washed in PBS, resuspended in SDS sample buffer, and heated at 95°C for 10 min. Thus, four fractions were analyzed by SDS-PAGE and Western blot: input (+ve), soluble supernatant (SN), carbonate supernatant (C), and pellet (P). Samples corresponding to approximately 1 × 10^7 parasites per lane were loaded. Anti-PfALD was used as a soluble-protein control and anti-PfEXP1 as a membrane-associated control.

5 References

Adl, S. M., D. Bass, C. E. Lane, J. Lukeš, C. L. Schoch, A. Smirnov, S. Agatha, et al. 2019. Revisions to the Classification, Nomenclature, and Diversity of Eukaryotes. *Journal of Eukaryotic Microbiology* 66: 4–119.

Aly, A. S. I., A. M. Vaughan, and S. H. I. Kappe. 2009. Malaria Parasite Development in the Mosquito and Infection of the Mammalian Host. *Annual Review of Microbiology* 63: 195–221.

Ansorge, I., K. Paprotka, S. Bhakdi, and K. Lingelbach. 1997. Permeabilization of the erythrocyte membrane with streptolysin O allows access to the vacuolar membrane of Plasmodium falciparum and a molecular analysis of membrane topology. *Molecular and Biochemical Parasitology* 84: 259–261.

Antinori, S., L. Galimberti, L. Milazzo, and M. Corbellino. 2012. BIOLOGY OF HUMAN MALARIA PLASMODIA INCLUDING PLASMODIUM KNOWLESI. *Mediterranean Journal of Hematology and Infectious Diseases* 4: e2012013.

Ashley, E. A., M. Dhorda, R. M. Fairhurst, C. Amaratunga, P. Lim, S. Suon, S. Sreng, et al. 2014. Spread of Artemisinin Resistance in *Plasmodium falciparum* Malaria. *New England Journal of Medicine* 371: 411–423.

Beck, J. R., and C.-M. Ho. 2021. Transport mechanisms at the malaria parasite-host cell interface B. F. C. Kafsack [ed.],. *PLOS Pathogens* 17: e1009394.

Bhatt, S., D. J. Weiss, E. Cameron, D. Bisanzio, B. Mappin, U. Dalrymple, K. E. Battle, et al. 2015. The effect of malaria control on Plasmodium falciparum in Africa between 2000 and 2015. *Nature* 526: 207–211.

Bozdech, Z., M. Llinás, B. L. Pulliam, E. D. Wong, J. Zhu, and J. L. DeRisi. 2003. The Transcriptome of the Intraerythrocytic Developmental Cycle of Plasmodium falciparum Gary Ward [ed.],. *PLoS Biology* 1: e5.

Bradley, P. J., and L. D. Sibley. 2007. Rhoptries: an arsenal of secreted virulence factors. *Current Opinion in Microbiology* 10: 582–587.

Buffet, P. A., I. Safeukui, G. Deplaine, V. Brousse, V. Prendki, M. Thellier, G. D. Turner, and O. Mercereau-Puijalon. 2011. The pathogenesis of Plasmodium falciparum malaria in humans: insights from splenic physiology. *Blood* 117: 381–392.

Bugge, K., K. Lindorff-Larsen, and B. B. Kragelund. 2016. Understanding single-pass transmembrane receptor signaling from a structural viewpoint—what are we missing? *The FEBS Journal* 283: 4424–4451.

Charpian, S., and J. M. Przyborski. 2008. Protein Transport Across the Parasitophorous Vacuole of *Plasmodium falciparum* : Into the Great Wide Open. *Traffic* 9: 157–165.

Coppel, R. L., J. M. Favaloro, P. E. Crewther, T. R. Burkot, A. E. Bianco, H. D. Stahl, D. J. Kemp, et al. 1985. A blood stage antigen of Plasmodium falciparum shares determinants with the sporozoite coat protein. *Proceedings of the National Academy of Sciences* 82: 5121–5125.

Cova, M. M., M. H. Lamarque, and M. Lebrun. 2022. How Apicomplexa Parasites Secrete and Build Their Invasion Machinery. *Annual Review of Microbiology* 76: 619–640.

Cowman, A. F., J. Healer, D. Marapana, and K. Marsh. 2016. Malaria: Biology and Disease. *Cell* 167: 610–624.

Cowman, A. F., C. J. Tonkin, W.-H. Tham, and M. T. Duraisingh. 2017. The Molecular Basis of Erythrocyte Invasion by Malaria Parasites. *Cell Host & Microbe* 22: 232–245.

Crary, J. L., and K. Haldar. 1992. Brefeldin A inhibits protein secretion and parasite maturation in the ring stage of Plasmodium falciparum. *Molecular and Biochemical Parasitology* 53: 185–192.

De Koning-Ward, T. F., P. R. Gilson, J. A. Boddey, M. Rug, B. J. Smith, A. T. Papenfuss, P. R. Sanders, et al. 2009. A newly discovered protein export machine in malaria parasites. *Nature* 459: 945–949.

Dondorp, A. M., C. I. Fanello, I. C. Hendriksen, E. Gomes, A. Seni, K. D. Chhaganlal, K. Bojang, et al. 2010. Artesunate versus quinine in the treatment of severe falciparum malaria in African children (AQUAMAT): an open-label, randomised trial. *The Lancet* 376: 1647–1657.

Fidock, D. A., and T. E. Wellems. 1997. Transformation with human dihydrofolate reductase renders malaria parasites insensitive to WR99210 but does not affect the intrinsic activity of proguanil. *Proceedings of the National Academy of Sciences* 94: 10931–10936.

Florentin, A., D. W. Cobb, H. M. Kudyba, and V. Muralidharan. 2020. Directing traffic: Chaperone-mediated protein transport in malaria parasites. *Cellular Microbiology* 22.

Francis, S. E., D. J. Sullivan, and A. D. E. Goldberg. 1997. HEMOGLOBIN METABOLISM IN THE MALARIA PARASITE *PLASMODIUM FALCIPARUM*. *Annual Review of Microbiology* 51: 97–123.

Fujiwara, T., K. Oda, S. Yokota, A. Takatsuki, and Y. Ikehara. 1988. Brefeldin A causes disassembly of the Golgi complex and accumulation of secretory proteins in the endoplasmic reticulum. *Journal of Biological Chemistry* 263: 18545–18552.

Gallup, J., and J. Sachs. 2001. The economic burden of malaria. *The American Journal of Tropical Medicine and Hygiene* 64: 85–96.

Garten, M., A. S. Nasamu, J. C. Niles, J. Zimmerberg, D. E. Goldberg, and J. R. Beck. 2018. EXP2 is a nutrient-permeable channel in the vacuolar membrane of Plasmodium and is essential for protein export via PTEX. *Nature Microbiology* 3: 1090–1098.

Geoghegan, N. D., C. Evelyn, L. W. Whitehead, M. Pasternak, P. McDonald, T. Triglia, D. S. Marapana, et al. 2021. 4D analysis of malaria parasite invasion offers insights into erythrocyte membrane remodeling and parasitophorous vacuole formation. *Nature Communications* 12: 3620.

Ginsburg, H., and W. D. Stein. 1987. New permeability pathways induced by the malarial parasite in the membrane of its host erythrocyte: Potential routes for targeting of drugs into infected cells. *Bioscience Reports* 7: 455–463.

Goldberg, D. E., and J. Zimmerberg. 2020. Hardly Vacuous: The Parasitophorous Vacuolar Membrane of Malaria Parasites. *Trends in Parasitology* 36: 138–146.

Grau, B., M. Javanainen, M. J. García-Murria, W. Kulig, I. Vattulainen, I. Mingarro, and L. Martínez-Gil. 2017. The role of hydrophobic matching on transmembrane helix packing in cells. *Cell Stress* 1: 90–106.

Gubbels, M.-J., and M. T. Duraisingh. 2012. Evolution of apicomplexan secretory organelles. *International Journal for Parasitology* 42: 1071–1081.

Günther, K., M. Tümmler, H.-H. Arnold, R. Ridley, M. Goman, J. G. Scaife, and K. Lingelbach. 1991. An exported protein of Plasmodium falciparum is synthesized as an integral membrane protein. *Molecular and Biochemical Parasitology* 46: 149–157.

Haldar, K., and N. Mohandas. 2009. Malaria, erythrocytic infection, and anemia. *Hematology* 2009: 87–93.

Hope, I. A., R. Hall, D. Ll. Simmons, J. E. Hyde, and J. G. Scaife. 1984. Evidence for immunological cross-reaction between sporozoites and blood stages of a human malaria parasite. *Nature* 308: 191–194.

Hope, I. A., M. Mackay, J. E. Hyde, M. Goman, and J. Scaife. 1985. The gene for an exported antigen of the malaria parasite *Plasmodium falciparum* cloned and expressed in *Escherichia coli*. *Nucleic Acids Research* 13: 369–379.

Huang, Z., G. Li, C. Zhang, and X.-H. Xing. 2016. A study on the effects of linker flexibility on acid phosphatase PhoC-GFP fusion protein using a novel linker library. *Enzyme and Microbial Technology* 83: 1–6.

Katris, N. J., G. G. Van Dooren, P. J. McMillan, E. Hanssen, L. Tilley, and R. F. Waller. 2014. The Apical Complex Provides a Regulated Gateway for Secretion of Invasion Factors in Toxoplasma L. D. Sibley [ed.],. *PLoS Pathogens* 10: e1004074.

Lambros, C., and J. P. Vanderberg. 1979. Synchronization of Plasmodium falciparum Erythrocytic Stages in Culture. *The Journal of Parasitology* 65: 418.

Lee, W.-C., B. Russell, and L. Rénia. 2019. Sticking for a Cause: The Falciparum Malaria Parasites Cytoadherence Paradigm. *Frontiers in Immunology* 10: 1444.

Lerch-Bader, M., C. Lundin, H. Kim, I. Nilsson, and G. Von Heijne. 2008. Contribution of positively charged flanking residues to the insertion of transmembrane helices into the endoplasmic reticulum. *Proceedings of the National Academy of Sciences* 105: 4127–4132.

Lingelbach, K., and K. A. Joiner. 1998. The parasitophorous vacuole membrane surrounding *Plasmodium* and *Toxoplasma:* An unusual compartment in infected cells. *Journal of Cell Science* 111: 1467–1475.

Lippincott-Schwartz, J., L. C. Yuan, J. S. Bonifacino, and R. D. Klausner. 1989. Rapid redistribution of Golgi proteins into the ER in cells treated with brefeldin A: Evidence for membrane cycling from Golgi to ER. *Cell* 56: 801–813.

Mace, K. E., N. W. Lucchi, and K. R. Tan. 2022. Malaria Surveillance — United States, 2018. *MMWR. Surveillance Summaries* 71: 1–35.

Maier, A. G., B. M. Cooke, A. F. Cowman, and L. Tilley. 2009. Malaria parasite proteins that remodel the host erythrocyte. *Nature Reviews Microbiology* 7: 341–354.

McFadden, G. I., and E. Yeh. 2017. The apicoplast: now you see it, now you don't. *International Journal for Parasitology* 47: 137–144.

Meibalan, E., and M. Marti. 2017. Biology of Malaria Transmission. *Cold Spring Harbor Perspectives in Medicine* 7: a025452.

Mesén-Ramírez, P., B. Bergmann, M. Elhabiri, L. Zhu, H. Von Thien, C. Castro-Peña, T.-W. Gilberger, et al. 2021. The parasitophorous vacuole nutrient channel is critical for drug access in malaria parasites and modulates the artemisinin resistance fitness cost. *Cell Host & Microbe* 29: 1774-1787.e9.

Mesén-Ramírez, P., B. Bergmann, T. T. Tran, M. Garten, J. Stäcker, I. Naranjo-Prado, K. Höhn, et al. 2019. EXP1 is critical for nutrient uptake across the parasitophorous vacuole membrane of malaria parasites. *PLoS biology* 17: e3000473.

Miller, L. H., D. I. Baruch, K. Marsh, and O. K. Doumbo. 2002. The pathogenic basis of malaria. *Nature* 415: 673–679.

Moras, M., S. D. Lefevre, and M. A. Ostuni. 2017. From Erythroblasts to Mature Red Blood Cells: Organelle Clearance in Mammals. *Frontiers in Physiology* 8: 1076.

O'Donnell, R. A., T. F. De Koning-Ward, R. A. Burt, M. Bockarie, J. C. Reeder, A. F. Cowman, and B. S. Crabb. 2001. Antibodies against Merozoite Surface Protein (Msp)-119 Are a Major Component of the Invasion-Inhibitory Response in Individuals Immune to Malaria. *The Journal of Experimental Medicine* 193: 1403–1412.

Park, E., and T. A. Rapoport. 2012. Mechanisms of Sec61/SecY-Mediated Protein Translocation Across Membranes. *Annual Review of Biophysics* 41: 21–40.

Pretini, V., M. H. Koenen, L. Kaestner, M. H. A. M. Fens, R. M. Schiffelers, M. Bartels, and R. Van Wijk. 2019. Red Blood Cells: Chasing Interactions. *Frontiers in Physiology* 10: 945.

Prudêncio, M., A. Rodriguez, and M. M. Mota. 2006. The silent path to thousands of merozoites: the Plasmodium liver stage. *Nature Reviews Microbiology* 4: 849–856.

Przyborski, J. M., and M. Lanzer. 2005. Protein transport and trafficking in *Plasmodium falciparum* -infected erythrocytes. *Parasitology* 130: 373–388.

Przyborski, J. M., B. Nyboer, and M. Lanzer. 2016. Ticket to ride: export of proteins to the *Plasmodium falciparum* -infected erythrocyte. *Molecular Microbiology* 101: 1–11.

Ressurreição, M., J. A. Thomas, S. D. Nofal, C. Flueck, R. W. Moon, D. A. Baker, and C. Van Ooij. 2020. Use of a highly specific kinase inhibitor for rapid, simple and precise synchronization of Plasmodium falciparum and Plasmodium knowlesi asexual blood-stage parasites G. Langsley [ed.],. *PLOS ONE* 15: e0235798.

Sachs, J., and P. Malaney. 2002. The economic and social burden of malaria. *Nature* 415: 680–685.

Schneider, A. F. L., and C. P. R. Hackenberger. 2017. Fluorescent labelling in living cells. *Current Opinion in Biotechnology* 48: 61–68.

Simmons, D., G. Woollett, M. Bergin-Cartwright, D. Kay, and J. Scaife. 1987. A malaria protein exported into a new compartment within the host erythrocyte. *The EMBO Journal* 6: 485–491.

Snow, R. W., B. Sartorius, D. Kyalo, J. Maina, P. Amratia, C. W. Mundia, P. Bejon, and A. M. Noor. 2017. The prevalence of Plasmodium falciparum in sub-Saharan Africa since 1900. *Nature* 550: 515–518.

Spielmann, T., D. J. P. Fergusen, and H.-P. Beck. 2003. *etramps* , a New *Plasmodium falciparum* Gene Family Coding for Developmentally Regulated and Highly Charged Membrane Proteins Located at the Parasite–Host Cell Interface G. Guidotti [ed.],. *Molecular Biology of the Cell* 14: 1529–1544.

Spielmann, T., D. L. Gardiner, H. Beck, K. R. Trenholme, and D. J. Kemp. 2006. Organization of ETRAMPs and EXP-1 at the parasite–host cell interface of malaria parasites. *Molecular Microbiology* 59: 779–794.

Spielmann, T., G. N. Montagna, L. Hecht, and K. Matuschewski. 2012. Molecular make-up of the Plasmodium parasitophorous vacuolar membrane. *International Journal of Medical Microbiology* 302: 179–186.

Srivastava, A., N. Philip, K. R. Hughes, K. Georgiou, J. I. MacRae, M. P. Barrett, D. J. Creek, et al. 2016. Stage-Specific Changes in Plasmodium Metabolism Required for Differentiation and Adaptation to Different Host and Vector Environments A. R. Odom [ed.],. *PLOS Pathogens* 12: e1006094.

Struck, N. S., S. De Souza Dias, C. Langer, M. Marti, J. A. Pearce, A. F. Cowman, and T. W. Gilberger. 2005. Re-defining the Golgi complex in *Plasmodium falciparum* using the novel Golgi marker *Pf* GRASP. *Journal of Cell Science* 118: 5603–5613.

Teese, M. G., and D. Langosch. 2015. Role of GxxxG Motifs in Transmembrane Domain Interactions. *Biochemistry* 54: 5125–5135.

Tilley, L., M. W. A. Dixon, and K. Kirk. 2011. The Plasmodium falciparum-infected red blood cell. *The International Journal of Biochemistry & Cell Biology* 43: 839–842.

Tonkin, C. J., J. A. Pearce, G. I. McFadden, and A. F. Cowman. 2006. Protein targeting to destinations of the secretory pathway in the malaria parasite Plasmodium falciparum. *Current Opinion in Microbiology* 9: 381–387.

Tonkin, C. J., G. G. Van Dooren, T. P. Spurck, N. S. Struck, R. T. Good, E. Handman, A. F. Cowman, and G. I. McFadden. 2004. Localization of organellar proteins in Plasmodium falciparum using a novel set of transfection vectors and a new immunofluorescence fixation method. *Molecular and Biochemical Parasitology* 137: 13–21.

Tribensky, A., A. W. Graf, M. Diehl, W. Fleck, and J. M. Przyborski. 2017. Trafficking of PfExp1 to the parasitophorous vacuolar membrane of *Plasmodium falciparum* is independent of protein folding and the PTEX translocon. *Cellular Microbiology* 19: e12710.

Virkki, M. T., C. Peters, D. Nilsson, T. Sörensen, S. Cristobal, B. Wallner, and A. Elofsson. 2014. The Positive Inside Rule Is Stronger When Followed by a Transmembrane Helix. *Journal of Molecular Biology* 426: 2982–2991.

Von Heijne, G. 1986. The distribution of positively charged residues in bacterial inner membrane proteins correlates with the trans-membrane topology. *The EMBO Journal* 5: 3021–3027.

White, N. J. 2022. Severe malaria. *Malaria Journal* 21: 284.

Zhao, R., D. S. Shin, A. Fiser, and I. D. Goldman. 2012. Identification of a functionally critical GXXG motif and its relationship to the folate binding site of the proton-coupled folate transporter (PCFT-SLC46A1). *American Journal of Physiology-Cell Physiology* 303: C673–C681.